José António Rodrigues Romero

Licenciado em Ciências de Engenharia Física

Optical Characterization of GaN

Dissertação para obtenção do Grau de Mestre em

Engenharia Física

Orientadores: Ana Gomes Silva, Prof. Dr., Faculdade de Ciências e Tecnologia da Universidade Nova de Lisboa

Kjeld Pedersen, Prof. Dr., Department of Physics and Nanotechnology of Aalborg University

Júri

Presidente:	Prof. Dr. Isabel Catarino
Arguente:	Prof. Dr. Reinhard Schwarz
Vogal:	Prof. Dr. Ana Gomes Silva

FACULDADE DE CIÊNCIAS E TECNOLOGIA
UNIVERSIDADE NOVA DE LISBOA

Março, 2017

Optical Characterization of GaN

Este documento foi gerado utilizando o processador (pdf)LaTeX, com base no template "unlthesis" [1] desenvolvido no Dep. Informática da FCT-NOVA [2].
[1] https://github.com/joaomlourenco/unlthesis [2] http://www.di.fct.unl.pt

Acknowledgements

I would like to express my gratitude prof. Ana Cristina and prof. Kjeld Pedersen whom were very patient and persevering in helping me throughout this dissertation, both the department of Physics and Nanotechnology from Aalborg University for providing me with the required equipment, and the Physics department of Faculdade de Ciências e Tecnologia da Universidade Nova de Lisboa (FCT-UNL) for the required preparation for this work.

I would like to thank my lab colleagues Rasmus Mørch and Thore Stig for helping me with the lab equipment, and my way around the laboratory.

I would also like to thank my family allowing me the chance to embark on this five year long journey, without their motivation, interest and sacrifices none of this would have been possible. I would also like to thank all my friends, old and new ones, for making these last five years a more pleasant experience.

Abstract

Gallium nitride is a direct bandgap semiconductor commonly used in LED's and lasers. Its wide bandgap, high thermal conductivity and ability to operate at high frequencies and power make it an attractive material in the semiconductor industry.

In this thesis two different samples of gallium nitride were characterized through four different linear and non-linear optical characterization techniques: a) optical second-harmonic generation, b) photoluminescence c) Raman spectroscopy and d) ellipsometry. Concepts in optics for anisotropic media and non-linear crystals required for the characterization techniques are discussed, and three of the most commonly used epitaxial growth techniques used for GaN growth for either thin films or bulk are described.

Moreover, to complement, and validate and to get a better understanding of the experimental results obtained computational simulations for ellipsometry and second harmonic generation were also implemented in the Python programming language.

Raman and photoluminesence spectra were compared with other published work, allowing us to compare the crystalinity and purity of the samples. Both mathematical models for ellipsometry and second harmonic generation were fitted to the experimental results, allowing us to conclude that it is possible to determine the thickness of a thick crystal through second harmonic generation, where ellipsometry no longer is a reliable method.

Keywords: Gallium Nitride, MBE, HVPE, MOCVD, SHG, Ellipsometry, Photoluminescence, Raman spectroscopy

Resumo

O nitreto de gálio é um semicondutor com um hiato de energia direto geralmente utilizado em lasers e LEDs. A seu grande hiato de energia, alta condutividade térmica e elétrica, e capacidade de operar em frequências e potências elevadas o tornaram num material apelativo na indústria de semicondutores.

Nesta tese duas amostras diferentes de nitreto de gálio foram caracterizadas por quatro técnicas óticas lineares e não-lineares diferentes: a) Geração ótica de segunda harmónica, b) fotoluminescência, c) Espectroscopia de Raman, e c) Elipsometría. Os conceitos de ótica em meios anisotrópicos e não-lineares necessários para as técnicas empregues são descritos, ao igual que três técnicas de crescimento epitaxial habitualmente usadas para crescer filmes e/ou cristais de nitreto de gálio.

Adicionalmente, como complemento a este trabalho foram desenvolvidos scripts na linguagem de programação Python, para simular resultados teóricos de forma a compreender melhor os resultados experimentais obtidos neste trabalho.

Enquanto que os espectros de Raman e fotoluminescência foram comparados com outras publicações de forma a comparar a cristalinidade e pureza das amostras. Por outro lado os modelos computacionais foram adaptados aos resultados experimentais dos espectros de elipsometria e segunda harmónica, de forma a determinar a espessura de uma amostra fina e um cristal de nitreto de gálio respetivamente, demonstrando que é possível determinar a espessura de um cristal grosso através de geração de segunda harmónica onde o mesmo não seria possível através de elipsometria.

Palavras-chave: Nitreto de gálio, MBE, HVPE, MOCVD, SHG, Elipsometria, Fotoluminescência, Espetroscopia de Raman

Contents

List of Figures

List of Tables

Acronyms

CCD	Charge-coupled Device.
CVD	Chemical Vapour Deposition.
HVPE	Hydride Vapour Phase Epitaxy.
HWP	Half Wave Plate.
IR	Infrared.
LED	Light Emitting Diode.
MBE	Molecular Beam Epitaxy.
MOCVD	Metalorganic Chemical Vapour Deposition.
MOSFET	Metal Oxide Semiconductor Field-effect Transistor.
Nd:YAG	Neodymium-doped Yttrium Aluminum Garnet.
OPO	Optical Parametric Oscillator.
PBN	Pyrolytic Boron Nitride.
PL	Photoluminescence.
PMT	Photomultiplier.

SHG Second Harmonic Generation.

UHV Ultra High Vacuum.

UV Ultraviolet.

Chapter 1

Introduction

Gallium Nitride is a group III-V compound semiconductor with a direct bandgap of 3.4 eV. Its wide bandgap has made it a popular material for optoelectronic devices such as LEDs, lasers and high power, high frequency and efficient electronic devices [1]. Only until recently it was discovered how to successfully grow GaN films on silicon substrates, allowing GaN devices to be compatible with current Si electronic devices. Compared to Si, GaN has a higher electron mobility, a higher breakdown voltage and a higher saturation mobility allowing a better performance at higher voltages and frequencies compared to Si [2]. GaN possesses many advantages over Si, by one side the bonds in a GaN crystal are stronger, this is the reason why GaN displays a smaller electrical resistance. Electronic devices based on GaN could become much smaller and operate at much higher temperatures, which is a key factor for power applications.

Alongside GaN, some other semiconductor materials have been considered as a replacement for Si, like SiC and GaAs. While SiC possesses a wide bandgap energy of 3.2 eV, this semiconductor can be used for high temperature and high voltages devices, however SiC price and availability make it less appealing as the next replacement of Si, making GaN the future option for widespread electronic devices and leaving SiC for higher end applications where the cost of production may not be the main concern [3]. GaAs is another popular semiconductor for making electronic devices such as Light Emitting Diodes (LEDs), lasers, solar cells, among many other applications, however its sole advantage is the fact that it is cheaper to mass produce and benefits from a more extensive period of research compared to GaN. Nonetheless GaN has proven to allow higher efficiencies, also it can operate at higher temperatures and higher voltages than GaAs, and at the same time adoption of GaN will likely make mass production of GaN a more affordable solution, likely replacing GaAs from the market.

GaN films are highly dependent on their growth process, therefore in order to achieve

the optimal characteristics in the produced films it's necessary to understand the growth processes used, and how it may affect the characteristics of the film. Once produced, it's also necessary to characterize these films to determine whether or not they obey fit the required criteria for their intended application. The characterization of the samples is done through performing several techniques, each of them providing a set of information of our samples.

Although gallium nitride is still a material which requires a more detailed understanding, specially when it comes to its production, some GaN devices can be currently found in the market, devices such as LEDs with wavelengths between the blue and UV spectra by adding aluminum or in the visible region by adding indium. GaN power Metal Oxide Semiconductor Field-effect Transistors (MOSFETs) can also be found since they display a better relationship between on-resistance and breakdown voltage compared to its silicon counterpart [4].

Future applications could include high bandwidth communication devices given that GaN can operate at higher frequencies compared to Si. One key disadvantage over silicon is its the production cost, although future adoption of GaN could lead to a drop of its cost.

Chapter 2

Electromagnetic Radiation and Optics

Most of the characterization methods applied for thin films consist on determining many of the optical properties of the films, this is due the fact that most of these characterization methods are non-destructive and contactless methods which is highly advantageous for these kind of devices that highly depend on the degree of purity and crystal quality of the layers, also the fact that the same sample can be reutilized on all these techniques is also a great advantage since the time and money required to produce these films can prove to be an inconvenient.

2.1 Electromagnetic Field

In classic electromagnetism, an electromagnetic field can be described by two fields, and those are the **E** and **H** which are the electromagnetic and magnetic field respectively. These fields obey a set of differential equations which are called Maxwell's equations. These equations are:

$$\nabla \times \mathbf{E} + \frac{\partial \mathbf{B}}{\partial t} = 0 \tag{2.1.1}$$

$$\nabla \times \mathbf{H} - \frac{\partial \mathbf{D}}{\partial t} = \mathbf{J} \tag{2.1.2}$$

$$\nabla \cdot \mathbf{D} = \rho \tag{2.1.3}$$

$$\nabla \cdot \mathbf{B} = 0 \tag{2.1.4}$$

Where **E** and **H** are the electric and magnetic field respectively, **D** is electric displacement, **B** is the magnetic induction field, **J** is the electric current density and ρ is the charge density.

The first equation is known as Faraday's law of induction, establishing that a non-conservative electric field will always induce by a time dependent magnetic field and vice-versa. The Electric field is said to be non-conservative because otherwise it's curl would equal to zero, which means that this same field cannot be spacially constant.

Eq.2.1.2 is known as Ampère's law, and establishes that any current or any changes in time of the electric displacement will induce a non-conservative magnetic field and vice versa, in other word any charge flow will induce a magnetic field in the area they pierce.

Both Equations 2.1.3 and 2.1.4 are Gauss's law for electric and magnetic fields respectively, the first one describes that the electric field that pierces a closed surface is proportional to the charge that is contained inside that same volume, the second one establishes the non existence of magnetic monopoles since the total magnetic flux that pierces a closed surface must always equal to zero (if there were any monopoles the divergence of the magnetic field in a volume could equal a value different that zero).

These same equations can also be expressed in their integral form opposed to the differential form applying both Gauss's divergence theorem (Eq.2.1.5) and Stoke's theorem (Eq.2.1.6), which allows to switch from a volume integral to a surface integral and from a surface integral to a line integral respectively.

$$\iiint_V (\nabla \cdot \mathbf{F})\, dV = \oiint_{\partial V} \mathbf{F} \cdot d\mathbf{S} \tag{2.1.5}$$

$$\oiint_S (\nabla \times \mathbf{F}) \cdot d\mathbf{S} = \oint_{\partial S} \mathbf{F} \cdot d\mathbf{l} \tag{2.1.6}$$

Where ∂S and ∂V represent the boundary of the closed surface S and closed volume V respectively. Applying both Equation 2.1.5 on Equations 2.1.3 and 2.1.4, and 2.1.6 on Equations 2.1.1 and 2.1.2, these same can also be written as:

$$\oint_{\partial S} \mathbf{E} \cdot d\mathbf{l} = -\oiint_S \frac{\partial \mathbf{B}}{\partial t} \cdot d\mathbf{S} \tag{2.1.7}$$

$$\oint_{\partial S} \mathbf{H} \cdot d\mathbf{l} = \oiint_S \left(\mathbf{J} + \frac{\partial \mathbf{D}}{\partial t} \right) \cdot d\mathbf{S} \tag{2.1.8}$$

$$\oiint_{\partial V} \mathbf{D} \cdot d\mathbf{S} = \iiint_V \rho\, dV \tag{2.1.9}$$

$$\oiint_{\partial V} \mathbf{B} \cdot d\mathbf{S} = 0 \tag{2.1.10}$$

These set of differential equations dictate the basis for classical electrodynamics and optics as well as electrical circuits. However before applying these equations it is necessary to know how the material respond to an electromagnetic field, this effect on the material is given by the electromagnetic constitutive equations for that given material.

$$\mathbf{D} = \varepsilon \mathbf{E} = \varepsilon_0 \mathbf{E} + \mathbf{P} \tag{2.1.11}$$

$$\mathbf{B} = \mu \mathbf{H} = \mu_0 \mathbf{H} + \mathbf{M} \tag{2.1.12}$$

Where Eq.2.1.11 is the electric displacement field and establishes how a medium reacts to an electric field, where ε is the permitivity of the medium, ε_0 is the permitivity of vacuum and $\mathbf{P}$ is the electric polarization, and Eq.2.1.12 is the magnetic field and establishes the interaction with a magnetic field where μ is the permeability, μ_0 is the permeability of vacuum and $\mathbf{M}$ is the magnetic polarization.

Throughout this subsection only linear mediums are going to be discussed, which means that both the magnetic and electric polarization are going to be proportional to the electric and magnetic field respectively. The same can be written as:

$$\mathbf{P} = \varepsilon_0 \chi_e \mathbf{E} \implies \mathbf{D} = \varepsilon_0 (1 + \chi_e)\mathbf{E} \tag{2.1.13}$$

$$\mathbf{M} = \mu_0 \chi_v \mathbf{H} \implies \mathbf{B} = \mu_0 (1 + \chi_v)\mathbf{H} \tag{2.1.14}$$

Where χ_e and χ_v are the electric and magnetic susceptibility respectively. As mentioned these equations assume a linear response of the medium, which will be valid for this subsection, and later on subsection 2.4 this assumption will no longer be valid, also only the electric polarization will be taken into account since the electric field in electromagnetic radiation is usually far stronger than the magnetic field, therefore the polarization intensity can be described as only the electric polarization. A material is said to be homogeneous if both χ_e and χ_v are independent of the position, also the medium is said to be isotropic if both susceptibilities can be expressed as scalar quantities, otherwise both vectors $\mathbf{P}$ and $\mathbf{D}$, and vectors $\mathbf{M}$ and $\mathbf{B}$ would not be parallel to each other and the medium is said to be anisotropic.

Most of electromagnetic waves can be expressed as sinusoidal waves, and can be either expressed by a pure real sinusoidal function or as a complex exponential function, where the real part would correspond to the same wave as the pure real counterpart. Let's take an electric field given by the following expression:

$$\mathbf{E} = \mathbf{E_0} e^{i(\mathbf{k}\cdot\mathbf{r} - \omega t)} \tag{2.1.15}$$

The electromagnetic wave is said to be monochromatic is we assume ω to be a constant, therefore having a constant wavelength λ. If we apply Gauss's law, and assume that the medium is both homogeneous and there are no free charges, thus $\rho = 0$, we also obtain:

$$\nabla \cdot \mathbf{D} = \rho \implies \nabla \cdot \mathbf{E} = \frac{\rho}{\varepsilon} \implies \nabla \cdot \mathbf{E} = 0 \tag{2.1.16}$$

$$\implies \nabla \cdot (\mathbf{E_0} e^{i(k_x x + k_y y + k_z z - \omega t)}) = 0 \tag{2.1.17}$$

$$\implies \mathbf{E_0} \cdot \mathbf{k} = 0 \tag{2.1.18}$$

What this means is that the electric field is perpendicular to the direction that the wave propagates, or in other words, that electromagnetic waves are transverse. Magnetic fields

can also be expressed through complex equations since they also behave as sinusoidal waves just as electric fields, and through Faraday's law it is possible to determine the magnetic field direction.

$$\mathbf{B} = \mathbf{B_0} e^{i(\mathbf{k}\cdot\mathbf{r}-\omega t)} \tag{2.1.19}$$

$$\nabla \times \mathbf{E} = -\frac{\partial \mathbf{B}}{\partial t} \implies i\mathbf{k} \times \mathbf{E} = -\frac{\partial \mathbf{B}}{\partial t} \tag{2.1.20}$$

$$\implies \mathbf{B} = \frac{1}{\omega}\mathbf{k} \times \mathbf{E} \tag{2.1.21}$$

Therefore it is possible to conclude that both the electric field and the magnetic field are perpendicular to each other and perpendicular to the direction of propagation of the wave.

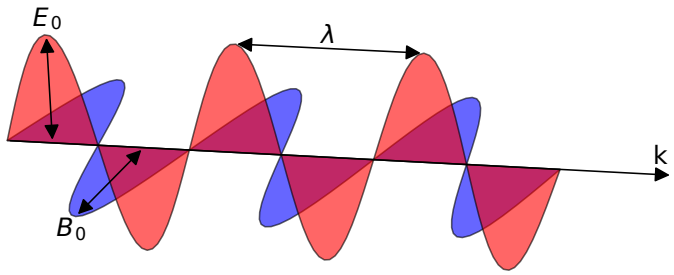

Figure 2.1: An electromagnetic wave is composed of both a magnetic (blue wave) and electric (red wave) fields.

Electromagnetic waves conservation of energy is also observed, this conservation of energy is expressed by Poynting's theorem, where it is established that the rate of change on time of the energy density on a closed volume for an electromagnetic field must equal to the flux of energy leaving that volume plus the work done to the free charges (or the free charge density) on the same volume. This theorem can be expressed as follows:

$$-\frac{\partial U}{\partial t} = \nabla \cdot \mathbf{S} + \mathbf{J} \cdot \mathbf{E} \tag{2.1.22}$$

Where U is the energy density per unit of volume of the electromagnetic field and $\mathbf{S}$ is the Poynting vector, and the same are defined as:

$$U = \frac{1}{2}(\mathbf{E} \cdot \mathbf{D} + \mathbf{H} \cdot \mathbf{B}) \tag{2.1.23}$$

$$\mathbf{S} = \mathbf{E} \times \mathbf{H} \tag{2.1.24}$$

However these equations are only true for non-complex equations, otherwise these quantities are expressed as follows:

$$U = \frac{1}{4} Re[\mathbf{E} \cdot \mathbf{D}^* + \mathbf{B} \cdot \mathbf{H}^*] \tag{2.1.25}$$

$$\mathbf{S} = \frac{1}{2} Re[\mathbf{E} \times \mathbf{H}^*] \tag{2.1.26}$$

The Poynting vector **S** represents the direction of the energy flux of an electromagnetic wave, this flux will have the same direction as the propagation of the wave, and the magnitude of this vector represents the power density per unit of area, therefore integrating this vector along a closed surface A this same vector pierces would give us the rate flow of energy along the same surface.

$$P_{rad} = \oint_A \mathbf{S} \cdot d\mathbf{A} \tag{2.1.27}$$

In Eqs.2.1.15 and 2.1.19, a wave vector **k**which propagates along the principal axis given by the vector **r** was introduced. This wavevector k is the vector of propagation in the medium, however the speed on how this wavevector propagates will depend on the refractive index of the material, and also all glasses display dispersion phenomenons, and what this means is that the refractive index of the material will vary with the wavelength of the incident beam.

$$k = n(\omega)\frac{\omega}{c} \tag{2.1.28}$$

This refractive index can be either a real number for a lossless medium, or a complex number, which depending on its extinction coefficient κ can be either an attenuating or stimulated amplifying medium, if κ possesses a negative or positive value respectively. This complex refractive index can be written as:

$$\tilde{n} = n + i\kappa \tag{2.1.29}$$

2.2 Polarization of Light

Terms such as polarized light or a polarizer are often used when dealing with radiation, specially with characterization techniques since in many substances the refractive index depend on the polarization of the incident light [5]. The direction of the electric field defines the state of polarization of light, therefore if an incident beam does not possess a well defined state of polarization then it's said to be non-polarized light, and a polarizer is an apparatus which allows to impose a state of polarization to a beam of light.

Let's assume an electromagnetic wave with its **k** vector in the z direction given by the following function:

$$\mathbf{E} = Re[\mathbf{E_0} e^{i(\omega t - kz)}] \tag{2.2.1}$$

Given that the wave propagates on the z direction, both electric and magnetic fields can only be contained in either the x or y planes, therefore the electric field can be separated in both a x and y components.

The respective E_x and E_y of the electric field are then given by:

$$E_x = E_{0x} cos(\omega t - kz + \Delta_x) \tag{2.2.2}$$

$$E_y = E_{0y} cos(\omega t - kz + \Delta_y) \tag{2.2.3}$$

These two expression can be further simplified in one single expression, relating both Δ_x and Δ_y, through some simple algebra.

$$\left(\frac{E_x}{E_{0x}}\right)^2 + \left(\frac{E_y}{E_{0y}}\right)^2 - \frac{2\cos(\Delta)}{E_{0y}E_{0x}} E_x E_y = \sin^2\Delta \tag{2.2.4}$$

$$\Delta = \Delta_y - \Delta_x,\ \Delta \in [-\pi, \pi] \tag{2.2.5}$$

Looking at Eq.2.2.4, the curve of this equation will be a ellipse, and the orientation of the ellipse will dictate the polarization state of the wave. From this curve, there are two special cases, when the ellipse is either a straight line or a circle, in which cases the light is said to be linearly and circularly polarized.

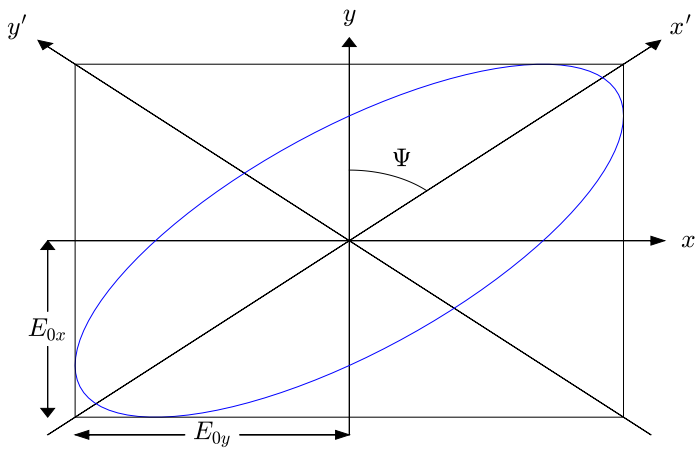

Figure 2.2: Polarization ellipse for $\Delta = \pi/4$.

If an electromagnetic wave is linearly polarized then:

$$\Delta = \Delta_y - \Delta_x = n\pi,\ n = 1, 2 \tag{2.2.6}$$

Otherwise the electromagnetic wave is said to be circularly polarized if:

$$\Delta = \Delta_y - \Delta_x = n\frac{\pi}{2},\ n = -1, 1 \tag{2.2.7}$$

The electric field for both x and y components can also be written in a complex function, so that a complex ratio ρ between both E_y and E_x is given by:

$$E_y = E_{0y} e^{i(\omega t - kz + \Delta_y)} \tag{2.2.8}$$

$$E_x = E_{0x} e^{i(\omega t - kz + \Delta_x)} \tag{2.2.9}$$

$$\rho = \frac{E_y}{E_x} = e^{i\Delta} tan\ \Psi = \frac{E_{0y}}{E_{0x}} e^{\Delta_y - \Delta_x},\ \Psi \in [0, \pi/2] \tag{2.2.10}$$

2.3 Anisotropic Medium

Through section 2.1 the media was assumed to be isotropic, and as a consequence, the electric polarization vector **P** was assumed to be parallel to the induced electric field. However there are many materials that do not display this behavior such as calcite, quartz, KDP and liquid crystals [5]. Looking at Eq.2.1.13, the electric polarization in given as:

$$\mathbf{P} = \varepsilon_0 \overline{\overline{\chi}}_e \mathbf{E} \tag{2.3.1}$$

However for this equation hold true for anisotropic media, then the electric susceptibility must be then given by a rank 2 tensor, otherwise the electric polarization vector would always be parallel to the induced electric field, therefore the electric susceptibility can be written as:

$$\overline{\overline{\chi}}_e = \begin{pmatrix} \chi_{11} & \chi_{12} & \chi_{13} \\ \chi_{21} & \chi_{22} & \chi_{23} \\ \chi_{31} & \chi_{32} & \chi_{33} \end{pmatrix} \tag{2.3.2}$$

Therefore the electric displacement vector will be given as

$$\mathbf{D} = \varepsilon_0 (1 + \overline{\overline{\chi}}_e)\ \mathbf{E} = \overline{\overline{\varepsilon}}\ \mathbf{E} = \begin{pmatrix} \varepsilon_{11} & \varepsilon_{12} & \varepsilon_{13} \\ \varepsilon_{21} & \varepsilon_{22} & \varepsilon_{23} \\ \varepsilon_{31} & \varepsilon_{32} & \varepsilon_{33} \end{pmatrix} \cdot \begin{pmatrix} E_x \\ E_y \\ E_z \end{pmatrix} \tag{2.3.3}$$

$$D_i = \sum_{j=1}^{3} \varepsilon_{ij} E_j, \quad i = 1, 2, 3 \tag{2.3.4}$$

It is possible to demonstrate through conservation of energy as stated on Poyting's theorem that the dielectric tensor must be symmetric, so that there are only six independent term on the dielectric tensor matrix, therefore:

$$\varepsilon_{ij} = \varepsilon_{ji}, \quad i,j = 1,2,3 \tag{2.3.5}$$

However it is possible to choose a set of coordinates x y and z for the crystal so that non-diagonal members of the matrix are set to be zero, this set of coordinates are called the principal axis of the system, further simplifying the dielectric tensor as:

$$\overline{\overline{\varepsilon}} = \begin{pmatrix} \varepsilon_x & 0 & 0 \\ 0 & \varepsilon_y & 0 \\ 0 & 0 & \varepsilon_z \end{pmatrix} \tag{2.3.6}$$

For this matrix there are three possibilities:

$$\varepsilon_x = \varepsilon_y = \varepsilon_z \tag{2.3.7}$$

$$\varepsilon_x = \varepsilon_y \neq \varepsilon_z \tag{2.3.8}$$

$$\varepsilon_x \neq \varepsilon_y \neq \varepsilon_z \tag{2.3.9}$$

The first case is the same as studied before, an isotropic medium, where this same matrix could be also written as just simply a scalar, for the second case the medium is said to be uniaxial crystal and for the third case a biaxial crystal.

Let's assume an electric field and a magnetic field given by the following expressions:

$$\mathbf{E} = E_0 e^{i(\mathbf{k}\cdot\mathbf{r}-\omega t)} \tag{2.3.10}$$

$$\mathbf{H} = H_0 e^{i(\mathbf{k}\cdot\mathbf{r}-\omega t)} \tag{2.3.11}$$

Applying Maxwell's Eqs.2.1.1 and 2.1.2, andassuming there are no free charges, we get:

$$\mathbf{k}\times\mathbf{E} = \omega\overline{\overline{\mu}}\,\mathbf{H} \tag{2.3.12}$$

$$\mathbf{k}\times\mathbf{H} = -\omega\overline{\overline{\varepsilon}}\,\mathbf{E} \tag{2.3.13}$$

What this implies is that wavevector $\mathbf{k}$ will not be parallel to the Poynting vector, so the wave propagates along this vector however the planewave of this electromagnetic wave will not be parallel to the direction of it's propagation.

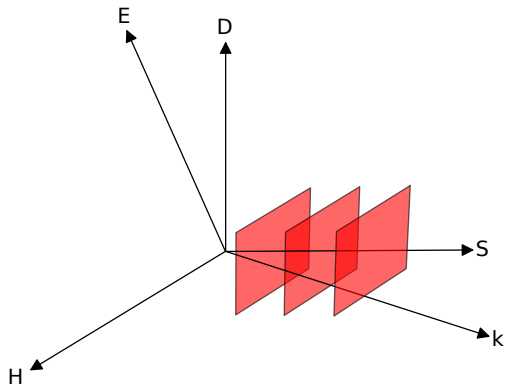

Figure 2.3: Plane waves in an anisotropic medium travel with the direction of the Poynting vector, however the planewaves will be parallel to the **k** vector.

Through Eqs.2.1.12 and 2.1.21, Eq.2.3.12 can be further simplified as:

$$\mathbf{B} = \frac{1}{\omega}\mathbf{k}\times\mathbf{E},\ \mathbf{B} = \mu\mathbf{H} \implies \overline{\overline{\mu}}\,\mathbf{H} = \frac{1}{\omega}\mathbf{k}\times\mathbf{E} \tag{2.3.14}$$

$$\implies \mathbf{k}\times(\mathbf{k}\times\mathbf{E}) = -\omega^2\overline{\overline{\mu}}\,\overline{\overline{\varepsilon}}\,\mathbf{E} \tag{2.3.15}$$

$$\implies (\mathbf{k}\cdot\mathbf{E})\mathbf{k} - (\mathbf{k}\cdot\mathbf{k})\mathbf{E} = -\omega^2\overline{\overline{\mu}}\,\overline{\overline{\varepsilon}}\,\mathbf{E} \tag{2.3.16}$$

Where just like ε, μ is a diagonal rank 2 tensor, which can be expressed as a constant for isotropic mediums.

$$\overline{\overline{\varepsilon}} = \begin{pmatrix} \varepsilon_x & 0 & 0 \\ 0 & \varepsilon_y & 0 \\ 0 & 0 & \varepsilon_z \end{pmatrix}, \qquad \overline{\overline{\mu}} = \begin{pmatrix} \mu_x & 0 & 0 \\ 0 & \mu_y & 0 \\ 0 & 0 & \mu_z \end{pmatrix} \tag{2.3.17}$$

From Eqn.2.3.16 we then get that:

$$\begin{pmatrix} \omega^2\mu_x\varepsilon_x - {k_y}^2 - {k_z}^2 & k_xk_y & k_xk_z \\ k_yk_x & \omega^2\mu_y\varepsilon_y - {k_x}^2 - {k_z}^2 & k_yk_z \\ k_zk_x & k_zk_y & \omega^2\mu_z\varepsilon_z - {k_x}^2 - {k_y}^2 \end{pmatrix} \cdot \begin{pmatrix} E_x \\ E_y \\ E_z \end{pmatrix} = 0 \tag{2.3.18}$$

From this linear system, we know the direction of propagation, therefore we know the components of the **k** vector, and the medium of propagation, therefore the elements of both tensors ε and μ are said to be know values, The remaining unknown variables are then the values of each element of the electric field which will correspond to the eigenvectors of the system, and the value for ω which will be related to the eigenvalues of the system. In order for non-trivial solutions exist on the system, the determinant must equal to zero.

$$\begin{vmatrix} \omega^2\mu_x\varepsilon_x - {k_y}^2 - {k_z}^2 & k_xk_y & k_xk_z \\ k_yk_x & \omega^2\mu_y\varepsilon_y - {k_x}^2 - {k_z}^2 & k_yk_z \\ k_zk_x & k_zk_y & \omega^2\mu_z\varepsilon_z - {k_x}^2 - {k_y}^2 \end{vmatrix} = 0 \tag{2.3.19}$$

Expanding this determinant a quadratic expression for ω^2 will be found, however only two of the four roots will be real ones, which will correspond to the two independent states of polarization for the propagation of the wave. By simplifying this determinant we then get:

$$\frac{{k_x}^2}{k^2 - \omega^2\mu_x\varepsilon_x} + \frac{{k_y}^2}{k^2 - \omega^2\mu_y\varepsilon_y} + \frac{{k_z}^2}{k^2 - \omega^2\mu_z\varepsilon_z} = 1 \tag{2.3.20}$$

By simplifying Eq.2.3.18, the direction of the electric field can be obtained.

$$\begin{pmatrix} E_x \\ E_y \\ E_z \end{pmatrix} = E_0 \begin{pmatrix} \dfrac{k_x}{k^2 - \omega^2\mu_x\varepsilon_x} \\ \dfrac{k_y}{k^2 - \omega^2\mu_y\varepsilon_y} \\ \dfrac{k_z}{k^2 - \omega^2\mu_z\varepsilon_z} \end{pmatrix} \tag{2.3.21}$$

where

$$E_0 = k_xE_x + k_yE_y + k_zE_z = \mathbf{k}\cdot\mathbf{E} \tag{2.3.22}$$

$$k^2 = {k_x}^2 + {k_y}^2 + {k_z}^2 \tag{2.3.23}$$

Since the medium is said to be anisotropic, each principal axis will have its own refractive index, this is, the refractive index of the system will also be given as a rank 2 tensor, which is given by:

$$\overline{\overline{n}} = \begin{pmatrix} n_x & 0 & 0 \\ 0 & n_y & 0 \\ 0 & 0 & n_z \end{pmatrix} = \sqrt{\frac{1}{\varepsilon_0\mu_0}} \begin{pmatrix} \sqrt{\varepsilon_x\mu_x} & 0 & 0 \\ 0 & \sqrt{\varepsilon_y\mu_y} & 0 \\ 0 & 0 & \sqrt{\varepsilon_z\mu_z} \end{pmatrix} \tag{2.3.24}$$

The **k** vector for a given anisotropic medium can be written as:

$$\begin{pmatrix} k_x \\ k_y \\ k_z \end{pmatrix} = \frac{\omega}{c} n \begin{pmatrix} s_x \\ s_y \\ s_z \end{pmatrix} \tag{2.3.25}$$

Where **s** is an unitary vector with the direction of propagation, and n is the effective refractive index. With both Eqs.2.3.24 and 2.3.25 it is possible to write Eq.2.3.20 as:

$$\frac{s_x^2}{n^2 - n_x^2} + \frac{s_y^2}{n^2 - n_y^2} + \frac{s_z^2}{n^2 - n_z^2} = \frac{1}{n^2} \tag{2.3.26}$$

and Eq.2.3.21 as:

$$\begin{pmatrix} E_x \\ E_y \\ E_z \end{pmatrix} = n^2(\mathbf{s} \cdot \mathbf{E}) \begin{pmatrix} \frac{s_x}{n^2 - {n_x}^2} \\ \frac{s_y}{n^2 - {n_y}^2} \\ \frac{s_z}{n^2 - {n_z}^2} \end{pmatrix} \tag{2.3.27}$$

Plotting Eq.2.3.20 in the **k** space, two shells will appear, with a maximum of four common points, depending on the values of n_x, n_y and n_z.

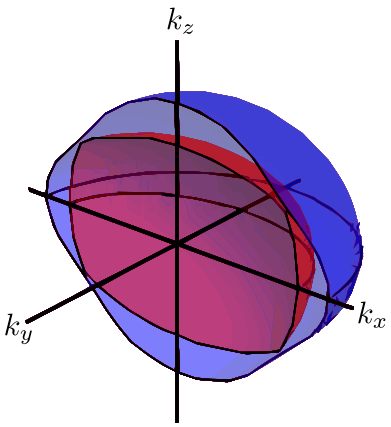

Figure 2.4: Half shell of the normal planes for a biaxial crystal.

For a biaxial crystal, intersecting the shells on the xz plane, will end up in two ellipsoids with four common points, these four points will set up the two optical axis of the crystal, so for a biaxial crystal two symmetry axis on the **k** space will be found (thus being called a biaxial crystal), similarly for an uniaxial crystal only two common points will arise therefore only one optical axis will be found, whereas for an isotropic crystal two overlapping spherical shapes will be found. For all cases two solutions will be found since the electromagnetic field is a transverse field.

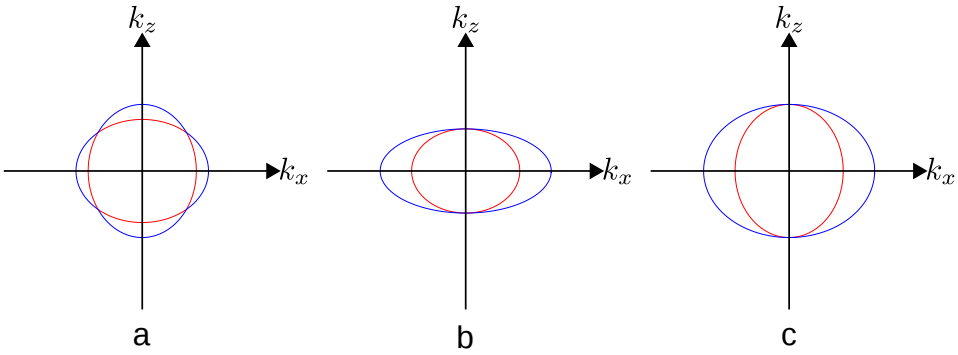

Figure 2.5: Intersection of the normal shells for (a) a biaxial crystal, (b) a positive uniaxial crystal and (c) a negative uniaxial crystal.

From Eq.2.1.23 we know that the energy density is given as:

$$U = \frac{1}{2}(\mathbf{E}\cdot\mathbf{D} + \mathbf{H}\cdot\mathbf{B}) \tag{2.3.28}$$

So it is possible to separate this energy density in both a magnetic and electric part.

$$U = \frac{1}{2}(U_E + U_B) \tag{2.3.29}$$

So if we look at the electric component of the energy density we get that:

$$2U_E = \left(\overline{\overline{\varepsilon}}^{-1}\mathbf{D}\right)\cdot\mathbf{D} \iff 2U_E = \frac{D_x^2}{\varepsilon_x} + \frac{D_y^2}{\varepsilon_y} + \frac{D_z^2}{\varepsilon_z} \tag{2.3.30}$$

$$\iff 1 = \frac{1}{2U_e}\left(\frac{D_x^2}{\varepsilon_x} + \frac{D_y^2}{\varepsilon_y} + \frac{D_z^2}{\varepsilon_z}\right) \tag{2.3.31}$$

$$\iff 1 = \frac{x^2}{\varepsilon_x} + \frac{y^2}{\varepsilon_y} + \frac{z^2}{\varepsilon_z} \tag{2.3.32}$$

Where

$$\mathbf{r} = \frac{\mathbf{D}}{\sqrt{2U_E}} = \begin{pmatrix} x \\ y \\ z \end{pmatrix} \tag{2.3.33}$$

However if we assume our crystal to be non-magnetic, then this would translate as:

$$\frac{1}{\mu_0}\overline{\overline{\mu}} = \overline{\overline{1}} \tag{2.3.34}$$

Then our refractive index tensor of our crystal can be further simplified as:

$$\overline{\overline{n}} = \frac{1}{\sqrt{\varepsilon_0}} \begin{pmatrix} \sqrt{\varepsilon_x} & 0 & 0 \\ 0 & \sqrt{\varepsilon_y} & 0 \\ 0 & 0 & \sqrt{\varepsilon_z} \end{pmatrix} \tag{2.3.35}$$

Then our electric displacement vector would yield:

$$\mathbf{D} = \overline{\overline{\varepsilon}}\, \mathbf{E} = \varepsilon_0 \begin{pmatrix} n_x^2 & 0 & 0 \\ 0 & n_y^2 & 0 \\ 0 & 0 & n_z^2 \end{pmatrix} \cdot \mathbf{E} \tag{2.3.36}$$

Then Eq.2.3.32 can be further simplified as:

$$1 = \frac{x^2}{\varepsilon_0 n_x^2} + \frac{y^2}{\varepsilon_0 n_y^2} + \frac{z^2}{\varepsilon_0 n_z^2} \tag{2.3.37}$$

However since ε_0 is a constant and to allow for a more compact notation, we then redefine $\mathbf{r}$ as:

$$\mathbf{r} = \frac{\mathbf{D}}{\sqrt{2\varepsilon_0 U_E}} = \begin{pmatrix} x \\ y \\ z \end{pmatrix} \tag{2.3.38}$$

Then Eq.2.3.32 would instead be given as:

$$\frac{x^2}{n_x^2} + \frac{y^2}{n_y^2} + \frac{z^2}{n_z^2} = 1 \tag{2.3.39}$$

This equation is known as the index ellipsoid or the optical indicatrix, and it serves as a graphical representation of the relative magnitude of the refractive indices for each direction of the crystal.

So for an uniaxial crystal, where n_x and n_y equal each other, Eq.2.3.39 can be rewritten as:

$$\frac{x^2}{n_o^2} + \frac{y^2}{n_o^2} + \frac{z^2}{n_e^2} = 1 \tag{2.3.40}$$

where

$$n_o = n_x = n_y \tag{2.3.41}$$

$$n_e = n_z \tag{2.3.42}$$

Since the normal shell for anisotropic media consists in two shells, which correspond to the two independent solutions for the polarization of the refracted waves for a given direction, then for an incident wave two refracted waves are going to be observed if the incident polarization consists of a linear combination of these two independent states.

Let us then consider a given anisotropic crystal with an incident wave with $\mathbf{k_0}$ as its propagation vector, and θ_0 as the angle between $\mathbf{k_0}$ and the normal of the crystal surface, then the kinematic conditions for the refracted waves are given as:

$$k_0 sin(\theta_0) = k_1 sin(\theta_1) = k_2 sin(\theta_2) \tag{2.3.43}$$

Where $\mathbf{k_1}$ and $\mathbf{k_2}$ are the propagation vectors for both refracted waves and θ_1 and θ_2 are their respective angles between the normal of the crystal surface.

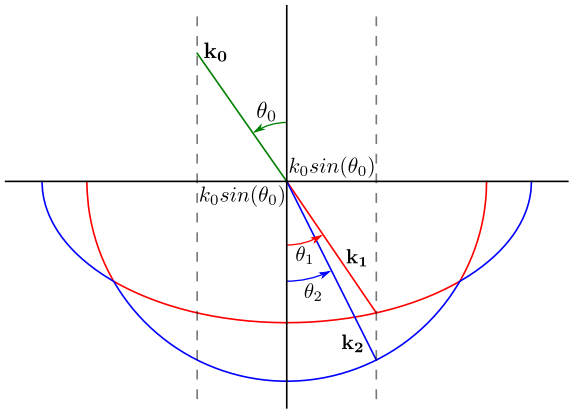

Figure 2.6: Double refraction for a biaxial crystal, where $n_x < n_y < n_z$, with an incident beam in the zx plane.

For an isotropic crystal we know that our normal shell consists of two overlapping spheres, so the values of $\mathbf{k_1}$ and $\mathbf{k_2}$ not only are going to equal each other, as they will not depend on the direction of propagation, however this will not be true for anisotropic media, thus resulting in a double refraction of light.

For an uniaxial crystal, one of the shells of the normal surface is always a sphere, so one of the solutions for the refracted waves will not depend on its direction of propagation, just like on an isotropic crystal, so for a given incident wave we can split this wave in the sum of two other waves, where one of these waves will have a parallel polarization with regards the optical axis of the crystal and the other one a perpendicular polarization, when refracted, the perpendicular component will follow Snell's law, and the refractive index for this refraction is called the ordinary refractive index (n_o), while the other refracted (or extraordinary ray) will not follow Snell's law. So for the ordinary ray we get:

$$n_i sin(\theta_0) = n_o sin(\theta_1) \tag{2.3.44}$$

Where n_i is the refractive index of the medium from the wave came before our crystal (usually 1 since its the air's refractive index).

2.4 Non-Linear Optics

Throughout this chapter all media were assumed to respond linearly to a electromagnetic field, however this assumption may not be valid for all crystals, so when exposed to an electromagnetic field, the induced polarization on the medium can be expressed in Taylor series, where the higher order terms will be responsible for any non-linear behavior. This non-linear behavior predominantly arises when the applied electric field is strong when compared to the atomic bonds of the crystal.

Let us then consider the polarization vector, where the ith component of this vector is given as:

$$P_i = \sum_{j=1}^{3} \varepsilon_0 \chi_{ij}^{(1)} E_j + \sum_{j=1}^{3}\sum_{k=1}^{3} \varepsilon_0 \chi_{ijk}^{(2)} E_j E_k + \sum_{j=1}^{3}\sum_{k=1}^{3}\sum_{l=1}^{3} \varepsilon_0 \chi_{ijkl}^{(3)} E_j E_k E_l + ... \tag{2.4.1}$$

In order to allow a more compact notation this same polarization component can be written as:

$$P_i = \varepsilon_0 \chi_{ij}^{(1)} E_j + \varepsilon_0 \chi_{ijk}^{(2)} E_j E_k + \varepsilon_0 \chi_{ijkl}^{(3)} E_j E_k E_l + ... \tag{2.4.2}$$

So looking at this equation, it can be seen that there are several non-linear coefficients, and while the third order coefficient $\chi_{ijkl}^{(3)}$ is always present for any material (although since its a higher order term its values can be really small for some materials, so that these materials can be studied as if they behaved linearly), while the second order term depending on the symmetry of the crystal may be zero, for instance centrosymmetric crystals will always have a zero second order non-linear coefficient.

Let us assume a given crystal with a centrosymmetric structure, if this same crystal is exposed by an electromagnetic wave, then inversion of symmetry must be observed (otherwise it wouldn't be a centrosymmetric crystal). Then $\mathbf{P}$ and $\mathbf{E}$ can be replaced in Eq.2.4.2 with $-\mathbf{P}$ and $-\mathbf{E}$ respectively, and the ith component must also verify the following equation:

$$-P_i = \varepsilon_0 \chi_{ij}^{(1)} (-E_j) + \varepsilon_0 \chi_{ijk}^{(2)} (-E_j)(-E_k) + \varepsilon_0 \chi_{ijkl}^{(3)} (-E_j)(-E_k)(-E_l) + ... \tag{2.4.3}$$

$$= -\varepsilon_0 \chi_{ij}^{(1)} E_j + \varepsilon_0 \chi_{ijk}^{(2)} E_j E_k - \varepsilon_0 \chi_{ijkl}^{(3)} E_j E_k E_l + ... \tag{2.4.4}$$

Comparing Eq.2.4.2 and Eq.2.4.4 we then get:

$$\varepsilon_0 \chi_{ijk}^{(2)} E_j E_k = -\varepsilon_0 \chi_{ijk}^{(2)} E_j E_k \tag{2.4.5}$$

Since **E** is an arbitrary vector and ε_0 a constant, this means that the only way for the same equation to be held true is if the second order coefficient is admitted to be zero, in fact if we were to consider a fourth order term the same would also equal zero for centrosymmetric crystals, so all even parity coefficients would equal zero for this kind of crystals. However this theory only applies if we only consider dipolar electrical interactions, discarding any dipolar magnetic, or any quadrupolar or higher order electrical interaction (which is the case in this analysis).

The second order non-linear behaviour of a crystal will be responsible for effects such as Second Harmonic Generation (SHG), frequency summation and differentiation, optical rectification, parametric amplification and oscillation [5]. Third order non-linear effects include Raman and Brillouin scattering, third harmonic generation, self focusing, and optical phase conjugation [5]. In this chapter we will only focus second order non-linear interactions, so third order interaction or higher order interactions will not be considered. Let us now assume that the polarization of a given crystal is given by only the first two terms of our Taylor expansion.

$$P_i = \varepsilon_0 \chi^{(1)}_{ij} E_j + \varepsilon_0 \chi^{(2)}_{ijk} E_j E_k \tag{2.4.6}$$

One important side note that must be taken care of, is the use of complex notation for describing the electric field, since the product of two complex numbers alter the real part. So for instance the jth component of the electric field could be written as:

$$E_j(t) = Re(E_{j0} e^{i(\mathbf{k}\cdot\mathbf{r}-\omega t)}) = \frac{1}{2}(E_{j0} e^{i(\mathbf{k}\cdot\mathbf{r}-\omega t)} + c.c.) \tag{2.4.7}$$

Where *c.c.* stands for the complex conjugate of the electric field equation. Lets consider that our electric field can be expressed just as a scalar quantity, then we can define our electric field as:

$$E = E_0 cos(\mathbf{k}\cdot\mathbf{r} - \omega t) \tag{2.4.8}$$

Then the polarization would be given as:

$$P = \varepsilon_0 \chi^{(1)} E_0 cos(\mathbf{k}\cdot\mathbf{r} - \omega t) + \varepsilon_0 \chi^{(2)} E_0^2 cos^2(\mathbf{k}\cdot\mathbf{r} - \omega t) \tag{2.4.9}$$

$$= \varepsilon_0 \chi^{(1)} E_0 cos(\mathbf{k}\cdot\mathbf{r} - \omega t) + \frac{1}{2}\varepsilon_0 \chi^{(2)} E_0^2 (1 + cos(2(\mathbf{k}\cdot\mathbf{r} - \omega t))) \tag{2.4.10}$$

Now from this polarization two important aspects appear, the first one is the fact that a time independent term appears, this term leads to the accumulation of charges on the surface of the crystal, and appears due the fact that the bound electrons of the crystal are no longer bound by a harmonic potential, so the average value of the polarization is

a non-zero value, thus the crystal will have a preferential direction for its polarization vector. The materials that exhibit this behaviour are said to have a quasi-DC polarization, and this phenomena is commonly referred as optical rectification. The second aspect is the fact that a harmonic electric dipole moment component with frequency 2ω appears, so the oscillating dipoles not only are going to have a preferential direction because of the time-independent term, their oscillations will be given as a superposition of two harmonic components with frequencies ω and 2ω.

Since an oscillating electric dipole emits electromagnetic radiation, this crystal will emit radiation with both frequencies ω and 2ω, so in fact a non-linear crystal can be used to generate an output beam of light with a frequency higher than its input beam, in this case twice the frequency to be precise, thus this phenomena is called second harmonic generation.

Let us then consider an electromagnetic wave which consists on the superposition of two waves of frequencies ω_1 and ω_2 respectively. Then our electric field can be written as:

$$E = E_1 cos(\mathbf{k_1} \cdot \mathbf{r} - \omega_1 t) + E_2 cos(\mathbf{k_2} \cdot \mathbf{r} - \omega_2 t) \tag{2.4.11}$$

Then our second order polarization term is given as:

$$P^{(2)} = \varepsilon_0 \chi^{(2)} (E_1 cos(\mathbf{k_1} \cdot \mathbf{r} - \omega_1 t) + E_2 cos(\mathbf{k_2} \cdot \mathbf{r} - \omega_2 t))^2 \tag{2.4.12}$$

$$= \varepsilon_0 \chi^{(2)} (E_1^2 cos^2(\mathbf{k_1} \cdot \mathbf{r} - \omega_1 t) + E_1 E_2 cos(\mathbf{k_1} \cdot \mathbf{r} - \omega_1 t) cos(\mathbf{k_1} \cdot \mathbf{r} - \omega_2 t) + E_2^2 cos(\mathbf{k_2} \cdot \mathbf{r} - \omega_2 t)) \tag{2.4.13}$$

Expanding further this equation, similarly like the previous one, a time independent term will arise and two harmonic terms with frequencies $2\omega_1$ and $2\omega_2$ respectively will also appear, however a harmonic term with frequency $\omega_1 + \omega_2$ will also appear which in this case its known as a phenomena known as frequency summation. Similarly if we take an electric field defined as:

$$E = E_1 cos(\mathbf{k_1} \cdot \mathbf{r} - \omega_1 t) - E_2 cos(\mathbf{k_2} \cdot \mathbf{r} - \omega_2 t) \tag{2.4.14}$$

Then a harmonic term with frequency $\omega_1 - \omega_2$ will appear, and in this case the phenomena is know as frequency differentiation. So in order for frequency summation or differentiation to be observed it is necessary to have at least two frequencies in our input beam, otherwise only second harmonic generation would be observed. However in order to have a high efficiency conversion for these non-linear effects, a set of phase matching conditions must be considered.

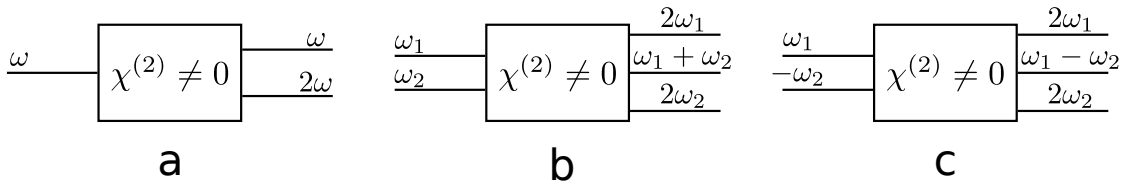

Figure 2.7: Non-linear effects observed when a crystal with a non centrosymmetric crystals is exposed to a beam with frequency (a) ω, (b) ω_1 and ω_2, and (c) ω_1 and -ω_2.

Let us take for another example an other electromagnetic wave, with its electric field defined as:

$$E = E_1 cos(\mathbf{k_1} \cdot \mathbf{r} - \omega t) + E_2 cos(\mathbf{k_2} \cdot \mathbf{r} - 2\omega t) \tag{2.4.15}$$

By replacing this electric field in the second order non-linear polarization equation we get five different terms. The first term is a time-independent term responsible for the optical rectification, while the other four terms are time dependent harmonic terms with frequencies ω, 2ω, 3ω and 4ω respectively. As previously stated the efficiency of these frequencies conversion is dependent on a set of phase matching conditions, however each frequency has its own phase matching conditions, that may or may not be the same for each frequency, thus while some terms might experience a high efficiency conversion other terms might not, thus the terms with negligible efficiency are often excluded.

We can rewrite the polarization as the sum of a linear and non-linear terms:

$$\mathbf{P} = \mathbf{P_L} + \mathbf{P_{NL}} = \varepsilon_0 \overline{\overline{\chi^{(1)}}} \mathbf{E} + \mathbf{P_{NL}} \tag{2.4.16}$$

Where the ith component of the non-linear polarization vector is given as:

$$(P_{NL})_i = \varepsilon_0 \chi^{(2)}_{ijk} E_j E_k \tag{2.4.17}$$

By replacing this non-linear polarization in Maxwell's equations, and if we assume there are no free charges or free currents in our material, we then get that:

$$\nabla \cdot \mathbf{E} = 0 \tag{2.4.18}$$

$$\nabla \cdot \mathbf{B} = 0 \tag{2.4.19}$$

$$\nabla \times \mathbf{E} = -\frac{\partial \mathbf{B}}{\partial t} \tag{2.4.20}$$

$$\nabla \times \mathbf{H} = \frac{\partial \mathbf{D}}{\partial t} = \frac{\partial}{\partial t}(\varepsilon_0 \mathbf{E} + \mathbf{P}) \tag{2.4.21}$$

To further simplify this relation, let us look at the following expression:

$$\nabla \times (\nabla \times \mathbf{E}) = \nabla(\nabla \cdot \mathbf{E}) - \nabla^2 \mathbf{E} \tag{2.4.22}$$

$$= -\nabla^2 \mathbf{E} \tag{2.4.23}$$

By replacing with our previous Maxwell's equations we get that:

$$\nabla \times \left(-\frac{\partial \mathbf{B}}{\partial t} \right) = -\Delta \mathbf{E} \tag{2.4.24}$$

$$\nabla^2 \mathbf{E} = \mu_0 \frac{\partial}{\partial t} (\nabla \times \mathbf{H}) \tag{2.4.25}$$

$$= \mu_0 \varepsilon_0 \left(\overline{\overline{1}} + \overline{\overline{\chi^{(1)}}} \right) \frac{\partial^2 \mathbf{E}}{\partial t^2} + \mu_0 \frac{\partial^2 \mathbf{P_{NL}}}{\partial t^2} \tag{2.4.26}$$

This condition must be met for both the waves with ω and 2ω frequencies.

$$\nabla^2 \mathbf{E}^{(\omega)} = \mu_0 \varepsilon_0 \left(\overline{\overline{1}} + \overline{\overline{\chi^{(1)}_{(\omega)}}} \right) \frac{\partial^2 \mathbf{E}^{(\omega)}}{\partial t^2} + \mu_0 \frac{\partial^2 \mathbf{P}^{(\omega)}_{\mathbf{NL}}}{\partial t^2} \tag{2.4.27}$$

$$\nabla^2 \mathbf{E}^{(2\omega)} = \mu_0 \varepsilon_0 \left(\overline{\overline{1}} + \overline{\overline{\chi^{(1)}_{(2\omega)}}} \right) \frac{\partial^2 \mathbf{E}^{(2\omega)}}{\partial t^2} + \mu_0 \frac{\partial^2 \mathbf{P}^{(2\omega)}_{\mathbf{NL}}}{\partial t^2} \tag{2.4.28}$$

This two equations dictate how the electromagnetic wave propagates in a non-linear media, however while in a linear media these two waves would propagate without interacting with each other, the non-linear polarization terms binds these two equations together, and these same non-linear polarization terms dictate how the two waves interact. A non-linear polarization term might lead to the generation of a different frequency, which would also need to satisfy this same conditions, thus these two set of equations need to be solved simultaneously.

Let us assume that both our waves at ω and 2ω frequencies travel along the z axis exclusively, then the electric field for these equations can be written as follows:

$$E^{(\omega)} = \frac{1}{2} \left(E_1 e^{i(k_1 z - \omega t)} + c.c. \right) \tag{2.4.29}$$

$$E^{(2\omega)} = \frac{1}{2} \left(E_2 e^{i(k_2 z - 2\omega t)} + c.c. \right) \tag{2.4.30}$$

So the total electric field on our crystal would be given as:

$$E = E^{(\omega)} + E^{(2\omega)} \tag{2.4.31}$$

Then the non-linear polarization term for our crystal would be given as:

$$P_{NL} = \frac{1}{4}\varepsilon_0 \chi^{(2)} \left(E_1 e^{i(k_1 z - \omega t)} + E_2 e^{i(k_2 z - 2\omega t)} + c.c. \right)^2 \tag{2.4.32}$$

By further expanding this non-linear polarization term, terms with frequencies ω and 2ω can be found, and they are given as follows:

$$P_{NL}^{(\omega)} = \frac{1}{2}\left(\varepsilon_0 \chi_{(\omega)}^{(2)} E_2 E_1^* e^{i((k_2 - k_1)z - \omega t)} + c.c. \right) \tag{2.4.33}$$

$$P_{NL}^{(2\omega)} = \frac{1}{4}\left(\varepsilon_0 \chi_{(2\omega)}^{(2)} E_1^2 e^{2i(k_1 z - \omega t)} + c.c. \right) \tag{2.4.34}$$

It is important to take notice on both E_1 and E_2 when dealing with these non-linear media, since both terms will also be functions of z, otherwise our non-linear polarization term would then equal to zero, and said crystal would be considered a linear medium. Lets us assume that for the electromagnetic wave $E^{(\omega)}$, E_1 is in fact independent of the z axis, then:

$$\frac{\partial^2 E^{(\omega)}}{\partial z^2} = -k_1^2 E^{(\omega)} = -\frac{k_1^2}{-\omega^2}\frac{\partial^2 E^{(\omega)}}{\partial t^2} = \frac{\omega^2}{c^2\omega^2}\varepsilon_r(\omega)\frac{\partial^2 E^{(\omega)}}{\partial t^2} \tag{2.4.35}$$

$$= \mu_0 \varepsilon_0 \left(1 + \chi^{(1)}(\omega)\right)\frac{\partial^2 E^{(\omega)}}{\partial t^2} \tag{2.4.36}$$

The only way for $E^{(\omega)}$ to satisfy Eq.2.4.27 would only be if its non-linear term $P_{NL}^{(\omega)}$ equals to zero, thus if our crystal is said to be a non-linear medium, then E_1 must be a function of z, otherwise the wave equation conditions for our crystal would not be met. So in order to fully study any non-linear process in our medium it is then necessary to obtain an expression for both $\frac{\partial^2 E^{(\omega)}}{\partial z^2}$ and $\frac{\partial^2 E^{(2\omega)}}{\partial z^2}$, however in some cases where the efficiency of the second harmonic signal is very small compared to the ω frequency signal, then $\frac{\partial^2 E^{(\omega)}}{\partial z^2}$ can be considered as constant to further simplify calculations.

Expanding these two partial derivatives we then get:

$$\frac{\partial^2 E^{(\omega)}}{\partial z^2} = \left(\frac{\partial^2 E_1}{\partial z^2} + \frac{2ik_1}{E_1}\frac{\partial E_1}{\partial z} + k_1^2\right)E^{(\omega)} = \left(\frac{\partial^2 E_1}{\partial z^2} + 2ik_1\frac{\partial E_1}{\partial z}\right)E^{(\omega)} + \frac{n_\omega^2}{c^2}\frac{\partial^2 E^{(\omega)}}{\partial t^2} \tag{2.4.37}$$

$$\frac{\partial^2 E^{(2\omega)}}{\partial z^2} = \left(\frac{\partial^2 E_2}{\partial z^2} + \frac{2ik_2}{E_2}\frac{\partial E_2}{\partial z} + k_2^2\right)E^{(2\omega)} = \left(\frac{\partial^2 E_2}{\partial z^2} + 2ik_2\frac{\partial E_2}{\partial z}\right)E^{(2\omega)} + \frac{n_{2\omega}^2}{c^2}\frac{\partial^2 E^{(2\omega)}}{\partial t^2} \tag{2.4.38}$$

By comparing this expressions with Eqs.2.4.27 and 2.4.28, we get:

$$\left(\frac{\partial^2 E_1}{\partial z^2} + 2ik_1\frac{\partial E_1}{\partial z}\right)E^{(\omega)} = \mu_0\frac{\partial^2 P_{NL}^{(\omega)}}{\partial t^2} \tag{2.4.39}$$

$$\left(\frac{\partial^2 E_2}{\partial z^2} + 2ik_2\frac{\partial E_2}{\partial z}\right)E^{(2\omega)} = \mu_0\frac{\partial^2 P_{NL}^{(2\omega)}}{\partial t^2} \tag{2.4.40}$$

If we assume that both E_1 and E_2 have a small variation on z so that:

$$\frac{\partial^2 E_1}{\partial z^2} \ll k_1 \frac{\partial E_1}{\partial z} \tag{2.4.41}$$

$$\frac{\partial^2 E_2}{\partial z^2} \ll k_2 \frac{\partial E_2}{\partial z} \tag{2.4.42}$$

Then the following approximations can be considered:

$$2ik_1 \frac{\partial E_1}{\partial z} E^{(\omega)} = \mu_0 \frac{\partial^2 P_{NL}^{(\omega)}}{\partial t^2} \tag{2.4.43}$$

$$2ik_2 \frac{\partial E_2}{\partial z} E^{(2\omega)} = \mu_0 \frac{\partial^2 P_{NL}^{(2\omega)}}{\partial t^2} \tag{2.4.44}$$

By simplifying these equations we then get:

$$\frac{\partial E_1}{\partial z} = i \frac{\omega}{2cn_\omega} \chi^{(2)}_{(\omega)} E_2 E_1^* e^{i\Delta k z} + c.c. \tag{2.4.45}$$

$$\frac{\partial E_2}{\partial z} = i \frac{\omega}{2cn_{2\omega}} \chi^{(2)}_{(2\omega)} E_1^2 e^{-i\Delta k z} + c.c. \tag{2.4.46}$$

where

$$\Delta k = k_2 - 2k_1 \tag{2.4.47}$$

Now if we assume that our input source only emits radiation with frequency ω, this means that our non-linear polarization term for 2ω must be our source of radiation at 2ω frequency.

By looking at this non-linear polarization term, it is possible to see that in fact it is also a traveling wave, thus it must also posses its own phase velocity, which is given as:

$$v_p\left(P_{NL}^{(2\omega)}\right) = \frac{2\omega}{2k_1} \tag{2.4.48}$$

Then this phase velocity should be equal to the phase velocity of $E^{(2\omega)}$

$$v_p\left(E^{(2\omega)}\right) = \frac{2\omega}{k_2} \implies \frac{2\omega}{k_2} = \frac{2\omega}{2k_1} \tag{2.4.49}$$

$$\implies \Delta k = 0 \tag{2.4.50}$$

This condition is called the phase matching condition, and it ensures that the interference between $E^{(2\omega)}$ and $P_{NL}^{2\omega}$ is always constructive, so when $\Delta k = 0$ then the efficiency of conversion from ω to 2ω is at its maximum.

Chapter 3

GaN Properties

Three different crystal structures can be achieved with GaN, and these are rocksalt, zincblende and wurtzite structures, however only the later one is stable for GaN, the other two structures are meta-stable structures which means that these structures will not be found in GaN films grown in stable conditions [6]. This wurtzite structure is asymmetrical on the c direction, which will lead to a polarization on the crystal since both the gallium and nitrogen atoms tend to form ionic bonds, this polarization of the material is called spontaneous polarization. This polarization can be highly increased by moving the atoms from their equilibrium position, this piezoelectric polarization can be achieved through a misfit of ether in the lattice or thermal expansion coefficient mismatch in hetero-structures or by adding impurities on the crystal [6].

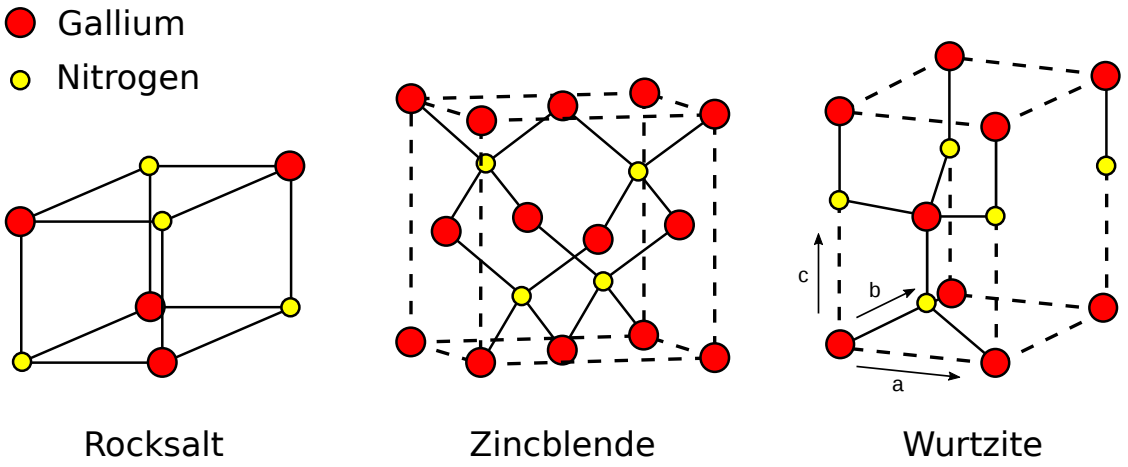

Figure 3.1: The different crystal structures a GaN crystal can display.

3.1 Optical Properties

GaN possess a wide bandgap of 3.4 eV, and unlike silicon, it is a direct bandgap semiconductor, which is a desirable trait for the semiconductor industry.

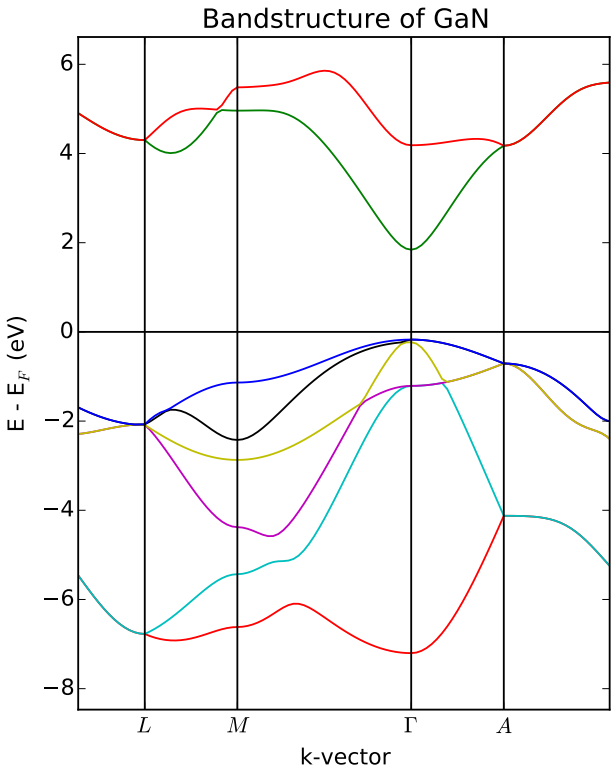

Figure 3.2: Simulated band structure of GaN.

For wurtzite GaN there are four possible optical vibrational modes, these are A_1, E_1, $2E_2$ and $2B_2$. While both A_1 and E_1 are polar modes (thus they are both Raman and Infrared (IR) active modes), E_1 modes are non-polar modes thus only Raman active, B_1 modes however are silent modes and aren't either Raman or IR active [7, 8].

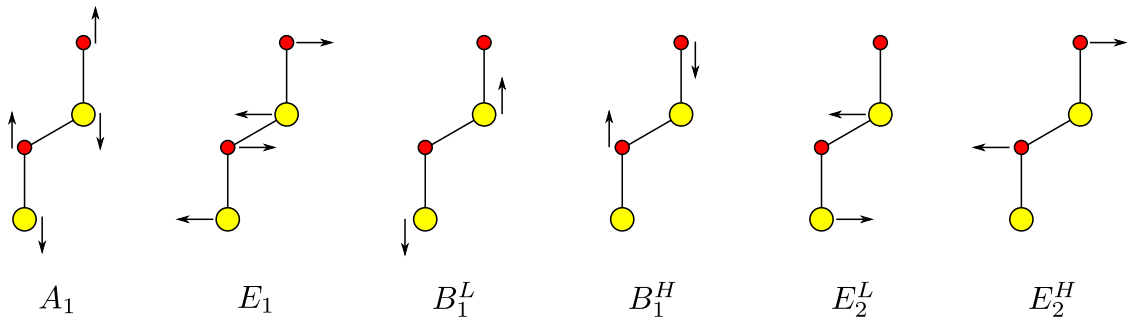

Figure 3.3: Vibrational modes for wurtzite GaN.

Both polar modes can be either transversely or longitudinally polarized (TO and LO respectively), and for each polarization state a different energy is associated. However depending on the scattering geometry only some of these vibrational modes are visible due to selection rules, which are described on the following table:

Mode	Configurations	Wavenumber (cm^{-1})
$A_1(TO)$	$x(y,y)\overline{x}$, $x(z,z)\overline{x}$, $y(x,x)\overline{y}$, $y(z,z)\overline{y}$	531.8
$A_1(LO)$	$z(x,x)\overline{z}$, $z(y,y)\overline{z}$	734.0
$E_1(TO)$	$x(z,y)\overline{x}$, $x(y,z)y$	558.8
$E_1(LO)$	$x(y,z)y$	741.0
E_2^H	$z(x,x)\overline{z}$, $z(x,y)\overline{z}$, $x(y,y)\overline{x}$	567.6
E_2^L	$z(x,x)\overline{z}$, $z(x,y)\overline{z}$, $x(y,y)\overline{x}$	144.0

Table 3.1: Raman active vibrational modes for wurtzite GaN [8].

Thus for incident light on the (0001) plane of the wurtzite crystal plane, only the vibrational modes $A_1(LO)$ and both E_2 modes should be observed. The configuration modes seen in Table 3.1, are expressed with Porto's notation, where the first term is the incidence propagation axis, the second term is the polarizer's axis, the third term is the analyzer's axis, and the fourth term is the axis at which the scattered light propagates.

3.2 Non-linear Properties

Wurtzite GaN is a non-centrosymmetric crystal, thus second order effects such as second harmonic generation, frequency sum and differentiation, and optical rectification should be observable. For wurtzite GaN the only independent non-vanishing elements of the second order susceptibility tensor are $\chi^{(2)}_{zxx}$, $\chi^{(2)}_{zyy}$, $\chi^{(2)}_{zzz}$, $\chi^{(2)}_{xzx}$ and $\chi^{(2)}_{yzy}$,additionally for an ideally perfect wurtzite structure [9]:

$$\chi^{(2)}_{zxx} = \chi^{(2)}_{zyy} = \chi^{(2)}_{xzx} = \chi^{(2)}_{yzy}$$
$$\chi^{(2)}_{zxx} = -\frac{\chi^{(2)}_{zzz}}{2}$$

Some experimental values for these non-linear susceptibilities are [10]:

$$\left|\chi^{(2)}_{zxx}\right| = 14.7 \pm 0.2 pm/V \quad \left|\chi^{(2)}_{xzx}\right| = 14.4 \pm 0.2 pm/V \quad \left|\chi^{(2)}_{zzz}\right| = 29.7 \pm 0.7 pm/V$$

Since these values are relatively low, a very low efficiency should be expected for a SHG signal, thus for thin GaN crystals the SHG process can be interpreted as having an undepleted source, or in other words, the intensity of the fundamental frequency can be seen as a constant.

3.3 Thermal and Mechanical Properties

GaN is not only desired in the semiconductor industry for its wide energy bandgap, but also for its good thermal stability which allows it to operate at higher temperatures and high power demands. As previously mentioned, GaN crystals are mostly found in wurtzite crystalline structures.

Property	Value	Range
Lattice constant (nm)	a = 0.318843	300K
	c = 0.518525	
Thermal expansion coefficient (K^{-1})	$3.17 \times 10^{-6} \parallel c-axis$	300-700K
	$7.75 \times 10^{-6} \parallel c-axis$	700-900K
	$5.59 \times 10^{-6} \parallel a-axis$	300-900K
Thermal conductivity (W $cm^{-1}K^{-1}$)	2.1	300K

Table 3.2: Thermal and mechanical properties of GaN [11, 12].

Chapter 4

Epitaxial Growth of GaN

In this chapter a brief introduction to the three most common techniques of epitaxial growth employed on GaN devices will be discussed, their advantages and disadvantages, as well the role that the substrate has when growing these films and the required treatment the same should undergo in order to grow good quality GaN films.

4.1 Substrate

GaN devices are highly dependent on the properties and quality of the substrate on which they are grown, properties such as lattice constants, thermal constants, roughness, terrace width, wetting behavior, surface temperature, both thermal and electrical conductivity, cleavability, price and availability [2, 12], at the same time the substrate can undergo a thermal annealing process to improve its quality and in order to overcome some issues such as lattice mismatches, a buffer layer between the GaN layer and the substrate can be deposited or by nitriding the substrate to improve the crystallinity of the GaN layer [13]. Unlike most other semiconductor materials, GaN is mostly grown on a foreign substrate, or in other words heteroepitaxial films [12]. GaN films are commonly grown in either silicon carbide, sapphire or more recently silicon substrates since bulk GaN can be difficult to obtain. Some of the criteria for choosing a substrate are:

- Lateral mismatch (a-lattice constant), a severe lateral mismatch will lead to high dislocation densities, leading to high device leakage currents and reducing the minority carriers lifetime, also reducing the thermal conductivity of the deposited layer and increasing the diffusion of impurities along the threading dislocations causing a non-uniform distribution of the impurities on the layer [12, 14];

- Vertical mismatch (c-lattice constant), this mismatch can lead to inversion domain boundaries, a high density of these defects leads to a smaller Young coefficient of the film, thus reducing the layer's stiffness making it more prone to cracking [15], antiphase boundaries are also related to these kind of mismatches [12] which can lead to an ansitropic crystal structure of the GaN layer [16, 17];

- Thermal conductivity, low thermal conductivity which can lead to overheating issues due to a low thermal dissipation;

- Difference in the chemical composition between the substrate and the epitaxial film, for instance when growing GaN on a Si substrate due to the chemical incompatibility of GaN and Si can lead to a melt-back of the GaN layer;

- Thermal expansion coefficients, if these coefficients greatly differ from the deposited layer, this could lead to cracks in the GaN layer;

- Availability and prize

4.1.1 SiC

Silicon carbide presents the best characteristics for GaN growth when compared to other materials other than GaN itself. SiC has a wide variety of polytipes, however only three of these are of our interest, 3C, 4H and 6H, both 4H and 6H exhibit low lattice constant mismatch of ~3%, all three forms possess a relatively high thermal conductivity and are good electrical conductors [2, 18]. The fact that SiC bulk layers are good electrical conductors allows for an easier design of electronic devices, however SiC substrates can be quite expensive as they are difficult to produce, for instance a 4 inch high quality wafer can cost around 3000$ [14].

Property	Polytype	Value
Lattice constant (nm)	3C	a = 0.43596
	4H	a = 0.30730
		c = 1.0053
	6H	a = 0.30806
		c = 1.51173
Thermal expansion coefficient (K^{-1})	3C	3.9×10^{-6}
	6H	4.46^{-6} a-axis
		4.16^{-6} c-axis
Thermal conductivity (W $cm^{-1}K^{-1}$)	3C	3.6
	4H	3.7
	6H	4.9

Table 4.1: Structural and thermal properties of SiC at room temperature [12].

4.1.2 Sapphire

Sapphire remains a very common substrate choice for GaN epitaxial growth. It has a lattice mismatch of ~15% which can lead to a high defect dislocation density [12], another problem with sapphire is that it possess a higher expansion coefficient than GaN and its thermal conductivity is rather poor compared to other substrate materials, however compared to SiC, sapphire is a more commercially available and cheaper than the latter.

Property	Value	Range
Lattice constant (nm)	a = 0.4765	20°C
	c = 1.2982	
Thermal expansion coefficients (K^{-1})	6.66×10^{-6} $\parallel$ c – axis	20 – 50°C
	9.03×10^{-6} $\parallel$ c – axis	20 – 1000°C
	5.0×10^{-6} $\perp$ c – axis	20 – 1000°C
Thermal conductivity (W $cm^{-1}K^{-1}$)	0.23 $\parallel$ c – axis	296K
	0.25 $\parallel$ a – axis	299K

Table 4.2: Structural and thermal properties of Sapphire [12].

4.1.3 Si

Silicon is a very desired material choice for growing GaN on due to its excellent physical properties, high availability and competitive price for mostly perfect and smooth surfaces. However growing GaN on silicon can prove to be a challenge since the lattice mismatch between silicon and GaN is roughly 17%, and the thermal expansion coefficient of Si is more than two times lower than of GaN, which can lead to the cracking of the deposited layers when cooling down. These inconvenients are solved by using buffer layers made of materials such as AlN [14]. Another problem with Si substrates is its tendency to form amorphous silicon nitride when exposed to nitrogen sources [12], which are required to produce GaN.

Property	Value
Lattice constant (nm)	0.543102
Thermal expansion coefficient (K^{-1})	2.616
Thermal conductivity (W $cm^{-1}K^{-1}$)	1.56

Table 4.3: Structural and thermal properties of Si at room temperature [12].

4.2 Molecular Beam Epitaxy

Molecular Beam Epitaxy (MBE) is a growing technique for thin films mostly used for compound semiconductors [19]. It consists on growing a thin film on top of a crystalline substrate with a very clean and defect free surface through a beam of molecules or atoms

produced on an effusion cell. Contrary to any vapour phase epitaxy this technique does not require a high pressure, in fact a very low pressure is required, therefore this growing method must always be accompanied with a set of Ultra High Vacuum (UHV) chambers and pumps to allow the required low pressure, this low pressure is needed to ensure a clean surface of the substrate before any growth, ensure that the films grown are chemically as pure as possible and to allow the molecular beam a high mean free path before hitting the substrate (otherwise the growth rate would be low).

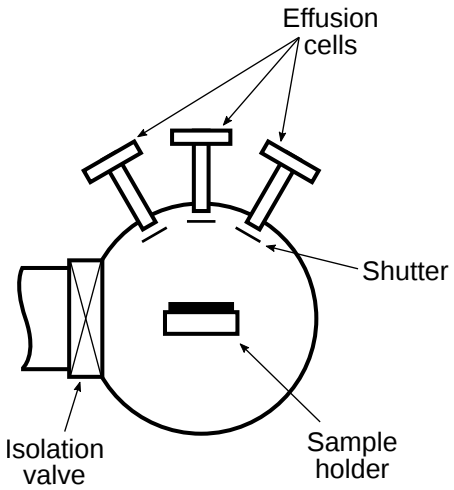

Figure 4.1: Some of the essential components that can be found on any MBE system.

As shown on the picture, a MBE system may contain more than one effusion cell, the amount of these cells will depend on the desired film to be grown. The most common effusion cell used in these systems are Knudsen cells, these cells rely on low partial pressure elements as a source for evaporation. These effusion cells evaporate the source contained in a crucible often made of Pyrolytic Boron Nitride (PBN), quartz, tungsten or graphite [20], the material chosen for the crucible will dependent on what element source will be evaporated as well as the temperature at which the same source element will be evaporated. PBN crucibles are the industry standard for both GaN and GaAs crystal production [21], some of the properties that make PBN an attractive choice for these particular setups are [20, 21]:

- Good thermal conductivity and stability
- High insulation resistance and dielectric strength over wide temperature range
- Material's high purity and low outgassing
- Non-toxic and non-wetting
- Non-reactive to most other compounds

- Withstands high temperatures and rapid cooling
- Long lifetime

These effusion cells rely on thermal evaporation of the source material, and for this a set of heating filaments, often made of tantalum, are used close to the crucible, so that when a current is applied the source material will be forced to effuse through a small hole above the crucible.

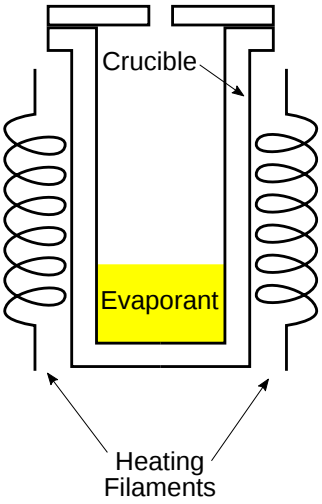

Figure 4.2: Simplified scheme of a Knudsen cell.

In theory the rate of evaporation is higher when the number of molecules evaporated correspond to the required amount of molecules to keep the vapor pressure while none of these evaporated molecules return [22]. In order to achieve this ideal rate of evaporation pressure on the chamber must equal to zero, therefore the lower the pressure of the chamber the higher the rate of evaporation, where the rate of evaporation is given by:

$$\Phi_e = \frac{\alpha_e N_A (P_e - P_h)}{\sqrt{2\pi MRT}} \tag{4.2.1}$$

Looking at the expression it can seen that the maximum rate of evaporation will be achieved when the chamber pressure P_h equals to zero and when the evaporation coefficient equals to one, since the same can only hold values from zero to one, where M is the atomic weight of the evaporant, R is the ideal gas constant, N_A is the Avogadro number and T is the temperature and P_e is the vapor pressure.

The vapor pressure of the element can be found theoretically through the Clausius-Clapyeron equation, although empirical formulas and experimental data are used to find these vapor pressures [23]. The same equation is given as:

$$\frac{dP}{dT} = \frac{\Delta H(T)}{T\Delta V} \tag{4.2.2}$$

If we assume the gas to be an ideal gas, then solving the same equation yields:

$$ln\left(\frac{P}{P_0}\right) = \frac{H_e}{R}\left(\frac{1}{T_0} - \frac{1}{T}\right) \tag{4.2.3}$$

Where ΔH_e is the molar enthalpy of evaporation, and P_0 and T_0 are the pressure and temperature of a reference point.

If the pressure is expressed in Torr, then Eq.4.2.1 can be further simplified, also allowing to have a simplified equation for the mass evaporation rate Γ_e as follows:

$$\Phi_e \approx 3.513 \times 10^{22} \frac{P_e}{\sqrt{MT}} \quad [molecules\ cm^{-2}\ s^{-1}] \tag{4.2.4}$$

$$\Gamma_e = \Phi_e \frac{M}{N_A} \approx 5.834 \times 10^{-2} \sqrt{M/T}\ P_e \quad [g\ cm^{-2}\ s^{-1}] \tag{4.2.5}$$

However not all of this evaporated mass will eventually be deposited on the substrate, mainly because of the geometry between the substrate and the effusive source. First we define the total evaporated mass M_e as:

$$M_e = \int_0^t \int_{A_e} \Gamma_e\ dA_e dt \tag{4.2.6}$$

Where A_e is the surface area of the source from where the evaporated particles leave. Depending on the size of A_e, two cases will occur, the source will either be a point source or a surface source, and depending on either case the deposited mass per unit of area will have a different expression.

In the first case,a point source, the solid angle Ω is said to be equal to 4π since the source emits in all directions, this type of geometry is a simpler geometry on which only one angle must be taken into account to determine the deposited mass per unit of area.

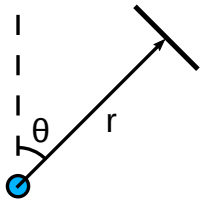

Figure 4.3: Deposition on a target substrate with a point source geometry.

Where the deposited mass per unit of area is given by:

$$\frac{dM_s}{dA_s} = \frac{M_e cos\theta}{\Omega r^2} = \frac{M_e cos\theta}{4\pi r^2} \tag{4.2.7}$$

In second case, a surface source, the solid angle is then said to equal 2π in contrast of the point source, since these sources will only emit in its upward face, also contrary to the later two angles must be taken into account, the second being the angle of inclination of the source surface.

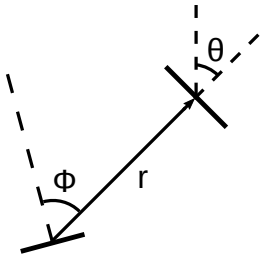

Figure 4.4: Deposition on a target substrate with a surface source geometry.

Where the deposited mass per unit of area is given by:

$$\frac{dM_s}{dA_s} = \frac{M_e cos\phi\ cos\theta}{\Omega r^2} = \frac{M_e cos\phi\ cos\theta}{2\pi r^2} \tag{4.2.8}$$

This model however assumes that the shape of the vapor cloud to be spherical. Nowadays deep narrow crucibles are used that allow the shape vapor cloud to a lobed shape, where the narrower the crucible is, the narrower the vapor cloud get, allowing for a more focused beam, where the deposited mass per area for these narrower crucibles is given by:

$$\frac{dM_s}{dA_s} = \frac{M_e(n+1)cos^n\phi\ cos\theta}{2\pi r^2}, \quad n \geq 0 \tag{4.2.9}$$

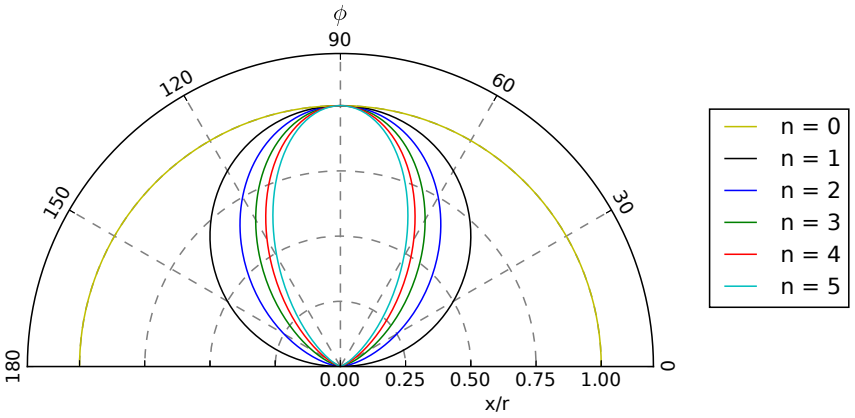

Figure 4.5: Different shapes of the vapor cloud for different n values.

From Fig.4.5 it is possible to see that for higher values of n, the vapor cloud becomes more directed, since n is related on how deep and narrow the crucible is, the deeper and narrower the crucible gets, the more directed the beam becomes, allowing for a smaller contamination of the UHV chamber and higher deposition rates.

Another important aspect of thin films deposition is the uniformity of the deposited layer, many industry applications rely on heavily uniform layers. The film density can be obtained through the following expression:

$$d = \frac{1}{\rho}\frac{dM_s}{dA_s} \tag{4.2.10}$$

Where ρ is the volumetric mass of the deposited material. However through Eqs.4.2.7, 4.2.8 and 4.2.9 we know that the angle of incidence of the beam will affect the deposition rate, and the maximum height will be when ϕ is 90°.

4.3 Metalorganic Chemical Vapour Deposition

Metalorganic Chemical Vapour Deposition (MOCVD) is a type of chemical vapor deposition technique that uses a metalorganic compound as a precursor for the group III element, in the case of GaN growth Trimethylgallium ($Ga(CH_3)_3$) is used.

The precursor needs to be a volatile compound, otherwise it becomes harder to allow a good flow throughout the reactor, thus allowing for faster deposition rates and more uniform growth rates.

There are several different geometries for MOCVD reactors, however all of them are either a vertical geometry or a horizontal geometry, depending on whether the flow is parallel to the wafer (horizontal geometry) or perpendicular (vertical geometry). Each geometry has its advantages and disadvantages however depending on what it to grown, one might perform better than the other.

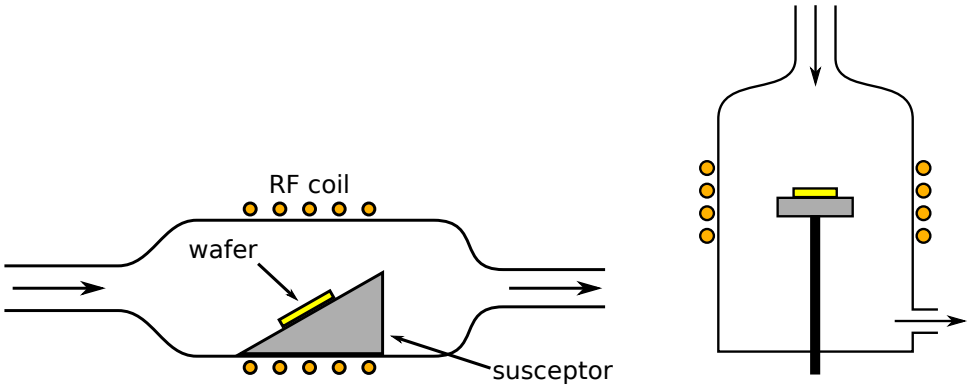

(a) Horizontal Geometry (b) Vertical Geometry

Figure 4.6: Schematics of two possible geometries for a MOCVD reactor.

The susceptor, usually made of graphite, is responsible for heating the substrate by converting an electromagnetic field into heat, in this case the field generated by the RF coil when passing a current through it, thus this susceptor needs to be a good thermal conductor.

All the by-products and the remaining unreacted reagents are to be expelled through the exhaust, however before releasing them to the atmosphere the same need to be filtered since they may contain toxic substances, thus the exhaust of the reactor is connected to a scrubber, which removes the toxicity of the by-products and then releases them to the atmosphere.

MOCVD reactors are usually made of quartz or other special ceramic or glasses, additionally the susceptor must be made of a material that is resistant to the metalorganic precursor used, otherwise it can get damaged and most of this metalorganic gas would end up being wasted. Another important aspect when designing a MOCVD reactor is the fact that some of the reagents used might be more reactive than others, thus if the inlet pipe for this particular reagent is too far from the wafer a lot of parasitic nucleation will occur, however if the inlet pipe for this particular reagent is positioned closer to the wafer then this side effect can be highly reduced.

High of low pressure MOCVD can be done, however while the deposition rate at atmospheric pressure or lower might be lower, some other advantages arise from using a lower pressure, advantages such as:

- Lowering the parasitic nucleation;
- Lowering the out-diffusion and auto-doping of the layers;
- Sharper layers for hetero-junctions;
- Lower temperatures required;
- Better homogeneity and uniformity of the deposited layers;
- Reduction of memory effects in the reactor

In order to grow uniform layers a laminar flow is required, this kind of flow is achieved when the viscous forces of the gas outnumber the inertial forces, in other words, for a laminar flow a relatively small Reynolds number is required, this coefficient is an adimensional quantity that provides the ratio between the inertial forces and the viscous forces (for most Chemical Vapour Deposition (CVD) reactors $Re < 100$ [24]), where the Reynolds number is given as:

$$Re = \frac{\rho v D}{\mu} \tag{4.3.1}$$

Where ρ is the density of the fluid, v is the average speed of the fluid, D is the diameter of the pipe where the gas flows and μ is the viscosity of the gas.

For a binary compound the growth rate is given as [25]:

$$g = \frac{MW_A}{k_B T d_A A_e} p_A F_A \tag{4.3.2}$$

Where p_A is the vapor pressure of the group III precursor gas, F_A is the flow rate, MW_A is the molecular weight, d_A is the solid density and A_e is the effective area. Growth rates for GaN through MOCVD are usually around $1 - 4\mu m/h$, however rates as high as $30\mu m/h$ have been reported [26].

4.4 Hydride Vapour Phase Epitaxy

Hydride Vapour Phase Epitaxy (HVPE) is a very similar technique to MOCVD since both are CVD techniques. HVPE reactors designs are also similar to MOCVD ones, both can be either vertically or horizontally oriented, and also a laminar flow is required. The main difference between HVPE and MOCVD, is the fact that different precursor gases are used, while for MOCVD a metalorganic gas was used, for HVPE a hydride is used, in the case of GaN growth, Hydrochloric acid (HCl) when heated in the presence of Gallium will form Gallium Chloride ($GaCl$), which then reacts with the group V precursor gas, in this case Ammonia (NH_3) forming Gallium Nitride on top of the wafer.

HVPE is usually employed for growing thick GaN bulk layers since it can reach very high deposition rates, up to hundreds of micrometers per hour [27]. These crystals are initially grown in a GaN template on either a Sapphire or SiC substrate and then removed by either reactive ion etching or by polishing [28].

Chapter 5

Characterization Techniques

In this chapter the basis of the four optical characterization techniques employed will be discussed. An optical characterization of the samples allowed to determine some of the physical characteristics of the samples in a non-destructive and contactless mode. Each technique has its merits and downfalls, and there is no single technique to provide all of the required information of the samples, thus multiple methods must be employed in order to characterize our samples.

5.1 Photoluminescence Spectroscopy

Photoluminescence (PL) spectroscopy is an optical characterization technique on which a sample is excited by a mostly monochromatic light source (in our case an Ar ion laser). When a molecule is excited by a photon, the same molecule undergoes through a series of electronic transitions before reaching its ground state, when doing so this same molecule can emit radiation on a given transition, this phenomena is called luminescence.

Luminescence is divided in two different categories, fluorescence and phosphorescence. When the excited electron of the molecule undergoes through a radiative allowed transition, the phenomena is called fluorescence, otherwise it is called phosphorescence. An allowed transition is said to be a transition where the total spin of the molecule is conserved. For instance when a molecule is in a singlet excited state an allowed transition would be to a lower level singlet state, so a transition to a triplet state would be a forbidden transition.

PL spectroscopy is widely used in the semiconductor industry for determining the badgap, presence of structural defects and possible presence of impurities. For this the sample must be excited with a monochromatic light source with a wavelength shorter than the one of the bandgap, causing the formation of holes and electrons in the valence

and conduction bands respectively, this will lead to the eventual recombination of the two when the sample goes through a relaxation process. This recombination can either be lead to the release of a photon (a direct bandgap semiconductor) or by the release of a phonon (indirect bandgap semiconductors).

The absorption or release of a phonon can be seen as the increase or decrease in momentum in the vibration of the interacting particles of the crystal. For a direct bandgap semiconductor when recombination occurs from an electron in the conduction band and a hole from the valence band occur, equates to the release of a phonon, since the lowest energy value from the conduction band and the highest energy value from the valence band, are not perfectly aligned in the momentum space, this non-radiative recombination will then to a loose of energy as the form of heat.

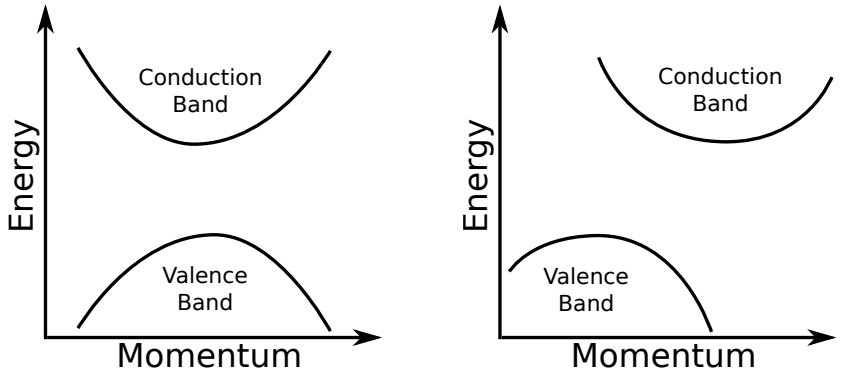

(a) Direct bandgap semiconductor (b) Indirect bandgap semiconductor

Figure 5.1: Possible energy bandgap diagrams for semiconductors.

However recombination from the conduction band and the valence band are on the only possible recombination processes, thus not necessarily the only source of luminescence for a semiconductor. Structural defects and the presence of impurities can be sources for radiative recombination. While these defects might always be seen as disadvantageous for a intrinsic semiconductor, impurities can deliberately be added to obtain higher wavelength peaks than the bandgap peak of the semiconductor. When p-type impurities are added, an acceptor level is created bellow the conduction band and above the valence band, otherwise, when n dopped, a donor level is created above the valence band and bellow the conduction band.

The addition of these impurities will always lead to a possible new peak at lower energies of the intrinsic bandgap, however some of the recombination from these donor and acceptor levels might not necessarily be radiative ones thus seen as defects rather than a dopant, leading to a decrease in luminescence efficiency and a increase in heat losses. The presence of luminescence defects in GaN samples is still an ongoing debate, however some recent studies have shown these luminescence to be related to transitions from either the conduction band or a shallow donor to a deep acceptor state [29].

5.2 Ellipsometry

As discussed in Chapter 2, a propagating electromagnetic wave has a direction of propagation perpendicular to both its electric field and magnetic field, and its polarization state is defined as the direction of the electric field. When a linearly polarized wave hits a surface, it can be polarized either in the plane of incidence or perpendicular to it, for the first case the wave is said to be p-polarized and for the later is said to be s-polarized.

However when hitting a interface between to different materials, part of the light will be reflected and part will be refracted, thought for each polarization state, the reflectivity of the material will be different.

Let us consider the following interface for a propagating wave:

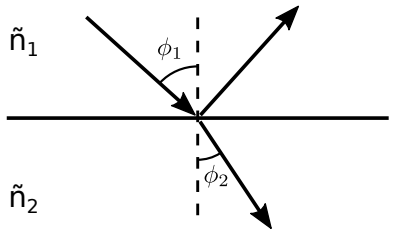

Figure 5.2: Interface between two mediums with different refractive indexes.

The Fresnel reflection coefficients for each state of polarization are then given as:

$$r_{12}^{p} = \frac{\tilde{n}_2 cos(\phi_1) - \tilde{n}_1 cos(\phi_2)}{\tilde{n}_2 cos(\phi_1) + \tilde{n}_1 cos(\phi_2)} \qquad r_{12}^{s} = \frac{\tilde{n}_1 cos(\phi_1) - \tilde{n}_2 cos(\phi_2)}{\tilde{n}_1 cos(\phi_1) + \tilde{n}_2 cos(\phi_2)} \tag{5.2.1}$$

Where the reflectance for this single interface is given as:

$$R^{p} = \left|r_{12}^{p}\right|^2 \qquad R^{s} = \left|r_{12}^{s}\right|^2 \tag{5.2.2}$$

Let us now consider the case where a intermediate layer exists, thus having two interfaces instead of one:

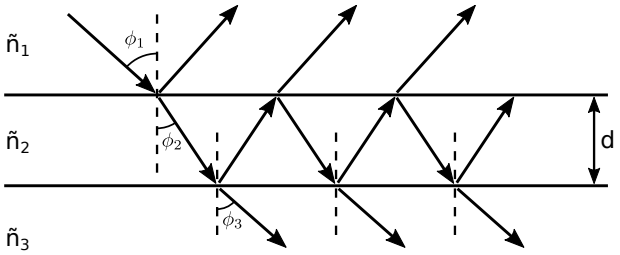

Figure 5.3: Light propagating along a two layered system with different refractive indexes.

The complex reflection coefficients for this system are given by the Airy formula:

$$r^p_{123} = \frac{r^p_{12} + r^p_{23} exp(-i2\beta)}{1 + r^p_{12} r^p_{23} exp(-i2\beta)} \tag{5.2.3}$$

$$r^s_{123} = \frac{r^s_{12} + r^s_{23} exp(-i2\beta)}{1 + r^s_{12} r^s_{23} exp(-i2\beta)} \tag{5.2.4}$$

Where β is the phase change in the polarization from the first to the second layer, and it is given as:

$$\beta = 2\pi \frac{d}{\lambda} \tilde{n}_2 cos(\phi_2) = 2\pi \frac{d}{\lambda} \sqrt{\tilde{n}_2 - \tilde{n}_1 sin^2(\theta_1)} \tag{5.2.5}$$

Thus the total reflectance of the system is then given as:

$$R^p = \left| r^p_{123} \right|^2 \qquad R^s = \left| r^s_{123} \right|^2 \tag{5.2.6}$$

An ellipsometer usually measures the Δ and Ψ ellipsometric parameter, where Δ is the phase difference induced by the total reflection, and Ψ is the ratio between the s and p polarization amplitudes. These can be related to the previous equation through the fundamental equation of ellipsometry.

$$\rho = \frac{r^p_{123}}{r^s_{123}} = tan(\Psi) exp(i\Delta) \tag{5.2.7}$$

Solving ρ we get:

$$\rho = \frac{r^p_{12} + r^p_{23} exp(-i2\beta)}{1 + r^p_{12} r^p_{23} exp(-i2\beta)} \frac{1 + r^s_{12} r^s_{23} exp(-i2\beta)}{r^s_{12} + r^s_{23} exp(-i2\beta)} \tag{5.2.8}$$

$$= \frac{AX^2 + BX + C}{DX^2 + EX + F} \tag{5.2.9}$$

where the constants A through F are given as:

$$A = r^p_{12} \quad B = r^p_{12} r^s_{12} r^s_{23} + r^p_{23} \quad C = r^p_{23} r^s_{12} r^s_{23} \tag{5.2.10}$$

$$D = r^s_{12} \quad E = r^s_{12} r^p_{12} r^p_{23} + r^s_{23} \quad F = r^s_{23} r^p_{12} r^p_{23} \tag{5.2.11}$$

and

$$X = exp(-i2\beta) \tag{5.2.12}$$

The roots for this quadratic expression are then given as:

$$X = \frac{-(\rho E - B) \pm \sqrt{(\rho E - B)^2 - 4(\rho D - A)(\rho F - C)}}{2(\rho D - A)} \tag{5.2.13}$$

If the ellipsometric parameters Ψ and Δ are known for our system, and the complex refractive indices $\tilde{N}_1$, $\tilde{N}_2$ and $\tilde{N}_3$, then the only unknown is the thickness d, which then can be solved. In the case of a system with four layers or more, these same equations can be used recursively from the bottom to the top layer.

If we then consider a four layer system then the complex reflectivity coefficients are then given as:

$$r^p_{1234} = \frac{r^p_{12} + r^p_{234} exp(-i2\beta_1)}{1 + r^s_{12} r^s_{234} exp(-i2\beta_1)} \qquad r^s_{1234} = \frac{r^s_{12} + r^s_{234} exp(-i2\beta_1)}{1 + r^s_{12} r^s_{234} exp(-i2\beta_1)} \tag{5.2.14}$$

$$r^p_{234} = \frac{r^p_{23} + r^p_{34} exp(-i2\beta_2)}{1 + r^p_{23} r^p_{34} exp(-i2\beta_2)} \qquad r^s_{234} = \frac{r^s_{23} + r^s_{34} exp(-i2\beta_2)}{1 + r_{23} spr^s_{34} exp(-i2\beta_2)} \tag{5.2.15}$$

The phase changes β_1 and β_2 are given as:

$$\beta_1 = 2\pi \frac{d_2}{\lambda} \tilde{n}_2 cos(\phi_2) \tag{5.2.16}$$

$$\beta_2 = 2\pi \frac{d_3}{\lambda} \tilde{n}_3 cos(\phi_3) \tag{5.2.17}$$

where d_2 and d_3 are the thicknesses of the second and third layer. The ellipsometric parameters for this system are then related as follows:

$$\rho = tan(\Psi) exp(i\Delta) = \frac{r^p_{1234}}{r^s_{1234}} \tag{5.2.18}$$

Ellipsometers often measure the Stokes parameters S_1 and S_2, which are given as:

$$S_1 = -cos(2\Psi) \tag{5.2.19}$$

$$S_2 = sin(2\Psi) cos(\Delta) \tag{5.2.20}$$

5.3 Raman Spectroscopy

Raman spectroscopy is an optical characterization technique based on the Raman scattering phenomena discovered in 1928 by Chandrasekhara Ventaka Raman. This inelastic scattering relies on the existence of vibrational modes that cause a change on the polarizability of a molecule in contrast of IR spectroscopy that relies on vibrational modes that cause a change on the dipole moment. Not all vibrational modes are Raman active, and while some modes might be Raman inactive they are IR active and vice versa, thus they complement each other, so in order to study all the vibrational modes of a molecule both IR and Raman spectroscopy are needed.

When exposed to an electric field, a dipole moment on the molecule will arise, since the atoms of the molecule will align themselves with the incident electric field. This electric dipole is given by:

$$\mathbf{P} = \overline{\overline{\varepsilon}}\mathbf{E} \tag{5.3.1}$$

Where **E** is the incident electric field and $\overline{\overline{\varepsilon}}$ is a symmetrical rank 2 tensor, this tensor dictates how easily a material can be polarized with an incident electric field. Let us assume an unidimensional case, where a molecule is exposed to a electric field given by the following expression:

$$E = E_0 cos(2\pi\nu t) \tag{5.3.2}$$

Then the induced dipole moment would be given as:

$$P = \varepsilon E_0 cos(2\pi\nu t) \tag{5.3.3}$$

As we know this electric field will induce a dipole moment on the molecule, however this dipole moment will not only depend on the applied electric field, the vibrational modes of this molecule might also induce a change on the polarizability. Since the electric dipole moment of the molecule will also depend on the frequency of its vibrational mode, the scattered photon will have a different energy which will depend on the frequency on which the molecule vibrates, thus this being a inelastic scattering.

If we define Q as our vibrational coordinate, for example either the angle of which the molecule is bending, or the distance at which the molecule is either stretching or contracting, then our polarizability will depend on this same coordinate. We can then expand our polarizability as s Maclaurin series.

$$\varepsilon = \varepsilon_0 + \left(\frac{\partial\varepsilon}{\partial Q}\right)_0 Q + ... \tag{5.3.4}$$

The first term, ε_0, corresponds to the polarizability when the molecule is in equilibrium, therefore for an unperturbed molecule, our polarizability would just equal to ε_0. The second term is what matters the most for Raman scattering, for a vibrational mode to be Raman active this second term cannot equal to zero when $Q \neq 0$.

$$\left(\frac{\partial \varepsilon}{\partial Q}\right)_0 = 0 \implies \text{Raman Inactive} \tag{5.3.5}$$

$$\left(\frac{\partial \varepsilon}{\partial Q}\right)_0 \neq 0 \implies \text{Raman Active} \tag{5.3.6}$$

These vibrations can be seen as small springs, thus the same vibrations can be studied as harmonic oscillators, therefore they can be expressed as sinusoidal waves.

$$Q = Q_0 cos(2\pi \nu_{vib} t) \tag{5.3.7}$$

Where ν_{vib} is the frequency at which the molecule vibrates. Then Eq.5.3.4 can be rewritten as:

$$\varepsilon = \varepsilon_0 + \left(\frac{\partial \varepsilon}{\partial Q}\right)_0 Q_0 cos(2\pi \nu_{vib} t) \tag{5.3.8}$$

Which then leads to:

$$P = \underbrace{\varepsilon_0 E_0 cos(2\pi \nu t)}_{\substack{\text{Rayleigh} \\ \text{Scattering}}} + \underbrace{\left(\frac{\partial \varepsilon}{\partial Q}\right)_0 Q_0 cos(2\pi \nu_t) cos(2\pi \nu_{vib} t)}_{\substack{\text{Raman} \\ \text{Scattering}}} \tag{5.3.9}$$

Then for our electric dipole moment we have an elastic scattering term, or Rayleigh scattering term and a inelastic term or Raman scattering term. Our Raman term can be further simplified if we admit the following trigonometric entity:

$$2cos(A)cos(B) = cos(A - B) + cos(A + B) \tag{5.3.10}$$

Then our Raman scattering term can be rewritten as:

$$\frac{1}{2}\left(\frac{\partial \varepsilon}{\partial Q}\right)_0 Q_0 E_0 (\underbrace{cos[2\pi(\nu - \nu_{vib})t]}_{\text{Stokes}} + \underbrace{cos[2\pi(\nu + \nu_{vib})t]}_{\text{Anti-Stokes}}) \tag{5.3.11}$$

So two inelastic lines will be seen on a Raman spectroscopy at both left and right side of the Rayleigh line with a shift of ν_{vib}.

As mentioned before, not all vibrational modes are Raman active, let us take for example a CO_2 molecule, and lets consider three of its vibrational modes, the symmetric and anti-symmetric stretches, and the bending mode.

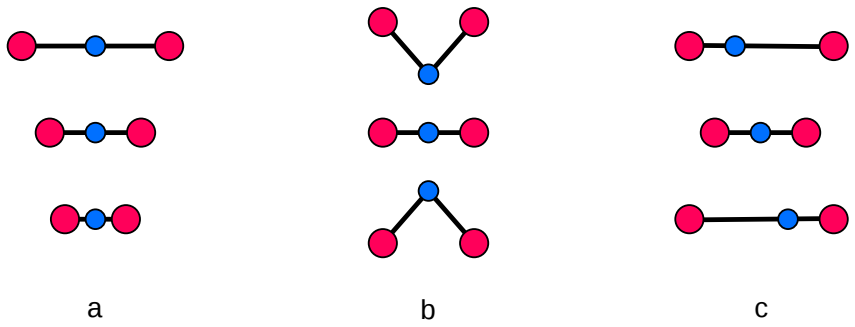

Figure 5.4: Three possible vibrational modes for a CO_2 molecule, (a) symmetric stretch, (b) bending, and (c) anti-symmetric stretch.

From Eq.5.3.7 we know that our vibration must be given by a sinusoidal wave, however from Fig.5.4 it is possible to see that the parity of each vibrational mode might differ from case to case. In the first case the symmetric stretch it will be an odd function, on the second case it must be an even function and for the third case we have a vibrational mode composed of two odd functions, however the product of either two even or odd parity functions must always equal an even parity function, thus for the third case we end up having an even parity function, so even parity vibrational modes are Raman inactive while odd parity ones are Raman active.

However studying the normal modes of a big molecule can prove to be difficult, so the selection rules can also be obtained through a quantum mechanics approach, where if the following integral equals zero then the vibrational mode is said to be Raman inactive:

$$\langle \Psi_0 | \varepsilon | \Psi_1 \rangle = \int_{-\infty}^{+\infty} \Psi_0^* \varepsilon \Psi_1 \, dQ \tag{5.3.12}$$

Where Ψ_0 is the wavefunction before the transition and Ψ_1 is the wavefunction after the transition. However for anisotropic media, we know that the polarizability is given by a symmetric rank 2 tensor, so we then define our polarizability as the following tensor:

$$\overline{\overline{\varepsilon}} = \begin{pmatrix} \varepsilon_{xx} & \varepsilon_{xy} & \varepsilon_{xz} \\ \varepsilon_{xy} & \varepsilon_{yy} & \varepsilon_{yz} \\ \varepsilon_{xz} & \varepsilon_{yz} & \varepsilon_{zz} \end{pmatrix} \tag{5.3.13}$$

However for any anistropic medium it is always possible to choose a set of coordinates so that only the diagonal member of these matrix are left as non-zero values.

Then for anisotropic media, the same kind of integral can be computed to determine the selection rules. If the integral for any given index equals a value different than zero then the vibrational mode is then said to be Raman active.

$$\langle \Psi_0 | \varepsilon_{ij} | \Psi_1 \rangle = \int_{-\infty}^{+\infty} \Psi_0^* \varepsilon_{ij} \Psi_1 dQ \tag{5.3.14}$$

We know that for a photon scattering, there are two possibilities, either the photon scatters elastically (Rayleigh scattering) or inelastically (Raman scattering), and if it does scatter inelastically either energy is lost (Stokes line) or energy is gained (Anti-Stokes line), however this Raman scattering occurs at a much lower rate compared to Rayleigh scattering, in fact the relative intensity of the Rayleigh scattered light compared to the Raman scattered one is often higher than 10^9 [30].

We know that for Rayleigh scattering the intensity of the scattered light is proportional to ν^4, for Raman scattering this proportionality is also observed, so for smaller wavelengths the intensity of the Raman spectra should increase, thus explaining why visible or Ultraviolet (UV) wavelengths are used instead of IR, however the use of smaller wavelengths in the UV region allow the occurrence of fluorescence which is undesired on a Raman spectra, thus visible light then being usually preferred for Raman spectroscopy.

$$I \propto \nu^4 \tag{5.3.15}$$

Then the ratio between both Stokes and Anti-Stokes is given as:

$$\frac{I_{Stokes}}{I_{Anti-Stokes}} = \left(\frac{\nu - \nu_{vib}}{\nu + \nu_{vib}} \right)^4 \tag{5.3.16}$$

However this is known to be false, since Stokes lines are clearly more intense on any Raman spectra. The reason behind this can be explained through the Boltzmann distribution. This distribution states that the probability to find a particle on a given energy state is given as:

$$P(E) = exp\left(-\frac{h\nu}{k_B T} \right) \tag{5.3.17}$$

Given that the Stokes lines correspond to our lowest energy lines, then the ratio between the both is given as:

$$\frac{I_{Stokes}}{I_{Anti-Stokes}} = \left(\frac{\nu - \nu_{vib}}{\nu + \nu_{vib}} \right)^4 exp\left(\frac{h\nu_{vib}}{k_B T} \right) \tag{5.3.18}$$

So in order to increase the ratio of Anti-Stokes lines scattering one should increase the temperature, however since both Stokes and Anti-Stokes lines provide the same information, usually only Stokes lines are acquired so no redundant information is displayed on a specter.

5.4 Second Harmonic Generation

As previously discussed on Section 2.4, when a non-linear crystal is exposed to an electromagnetic wave, and its electric field is strong enough, a non-linear polarization term arises due to its non-linear electric susceptibility. This non-linear polarization term will be responsible to generate electromagnetic radiation with a different wavelength of its source, however it is necessary to remember that this process does follow the energy conservation law.

In order to maximize the efficiency of this non-linear process for a given frequency, a phase-matching condition must be met, however for each frequency this phase-matching condition may differ, thus we only consider the frequencies at which we meet this phase-matching condition (all other frequencies will have a relatively small efficiency thus can be considered as zero).

In this section we will discuss the intensity of this non-linear therm, initially for isotropic media and later on for uniaxial crystals.

Let us now consider a non-linear crystal where only its linear and second order polarization terms are considered, then the polarization for this crystal would be given as follows:

$$\mathbf{P} = \varepsilon_0 \overline{\overline{\chi^{(1)}}}\mathbf{E} + \mathbf{P_{NL}} = \overline{\overline{\varepsilon}}\mathbf{E} + 2\varepsilon_0 \overline{\overline{d}}\mathbf{E}^2 \tag{5.4.1}$$

Since a the electric field is a traveling wave, then it must follow the wave equation.

$$\nabla^2\mathbf{E} = \frac{\mu_0\varepsilon_0}{2}\left(\overline{\overline{1}} + \overline{\overline{\chi^{(1)}}}\right)\frac{\partial^2\mathbf{E}}{\partial t^2} + \mu_0\frac{\partial^2\mathbf{P_{NL}}}{\partial t^2} + c.c. \tag{5.4.2}$$

Applying this wave equation to the ath component of the electric field we get:

$$\nabla^2 E_a = \frac{\mu_0\varepsilon_0}{2}\varepsilon_{bc}\frac{\partial^2 E_b}{\partial t^2} + \mu_0\frac{\partial^2 (P_{NL})_{abc}}{\partial t^2} + c.c. \tag{5.4.3}$$

Where the non-linear polarization is given as:

$$(P_{NL})_{abc} = \frac{\varepsilon_0 d_{abc}}{2}E_b E_c + c.c. \tag{5.4.4}$$

Where this non-linear term will be responsible for converting part of the incident radiation at frequency ω to radiation with frequency 2ω.

Since our non-linear crystal is converting radiation at frequency ω to radiation at frequency 2ω, then we can admit that our electric field is the superposition of two electric fields, with frequencies ω and 2ω.

$$E_a = E_a^{(\omega)} + E_a^{(2\omega)} \tag{5.4.5}$$

Where each wave is given as:

$$E_a^{(\omega)} = \frac{1}{2} E_{1a} exp\left[i(\mathbf{k_1}\cdot\mathbf{r} - \omega t)\right] + c.c. \tag{5.4.6}$$

$$E_a^{(2\omega)} = \frac{1}{2} E_{2a} exp\left[i(\mathbf{k_2}\cdot\mathbf{r} - 2\omega t)\right] + c.c. \tag{5.4.7}$$

For both cases the wave equation must be met, since both waves are also traveling waves.

$$\nabla^2 E_a^{(\omega)} = \frac{\mu_0 \varepsilon_0}{2} \varepsilon_{bc}^{(\omega)} \frac{\partial^2 E_c^{(\omega)}}{\partial t^2} + \mu_0 \frac{\partial^2 \left(P_{NL}^{(\omega)}\right)_{abc}}{\partial t^2} \tag{5.4.8}$$

$$\nabla^2 E_a^{(2\omega)} = \frac{\mu_0 \varepsilon_0}{2} \varepsilon_{bc}^{(2\omega)} \frac{\partial^2 E_c^{(2\omega)}}{\partial t^2} + \mu_0 \frac{\partial^2 \left(P_{NL}^{(2\omega)}\right)_{abc}}{\partial t^2} \tag{5.4.9}$$

Where the non-linear polarization terms for each frequency are given as:

$$\left(P_{NL}^{(\omega)}\right)_{abc} = \frac{\varepsilon_0 d_{abc}^{(\omega)}}{2} E_{1b}^* E_{2c} exp\left[i\left((\mathbf{k_2} - \mathbf{k_1})\cdot\mathbf{r} - \omega t\right)\right] + c.c. \tag{5.4.10}$$

$$\left(P_{NL}^{(2\omega)}\right)_{abc} = \frac{\varepsilon_0 d_{abc}^{(2\omega)}}{2} E_{1b} E_{1c} exp\left[i2(\mathbf{k_1}\cdot\mathbf{r} - \omega t)\right] + c.c. \tag{5.4.11}$$

By expanding the Laplacian vector for both both frequencies, we get that the ath component of these vectors are given as:

$$\nabla^2 E_a^{(\omega)} = \frac{1}{2} \sum_b^{x,y,z} \left(\frac{\partial^2 s E_{1a}}{\partial b^2} + \frac{i2k_{1bc}}{E_{1a}} \frac{\partial E_{1a}}{\partial b} - k_{1bc}^2 \right) E_a^{(\omega)} + c.c. \tag{5.4.12}$$

$$\nabla^2 E_a^{(2\omega)} = \frac{1}{2} \sum_b^{x,y,z} \left(\frac{\partial^2 s E_{2a}}{\partial b^2} + \frac{i2k_{2bc}}{E_{2a}} \frac{\partial E_{2a}}{\partial b} - k_{2bc}^2 \right) E_a^{(2\omega)} + c.c. \tag{5.4.13}$$

where

$$k_{1ab}^2 = \frac{\omega^2}{c^2} \varepsilon_{ab}^{(\omega)} \tag{5.4.14}$$

$$k_{2ab}^2 = \frac{4\omega}{c^2} \varepsilon_{ab}^{(2\omega)} \tag{5.4.15}$$

Both wave vectors $\mathbf{k_1}$ and $\mathbf{k_2}$ represent the direction of propagation of both electromagnetic waves at frequencies ω and 2ω frequencies as if they were not interfering with each other, thus we also call them as "free" waves.

These free waves represent the direction of propagation of each frequency when the non-linear polarization terms equal zero, however looking at the non-linear polarization therms, we can see that these terms also posses a wave-like equation, which will end up interfering with our free waves, since any oscillating dipole emits radiation. This also fits nicely with our wave equation, since this non-homogeneous differential equation will have as its solutions the sum of its homogeneous solution plus a particular solution.

The "free" waves correspond to our homogeneous solution, whereas the radiation from the non-linear polarization will be our particular solutions, which are also known as bound waves. The wave vectors for our bound waves are given as:

$$\mathbf{k_b^{(\omega)}} = \mathbf{k_2} - \mathbf{k_1} \tag{5.4.16}$$

$$\mathbf{k_b^{(2\omega)}} = 2\mathbf{k_1} \tag{5.4.17}$$

So for our free waves, the Laplacian vector would result as:

$$\nabla^2 E_{fa}^{(\omega)} = -\frac{1}{2} k_{1ab}^2 E_b^{(\omega)} + c.c. = \frac{\mu_0 \varepsilon_0}{2} \varepsilon_{ab}^{(\omega)} \frac{\partial^2 E_a^{(\omega)}}{\partial t^2} + c.c. \tag{5.4.18}$$

$$\nabla^2 E_{fa}^{(2\omega)} = -\frac{1}{2} k_{2ab}^2 E_b^{(2\omega)} + c.c. = \frac{\mu_0 \varepsilon_0}{2} \varepsilon_{ab}^{(2\omega)} \frac{\partial^2 E_a^{(2\omega)}}{\partial t^2} + c.c. \tag{5.4.19}$$

If we admit that our set of coordinates matches the principal set of coordinates of our crystal, then only the diagonal members of our dielectric tensor are non-zero values, also we consider the rate of change of the variation of the electric field along each direction to be negligible, thus all second derivatives can be considered as zero.

$$\nabla^2 E_a^{(\omega)} = \frac{1}{2} \left(\frac{i 2 k_{1bb}}{E_{1a}} \frac{\partial E_1 a}{\partial b} - k_{1bb}^2 \right) E_a^{\omega} + c.c. \tag{5.4.20}$$

$$\nabla^2 E_a^{(2\omega)} = \frac{1}{2} \left(\frac{i 2 k_{2bb}}{E_{2a}} \frac{\partial E_2 a}{\partial b} - k_{2bb}^2 \right) E_a^{2\omega} + c.c. \tag{5.4.21}$$

where

$$k_{1aa} = \frac{\omega}{c} n_a^{\omega} \tag{5.4.22}$$

$$k_{2aa} = \frac{2\omega}{c} n_a^{2\omega} \tag{5.4.23}$$

Comparing with the wave equation, we get for our particular solution:

$$\mu_0 \frac{\partial^2 \left(P_{NL}^{(\omega)} \right)_{abc}}{\partial t^2} = \frac{i k_{1bb}}{E_{1a}} \frac{\partial E_{1a}}{\partial b} E_a^{(\omega)} \tag{5.4.24}$$

$$\mu_0 \frac{\partial^2 \left(P_{NL}^{(2\omega)} \right)_{abc}}{\partial t^2} = \frac{i k_{2bb}}{E_{1a}} \frac{\partial E_{2a}}{\partial b} E_a^{(2\omega)} \tag{5.4.25}$$

Simplifying we get:

$$\frac{\partial E_{1a}}{\partial b} = -i\frac{\omega d_{acd}^{(\omega)}}{cn_b^{(\omega)}} E_{1c}^* E_{2d} exp\left[i\mathbf{\Delta k}\cdot\mathbf{r}\right] \tag{5.4.26}$$

$$\frac{\partial E_{2a}}{\partial b} = -i\frac{\omega d_{acd}^{(2\omega)}}{cn_b^{(2\omega)}} E_{1c} E_{1d} exp\left[-i\mathbf{\Delta k}\cdot\mathbf{r}\right] \tag{5.4.27}$$

where

$$\mathbf{\Delta k} = \mathbf{k_2} - 2\mathbf{k_1} \tag{5.4.28}$$

If we assume that the efficiency of conversion for the SHG process to be very low, then the intensity of the electric field $\mathbf{E_1}$ will vary very little, thus we can consider it as constant. We can assume this partial derivative to be equal to its correspondent total derivative, since each of the x, y and z spatial variables are independent of each other.

$$\frac{dE_{2a}}{db} = \frac{\partial E_{2a}}{\partial b}\frac{db}{db} + \frac{\partial E_{2a}}{\partial a}\frac{da}{db} + \frac{\partial E_{2a}}{\partial c}\frac{dc}{db} = \frac{\partial E_{2a}}{\partial b} \tag{5.4.29}$$

So by integrating we get:

$$E_{2a} = \int_0^L \frac{\partial E_{2a}}{\partial b} db = -i\frac{\omega d_{acd}^{(2\omega)}}{cn_b^{(2\omega)}} E_{1c} E_{1d} \frac{exp\left[-i\mathbf{\Delta k}\cdot\mathbf{r}\right] - 1}{-i\Delta k_b} \tag{5.4.30}$$

The solution of our non-homogeneous differential equation consists in the sum of the sum of a free and bound wave. The electric field for these bound and free waves is given as:

$$E_a^{(2\omega)} = E_{2a} exp[i(\mathbf{k_2}\cdot\mathbf{r} - 2\omega t)] \tag{5.4.31}$$

$$= \left(E_a^{(2\omega)}\right)_{free} exp[i(\mathbf{k_2}\cdot\mathbf{r} - 2\omega t)] + \left(E_a^{(2\omega)}\right)_{bound} exp[i2(\mathbf{k_1}\cdot\mathbf{r} - \omega t)] \tag{5.4.32}$$

were

$$\left(E_a^{(2\omega)}\right)_{free} exp[i(\mathbf{k_2}\cdot\mathbf{r} - 2\omega t)] = -\sum_{b,c,d}^{x,y,z} \frac{\omega d_{acd}^{(2\omega)}}{cn_b^{(2\omega)}} E_{1c} E_{1d} \frac{exp[i(\mathbf{k_2}\cdot\mathbf{r} - 2\omega t)]}{\Delta k_b} \tag{5.4.33}$$

$$\left(E_a^{(2\omega)}\right)_{bound} exp[i2(\mathbf{k_1}\cdot\mathbf{r} - \omega t)] = \sum_{b,c,d}^{x,y,z} \frac{\omega d_{acd}^{(2\omega)}}{cn_b^{(2\omega)}} E_{1c} E_{1d} \frac{exp[i2(\mathbf{k_1}\cdot\mathbf{r} - \omega t)]}{\Delta k_b} \tag{5.4.34}$$

We are interested however in both the reflected and transmitted beams from a crystal with parallel faces, for this we need to take into consideration continuity conditions at our boundaries.

Let us now consider an electromagnetic wave traveling on the xz plane of the principal set of coordinates of our crystal, with a incidence angle θ_0.

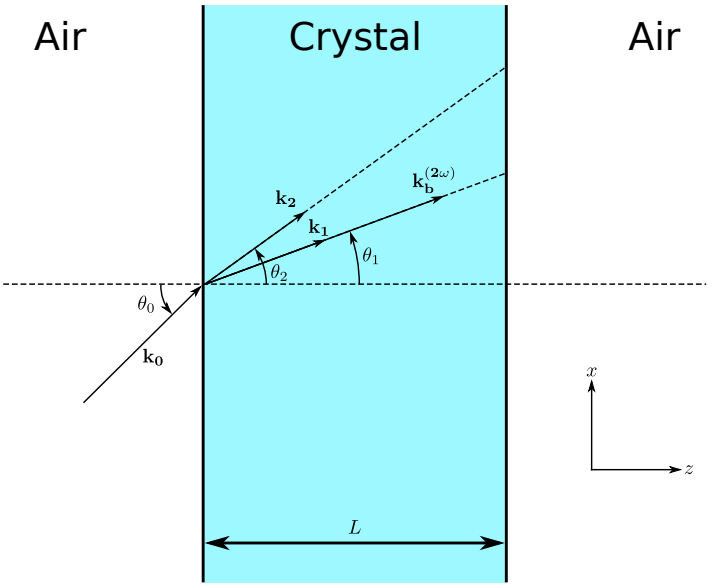

Figure 5.5: Representation of the free, bound waves for a non-linear crystal.

Our propagation vectors are then given as:

$$\mathbf{k_0} = \frac{\omega}{c} n_{air} \begin{pmatrix} sin(\theta_0) \\ 0 \\ cos(\theta_0) \end{pmatrix} \qquad \mathbf{k_1} = \frac{\omega}{c} n_1 \begin{pmatrix} sin(\theta_1) \\ 0 \\ cos(\theta_1) \end{pmatrix} \tag{5.4.35}$$

$$\mathbf{k_2} = \frac{2\omega}{c} n_2 \begin{pmatrix} sin(\theta_2) \\ 0 \\ cos(\theta_2) \end{pmatrix} \qquad \mathbf{k_b^{(2\omega)}} = \frac{2\omega}{c} n_1 \begin{pmatrix} sin(\theta_1) \\ 0 \\ cos(\theta_1) \end{pmatrix} \tag{5.4.36}$$

For this direction of propagation two independent states of polarization are possible, either parallel to the plane of incidence (p-polarized), or perpendicularly (s-polarized). The electric fields for the incident beam, for these two states of polarization are then given as:

$$\mathbf{E_0^S} = \begin{pmatrix} 0 \\ E_0 \\ 0 \end{pmatrix} \qquad \mathbf{B_0^S} = \frac{n_{air}}{c} \begin{pmatrix} E_0 sin(\theta_0) \\ 0 \\ -E_0 cos(\theta_0) \end{pmatrix} \tag{5.4.37}$$

$$\mathbf{E_0^P} = \begin{pmatrix} E_0 sin(\theta_0) \\ 0 \\ -E_0 cos(\theta_0) \end{pmatrix} \qquad \mathbf{B_0^P} = \frac{n_{air}}{c} \begin{pmatrix} 0 \\ E_0 \\ 0 \end{pmatrix} \tag{5.4.38}$$

The boundaries conditions demand that both the net electric and magnetic field for both reflected and transmitted SHG signal to be equal at the interface. However this boundary problem needs to be solved differently for each independent state of polarization. Let us assume that the electric field oscillates perpendicularly to the plane of incidence, then we get:

$$\left(E^{(2\omega)}\right)_{rfl} = \left(E^{(2\omega)}\right)_{free} + \left(E^{(2\omega)}\right)_{bound} \tag{5.4.39}$$

$$\left(B^{(2\omega)}\right)_{rfl} = \left(B^{(2\omega)}\right)_{free} + \left(B^{(2\omega)}\right)_{bound} \tag{5.4.40}$$

Replacing we get

$$\left(E^{(2\omega)}\right)_{free} = -\frac{cos(\theta_0) + n_1 cos(\theta_1)}{n_2 cos(\theta_2) + cos(\theta_0)} \left(E^{(2\omega)}\right)_{bound} \tag{5.4.41}$$

At the second boundary we can have either transmitted or reflected SHG rays from either bound or free waves, however the transmitted rays are free waves since air is assumed to be linear, as for the reflected rays, we neglect any bound reflected rays, thus we get:

$$\begin{aligned}\left(E^{(2\omega)}\right)_{tr} exp[i2\mathbf{k_0}\cdot\mathbf{z}L] = &\left(E^{(2\omega)}\right)_{bound} exp[i2\mathbf{k_1}\cdot\mathbf{z}L] + \\ &+ \left(E^{(2\omega)}\right)_{bound} exp[i\mathbf{k_2}\cdot\mathbf{z}L] + \left(E^{(2\omega)}\right)^{rfl}_{bound} exp[i\mathbf{k_2}\cdot\mathbf{z}L]\end{aligned} \tag{5.4.42}$$

$$\begin{aligned}\left(B^{(2\omega)}\right)_{tr} exp[i2\mathbf{k_0}\cdot\mathbf{z}L] = &\left(B^{(2\omega)}\right)_{bound} exp[i2\mathbf{k_1}\cdot\mathbf{z}L] + \\ &+ \left(B^{(2\omega)}\right)_{bound} exp[i\mathbf{k_2}\cdot\mathbf{z}L] + \left(B^{(2\omega)}\right)^{rfl}_{bound} exp[i\mathbf{k_2}\cdot\mathbf{z}L]\end{aligned} \tag{5.4.43}$$

replacing we get:

$$\begin{aligned}\left(E^{(2\omega)}\right)_{tr} exp[i2\mathbf{k_0}\cdot\mathbf{z}L] = &\frac{2n_1 cos(\theta_1)}{cos(\theta_0) + n_2 cos(\theta_2)} \left(E^{(2\omega)}\right)_{free} exp[i\mathbf{k_2}\cdot\mathbf{z}L] + \\ &+ \frac{n_1 cos(\theta_1) + n_2 cos(\theta_2)}{cos(\theta_0) + n_2 cos(\theta_2)} \left(E^{(2\omega)}\right)_{bound} exp[i2\mathbf{k_1}\cdot\mathbf{z}L]\end{aligned} \tag{5.4.44}$$

Thus the transmitted power of SHG signal is:

$$\left(P^{(2\omega)}\right)_{tr} = \frac{cn_2\varepsilon_0}{2}\left|\left(\mathbf{E}^{(2\omega)}\right)_{tr} \times \left(\mathbf{H}^{(2\omega)}\right)^*_{tr}\right| S = \frac{c\varepsilon_0}{2}\left|\left(E^{(2\omega)}\right)_{tr}\right|^2 S \tag{5.4.45}$$

$$= \frac{cn_2\varepsilon_0}{2}\left|\left(E^{(2\omega)}\right)_{bound}\right|^2 \left(T^{(2\omega)} sin^2\left[\frac{\mathbf{\Delta k}\cdot\mathbf{z}L}{2}\right] + T_0^{(2\omega)}\right) S \tag{5.4.46}$$

Where $T^{(2\omega)}$ and $T_0^{(2\omega)}$ are transmission factors, however $T_0^{(2\omega)}$ can be in some cases disregarded as it becomes considerably small.

These transmission factors are given as:

$$T^{(2\omega)} = \frac{8n_2cos(\theta_2)[cos(\theta_0)+n_1cos(\theta_1)][n_1cos(\theta_1)+n_2cos(\theta_2)]}{(n_2cos(\theta_2)+cos(\theta_0))^3} \tag{5.4.47}$$

$$T_0^{(2\omega)} = \frac{(n_1cos(\theta_1)-n_2cos(\theta_2))^2}{(n_2cos(\theta_2)+cos(\theta_0)))^4}(n_2cos(\theta_2)-cos(\theta_0))^2 \tag{5.4.48}$$

In a similar manner transmission factors for P polarized light from the boundary conditions are given as:

$$T^{(2\omega)} = \frac{8n_2cos(\theta_2)[cos(\theta_1)+n_1cos(\theta_0)][n_1cos(\theta_2)+n_2cos(\theta_1)]}{(n_2cos(\theta_0)+cos(\theta_2))^3} \tag{5.4.49}$$

$$T_0^{(2\omega)} = \frac{(n_1cos(\theta_2)-n_2cos(\theta_1))^2}{(n_2cos(\theta_0)+cos(\theta_2)))^4}(n_2cos(\theta_0)-cos(\theta_2))^2 \tag{5.4.50}$$

If we admit our crystal to be uniaxial crystal, then the effective refractive index for vertical and horizontal polarization will be different. For our chosen geometry, a S polarized ray should be a ordinary ray and a P polarized ray a extraordinary ray, the effective refractive indices for ordinary and extraoridinary rays are given as:

$$N_o^{(\omega)} = n_o \tag{5.4.51}$$

$$N_e^{(\omega)} = \left(\left(\frac{cos(\theta_0)}{n_o}\right)^2 + \left(\frac{sin(\theta_0)}{n_e}\right)^2\right)^{-1/2} \tag{5.4.52}$$

Given that our SHG signal is proportional to the amplitude of the transmitted ray at pump frequency (E_1), boundary conditions must be taken into account to determine its transmission factor. Assuming our source to be undepleted, then the transmission factors at frequency ω are given as:

$$E_1^S = E_0 t_o^{(\omega)} = E_0 \frac{2cos(\theta_0)}{N_o^{(\omega)}cos(\theta_1)+cos(\theta_0)} \tag{5.4.53}$$

$$E_1^P = E_0 t_e^{(\omega)} = E_0 \frac{2cos(\theta_0)}{N_e^{(\omega)}cos(\theta_0)+cos(\theta_1)} \tag{5.4.54}$$

The amplitude of the electric field for both S and P polarization, when taking the anisotropy of the crystal into account, are given as:

$$\left|\left(E^{(2\omega)}\right)_{bound}^S\right| = \frac{\omega d^{(2\omega)}}{cN_o^{(\omega)}}E_0^2\left(t_o^{(\omega)}\right)^2 \frac{p_S}{\frac{\omega}{c}(N_o^{(2\omega)}cos(\theta_2)-N_o^{(\omega)}cos(\theta_1))} \tag{5.4.55}$$

$$\left|\left(E^{(2\omega)}\right)_{bound}^P\right| = \frac{\omega d^{(2\omega)}}{cN_e^{(\omega)}}E_0^2\left(t_o^{(\omega)}\right)^2 \frac{p_P}{\frac{\omega}{c}(N_e^{(2\omega)}cos(\theta_2)-N_e^{(\omega)}cos(\theta_1))} \tag{5.4.56}$$

Where p_P and p_S are projection factors from the second order dielectric tensor. Let us take for example wurtzite GaN, since it is a C_{6v}, the its second order dielectric tensor is given as:

$$\overline{\overline{d}} = \begin{pmatrix} 0 & 0 & 0 & 0 & d_{15} & 0 \\ 0 & 0 & 0 & d_{15} & 0 & 0 \\ d_{31} & d_{31} & d_{33} & 0 & 0 & 0 \end{pmatrix} = \begin{pmatrix} 0 & 0 & 0 & 0 & d & 0 \\ 0 & 0 & 0 & d & 0 & 0 \\ d & d & -2d & 0 & 0 & 0 \end{pmatrix} \tag{5.4.57}$$

Then for S and P polarizations, the form factors are given as:

$$\overline{\overline{d}} \cdot \mathbf{E_0^S}^2 = \begin{pmatrix} 0 & 0 & 0 & 0 & d & 0 \\ 0 & 0 & 0 & d & 0 & 0 \\ d & d & -2d & 0 & 0 & 0 \end{pmatrix} \cdot \begin{pmatrix} 0 \\ E_0^2 \\ 0 \\ 0 \\ 0 \\ 0 \end{pmatrix} = \begin{pmatrix} 0 \\ dE_0^2 \\ 0 \end{pmatrix} \tag{5.4.58}$$

$$\overline{\overline{d}} \cdot \mathbf{E_0^P}^2 = \begin{pmatrix} 0 & 0 & 0 & 0 & d & 0 \\ 0 & 0 & 0 & d & 0 & 0 \\ d & d & -2d & 0 & 0 & 0 \end{pmatrix} \cdot \begin{pmatrix} E_0^2 sin^2(\theta_0) \\ 0 \\ E_0^2 cos^2(\theta_0) \\ 0 \\ -E_0^2 sin(\theta_0) cos(\theta_0) \\ 0 \end{pmatrix} = \begin{pmatrix} dE_0^2 cos(\theta_0) sin(\theta_0) \\ 0 \\ \frac{dE_0^2}{2}(3 + cos(2\theta_0)) \end{pmatrix} \tag{5.4.59}$$

$$\left| \overline{\overline{d}} \cdot \mathbf{E_0^S}^2 \right| = dE_0^2 p_S = dE_0^2 \tag{5.4.60}$$

$$\left| \overline{\overline{d}} \cdot \mathbf{E_0^S}^2 \right| = dE_0^2 p_P = dE_0^2 \sqrt{\frac{3 + 3cos(2\theta_0) + 2cos(4\theta_0)}{2}} \tag{5.4.61}$$

Then the transmitted power for both ordinary and extraordinary rays at $(x, y, z) = (0, 0, L)$ is given as:

$$\left(P^{(2\omega)}\right)_{tr}^{S} = \frac{P_{pump}^2}{S} \frac{8\pi^2 \left(d^{(2\omega)}\right)^2}{\lambda^2 c \left(N_o^{(\omega)}\right)^2 N_o^{(2\omega)} \varepsilon_0} \left(t_o^{(\omega)}\right)^4 p_S^2 \left(\frac{T_o^{(2\omega)} sin^2(\Psi_o) + \left(T_0^{(2\omega)}\right)_o}{\Psi_o^2} \right) L^2 \tag{5.4.62}$$

$$\left(P^{(2\omega)}\right)_{tr}^{P} = \frac{P_{pump}^2}{S} \frac{8\pi^2 \left(d^{(2\omega)}\right)^2}{\lambda^2 c \left(N_e^{(\omega)}\right)^2 N_e^{(2\omega)} \varepsilon_0} \left(t_e^{(\omega)}\right)^4 p_P^2 \left(\frac{T_e^{(2\omega)} sin^2(\Psi_e) + \left(T_0^{(2\omega)}\right)_e}{\Psi_e^2} \right) L^2 \tag{5.4.63}$$

Where Ψ is the phase change due to interference in the medium, responsible for the Maker fringes.

These interference factors are given as:

$$\Psi_o = \frac{2\pi}{\lambda}(N_o^{(2\omega)}cos(\theta_2) - N_o^{(\omega)}cos(\theta_1))L \tag{5.4.64}$$

$$\Psi_e = \frac{2\pi}{\lambda}(N_e^{(2\omega)}cos(\theta_2) - N_e^{(\omega)}cos(\theta_1))L \tag{5.4.65}$$

And the transmission factors are given as:

$$t_o^{(\omega)} = \frac{2cos(\theta_0)}{N_o^{(\omega)}cos(\theta_1) + cos(\theta_0)} \tag{5.4.66}$$

$$t_e^{(\omega)} = \frac{2cos(\theta_0)}{N_e^{(\omega)}cos(\theta_0) + cos(\theta_1)} \tag{5.4.67}$$

$$T_o^{(2\omega)} = \frac{8N_o^{(2\omega)}cos(\theta_2)\left(cos(\theta_0) + N_o^{(\omega)}cos(\theta_1)\right)\left(N_o^{(\omega)}cos(\theta_1) + N_o^{(2\omega)}cos(\theta_2)\right)}{\left(N_o^{(2\omega)}cos(\theta_2) + cos(\theta_0)\right)^3} \tag{5.4.68}$$

$$T_e^{(2\omega)} = \frac{8N_e^{(2\omega)}cos(\theta_2)\left(cos(\theta_1) + N_e^{(\omega)}cos(\theta_0)\right)\left(N_e^{(2\omega)}cos(\theta_1) + N_e^{(\omega)}cos(\theta_2)\right)}{\left(N_e^{(2\omega)}cos(\theta_0) + cos(\theta_2)\right)^3} \tag{5.4.69}$$

$$\left(T_0^{(2\omega)}\right)_e = \frac{\left(N_o^{(\omega)}cos(\theta_1) - N_o^{(2\omega)}cos(\theta_2)\right)^2}{\left(N_o^{(2\omega)}cos(\theta_2) + cos(\theta_0)\right)^4}\left(N_e^{(2\omega)}cos(\theta_2) - cos(\theta_0)\right)^2 \tag{5.4.70}$$

$$\left(T_0^{(2\omega)}\right)_o = \frac{\left(N_e^{(\omega)}cos(\theta_2) - N_e^{(2\omega)}cos(\theta_1)\right)^2}{\left(N_e^{(2\omega)}cos(\theta_0) + cos(\theta_2)\right)^4}\left(N_e^{(2\omega)}cos(\theta_0) - cos(\theta_2)\right)^2 \tag{5.4.71}$$

We know from the wave equation, that the Maker fringes interference pattern must be observed for the SHG signal transmitted from a non-linear crystal. Non linear behaviors should also be observed in reflected waves, however contrary to the transmitted wave, the reflected SHG signal should not display any Maker fringes pattern, given that this wave while needs a non-linear crystal to be produced, the same does not travel in the non-linear medium, thus the wave equation for the reflected wave should not contain any non-linear polarization term except that one coming from the interface. In other words, one could see the interface of the non-linear crystal as a source of radiation at frequency ω_2.

Obtaining an accurate expression for the reflected wave would involves a much more difficult analysis with further details, given that the boundary conditions problem cannot be solved so easily since the superposition principle is not valid for non-linear behaviors. Moreover while the reflected wave should not display any Maker fringes interference pattern, experimental results might show otherwise, which does not contradict any theory, since the reflected waves at the second interface of the non-linear crystal can also

reflect some of the SHG waves, which then would lead to a problem similar to the one in ellipsometry, where multiple reflections should be accounted for, this behavior though is hardly seen in thick crystals, where is more difficult to obtain really flat and parallel surfaces.

While obtaining an expression for the reflected waves is difficult, this thorough analysis would only be needed for determining the second order susceptibility of a non-linear crystal, however the Maker fringes interference pattern allows to have an approximation of how thick a crystal might be without the need of knowing an absolute value of $\chi^{(2)}$, where ellipsometry no longer becomes an option, in this case measurements of the reflected wave are useful as a means of normalizing the data without worrying with the response curves of the photo-detectors and any optical filters used.

Chapter 6

Experimental Procedure and Equipment

Four different optical characterization techniques where employed on two GaN samples grown through different epitaxial techniques. The first sample was a 500nm thick undoped GaN crystal grown through MOCVD with an AlN buffer layer roughly 100nm thick, the second sample used was a 0.35mm thick undoped GaN single crystal grown through HVPE reference sample.

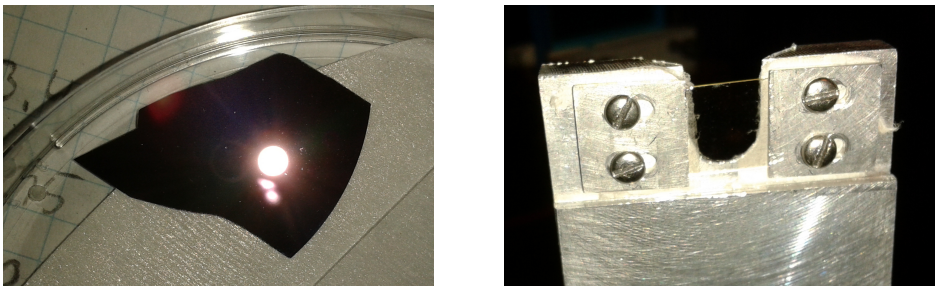

(a) GaN on Si sample. (b) GaN single crystal sample.

Figure 6.1: GaN samples used for the four optical characterization techniques.

6.1 Photoluminescence Spectroscopy

The experimental setup for this experiment was relatively simple compared to the other three techniques. It consisted in an unfocused Ar ion laser beam passing through a band pass filter (F1, 340 ± 26nm) so that only the 351nm laser line would hit our sample.

While the GaN single crystal is a transparent, the GaN on Si is not, since the Si substrate is very reflective, so for the GaN single crystal the measurement was made in transmission mode, while for the GaN on Si in reflection mode with roughly a 90° geometry.

The output beam of the sample was then focused with a set of focusing lenses L1 and L2 with focal a length of 25mm and 50mm respectively, and then filtered through a long pass filter of 355nm (so that the more intense laser line would not saturate the detector) and then sent to a spectrometer through an optic fiber.

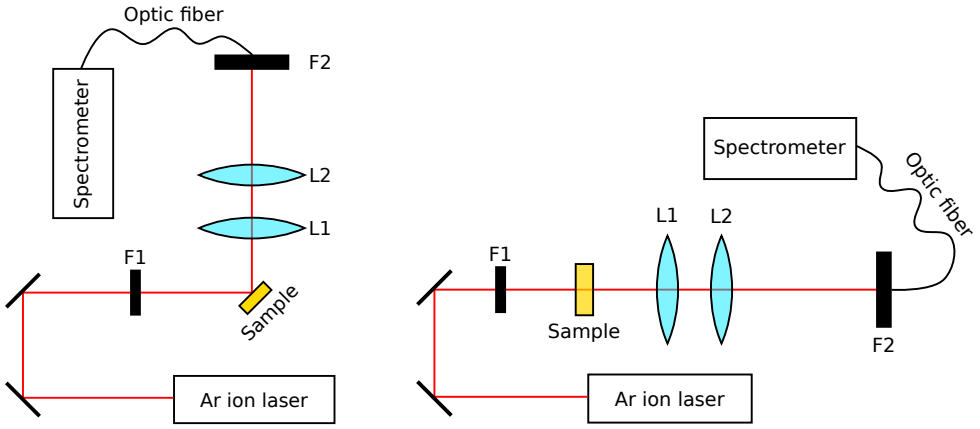

(a) Reflection mode (b) Transmission mode

Figure 6.2: Experimental setup used for measuring PL spectra.

Both samples were recorded with a 150 lines per mm grating with background subtraction and 10×1s accumulation time, the intensity used of the laser beam was low enough to avoid saturating the defects luminescence (output power of roughly 1 mW) on both cases as well. All measurements were made at room temperature.

6.2 Ellipsometry

For this experiment only the GaN on Si sample was studied, given that our GaN single crystal was a very thick sample, and the spectrometer's resolution would not be good enough to distinguish the peaks, for the wavelength range measured for this sample.

A commercially available ellipsometer from Sentech was used, the model used was the SE 850, which consists on typical ellipsometric setup, with a polychromatic non-polarized light source (a light bulb) and a polarizer, the reflected light from the sample passes through an analyzer before being measured through a detector (in this case a spectrometer so that each wavelength component could be split and measured).

Before starting any measurement, it was necessary to ensure a proper alignment of the beam, this alignment was made through the ellipsometer's software which allowed to displace on the x and y axis the spot where the incident light hits the sample, the same spot was aligned on the (0,0) coordinates. The input polarization angle used was 45°.

The same ellipsometer's software output format provided the ellipsometric parameters s1 and s2 as functions of the wavelength λ, and the wavelength ranged measured was from 340nm to 820nm.

The incidence and detection angle, and the polarization of both the polarizer and the analyzer can be arbitrarily set through the manufacturer's software. The angle used for this experiment was set to 65° with a perpendicular polarization for both the polarizer and the analyzer.

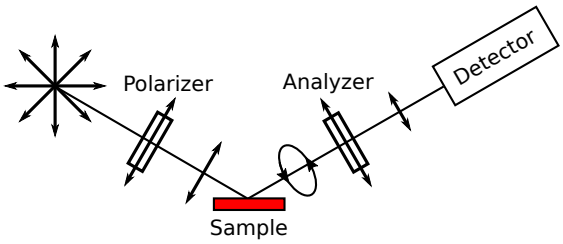

Figure 6.3: Schematic of the ellipsometric system used.

6.3 Raman Spectroscopy

For this experiment an Argon Ion laser was used, the beam from the laser was focused through an optical microscope, which had a manual shutter which allowed to block all the incoming light from the laser to pass through the objective so that focusing could be possible without damaging the eyes with the very intense beam from the laser.

Since the Ar ion laser has many emission lines, and a mostly monochromatic beam was desired, a filter (F1) was needed before hitting the sample, in this case the 488nm emission line was used.

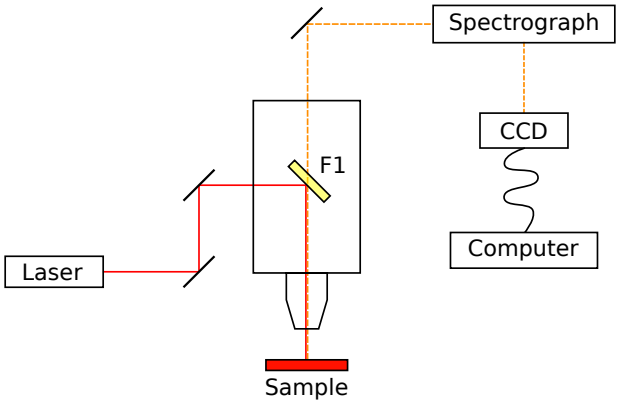

Figure 6.4: Experimental setup used for Raman spectroscopy.

Additionally a filter (F2) was also needed after hitting the sample (a notch filter), for cutting out the highly more intense Rayleigh peak, to avoid any saturation of our detector.

While only one measurement for the GaN on Si sample was made (from 300 nm to 1100 nm), two measurements where made for the GaN single crystal, for each measurement a different face of the crystal was facing the light source's input. Raman spectra could be acquired either through a Charge-coupled Device (CCD) (most suited for fast

real time spectra while focusing the microscope), or through a spectrometer for a higher resolution spectrum.

6.4 Second Harmonic Generation

SHG measurements consisted in two parts, first the reflected SHG signal was measured and then the transmitted SHG signal was measured, however for each case a different setup was used, however even though the signal measured for the GaN on Si sample was the transmitted one, the setup used for this measurement was the same setup as for the reflected SHG measurements was used given that the Si substrate is highly reflective (even though the reflected signal was also measured alongside the transmitted one for this sample, the transmitted signal through the GaN layer is more intense, so the reflected signal could be disregarded).

Given that the laser used had a p-polarized output, for all s polarization measurements a Half Wave Plate (HWP) was used, whereas for p polarization the HWP was removed (the rest of the setup remained the same).

Only a quartz sample was measured in reflection mode, to be used as a reference signal for normalizing our data, in transmission mode, both the GaN single crystal and GaN on Si were measured and also the same quartz crystal.

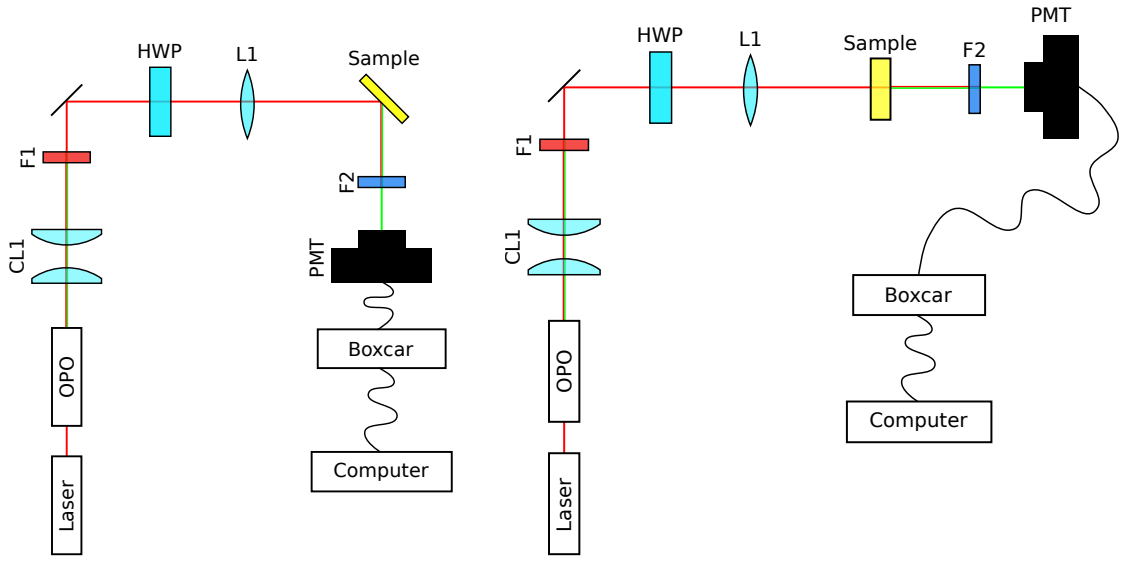

(a) Reflection mode

(b) Transmission mode

Figure 6.5: Experimental setups for SHG spectra.

For the SHG signal from quartz in transmission mode, an incidence angle of 15° was used with s polarization, for the GaN single crystal measurements with 15°, 30°and45° where made with s polarization, and for the 0° measurement a p polarization was used, for the GaN on Si sample p polarization was used with an incidence angle of 45°.

The laser used for this experiment was a q-switched, Neodymium-doped Yttrium Aluminum Garnet (Nd:YAG) nanosecond laser, however since the same had a fixed 1064nm emission line (frequency doubled to 532nm), an Optical Parametric Oscillator (OPO) was used at the output of the same, the same was controlled through a homemade software, which allowed us to shift the wavelength of the laser, so that a range of wavelengths could be analyzed. However the output of the OPO contained various wavelengths, apart from the desired wavelength, so a filter (F1) had to be put at its output so that the sample would be hit by mostly monochromatic radiation, additionally a filter before the Photomultiplier (PMT) (F2), was necessary to cutout any non SHG signal from being detected, since the efficiency of the SHG process was very low.

A set of collimating lenses (CL1) were used to reduce the divergence of the beam, an input filter F1 was needed to cutout the residual and idler signals from the OPO, and an output filter F2 to cutout any non SHG from reaching the PMT. All measurements from the PMT were averaged through a boxcar averager, a 1 nm wavelength step was used for all GaN single crystal spectra with 100 samples per point, and 4 nm step with 100 samples per point for the remaining spectra. The output power of the laser was roughly 5 mW, and the beam diameter was roughly 20 to 50μm, however the output from the signal beam of the OPO varied with the desired wavelength (along side from the filters optical response, and the PMT's response, being the reasons why a normalization sample was required).

CHAPTER 7

Experimental Results and Discussion

Overall the experimental results do match what would be theoretically predicted, in all cases (except for ellipsometry wereonly the GaN on Si sample was studied), the GaN single crystal does provided higher intensity signals, since the GaN on Si sample was very thin compared to the GaN crystal grew through HVPE.

7.1 Photoluminescence Spectroscopy

Both PL spectra shown a sharp peak at around 365 nm, which does match the 3.4 eV bandgap of undoped GaN, as shown in the image bellow.

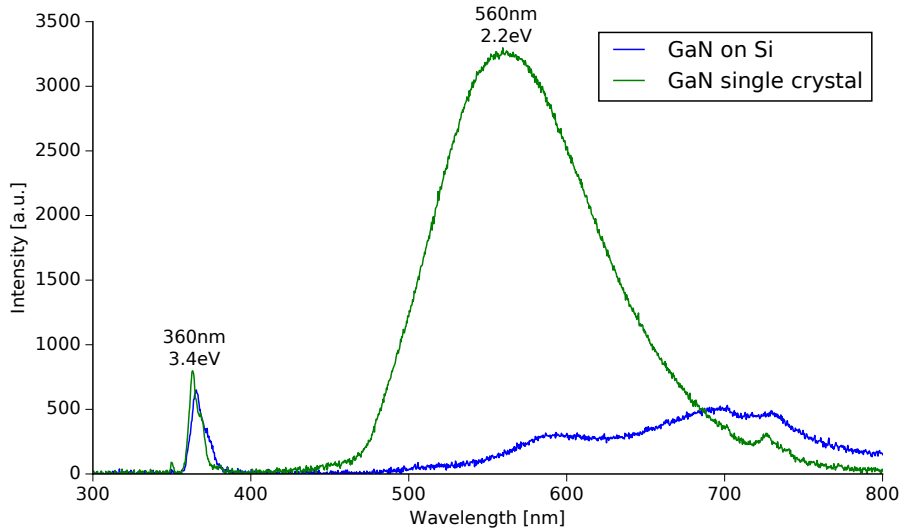

Figure 7.1: PL spectra obtained for both samples.

While both samples do seem to have to 3.4 eV bandgap peak, both samples show different defects luminescence. A stronger defect band can be seen for the GaN single crystal sample peaking at 560 nm, whereas for the GaN on Si sample, two different luminescence defect peaks could be observed at 695 and 590 nm.

Both samples exhibited a peak at 720 nm, however this peak is due to second order diffraction of the bandgap luminescence from grating of the spectrometer.

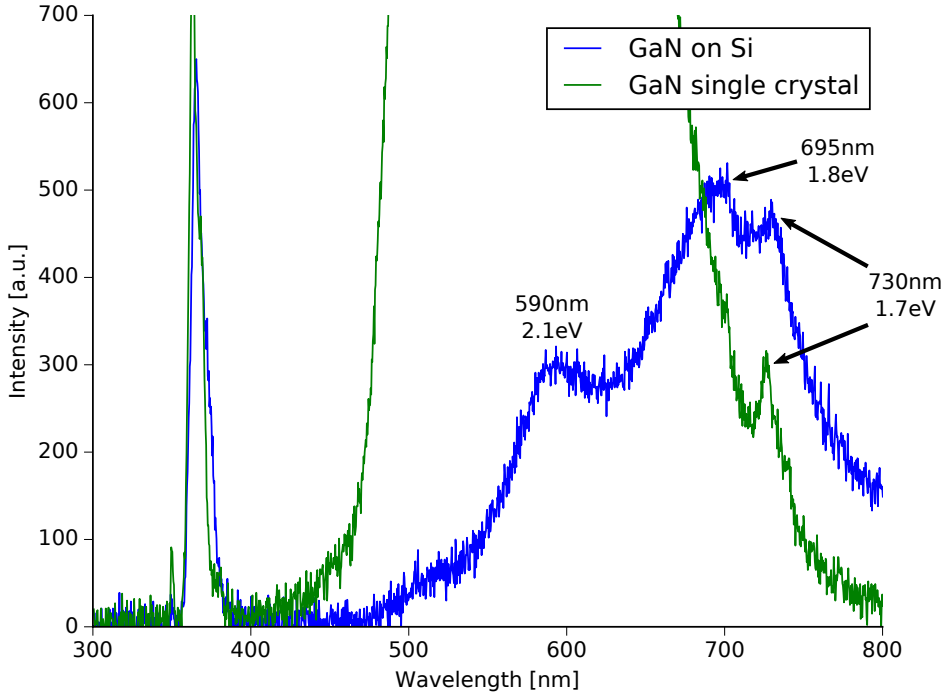

Figure 7.2: Closeup of the PL defects of the GaN on Si sample.

The 560 nm peak for the GaN single crystal matches the 2.2 eV from the yellow luminescence band [31, 32], however for the GaN on Si sample, a broad luminescence peak around 1.8 eV can be seen that matches the red luminescence band [31], this same peak also seem to have interference fringes (at 590 and 695 nm), are related to multiple reflection between the GaN and AlN layers and the Si substrate.

7.2 Ellipsometry

For this experiment the ellipsometric parameters S_1 and S_2 were measured with the ellipsometer, and then compared with the expected theoretical results simulated through a Python script. The estimated thickness for the GaN layer was 585nm and 85nm for the AlN buffer layer.

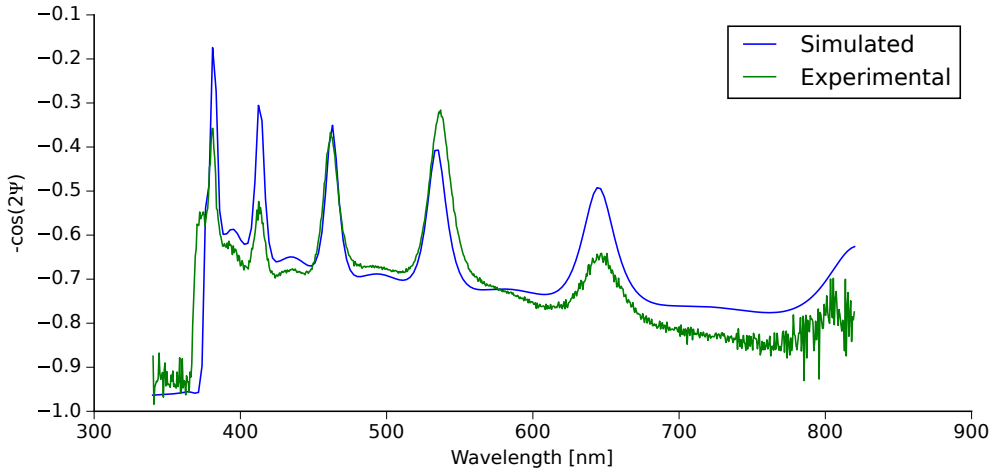

Figure 7.3: Experimental results for the S_1 ellipsometric parameter.

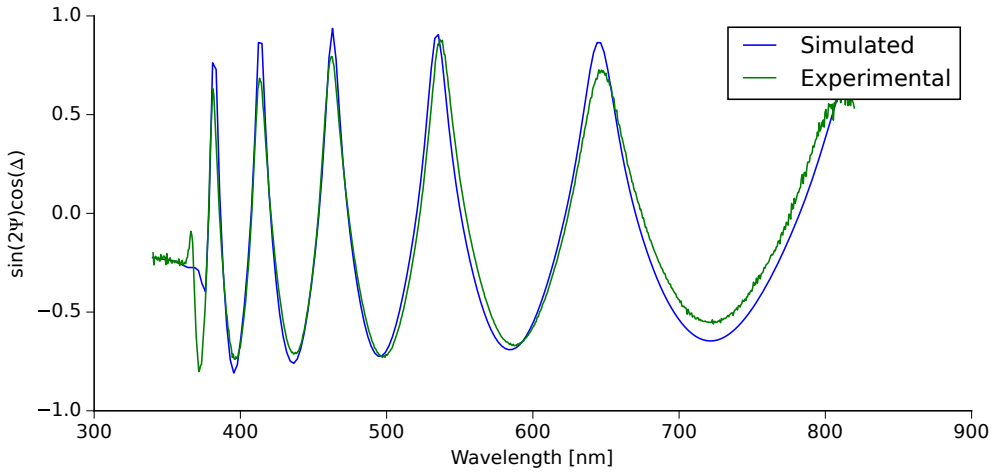

Figure 7.4: Experimental results for the S_2 ellipsometric parameter.

For the simulated values a table with the dispersion values for the refractive index and extinction coefficient were used [33, 34], and then interpolated by linear splines (higher order interpolation, such as cubic splines, caused big oscillations for the refractive indices and extinction coefficients).

7.3 Raman Spectroscopy

For the GaN on Si sample a variety of peaks were encountered, as expected, both $A_1(LO)$ and E_2^H were encountered (the E_2^L peak was bellow the scanned domain thus it wasn't visible), however Raman modes from the silicon substrate and the buffer layer were also encountered.

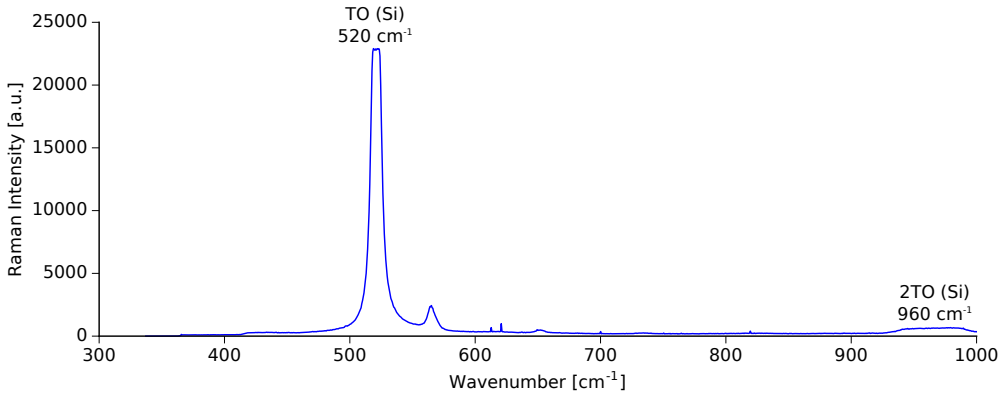

Figure 7.5: Raman spectra of the GaN on Si sample.

The peak at 520 cm^{-1} matches the TO peak of Si, and the peak at 960 cm^{-1} matches $2TO$ from Si, also the peak at 650 cm^{-1} matches E_2^H from wurtzite AlN, which is expected given that an AlN buffer layer was used for this film.

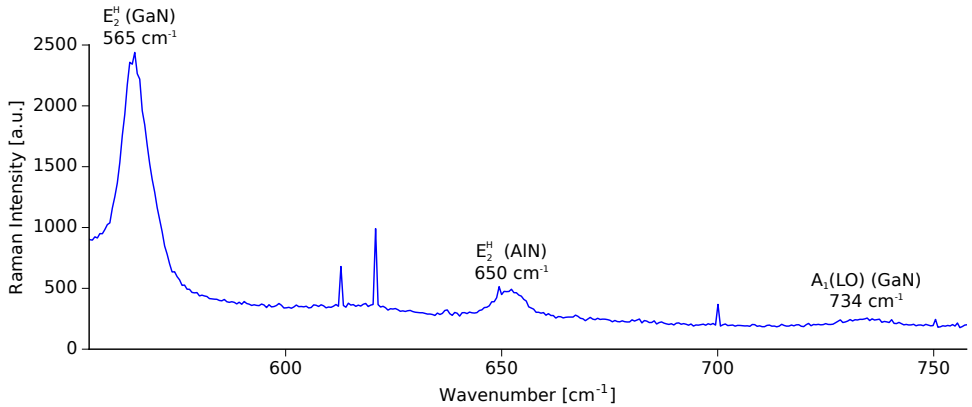

Figure 7.6: Closer look of the Raman modes found for the GaN on Si sample.

Given that the only Raman modes found for GaN were $A_1(LO)$ and E_2^H, this suggests that the deposited GaN layer was oriented on its (0001) plane, additionally the fact that the Raman peaks for GaN were considerably weaker than the silicon peaks relates to the fact the deposited layer was indeed very thin.

For the GaN single crystal only E_2^H and $A_1(LO)$ Raman modes were encountered, which again means that the crystal was oriented in the (0001) plane.

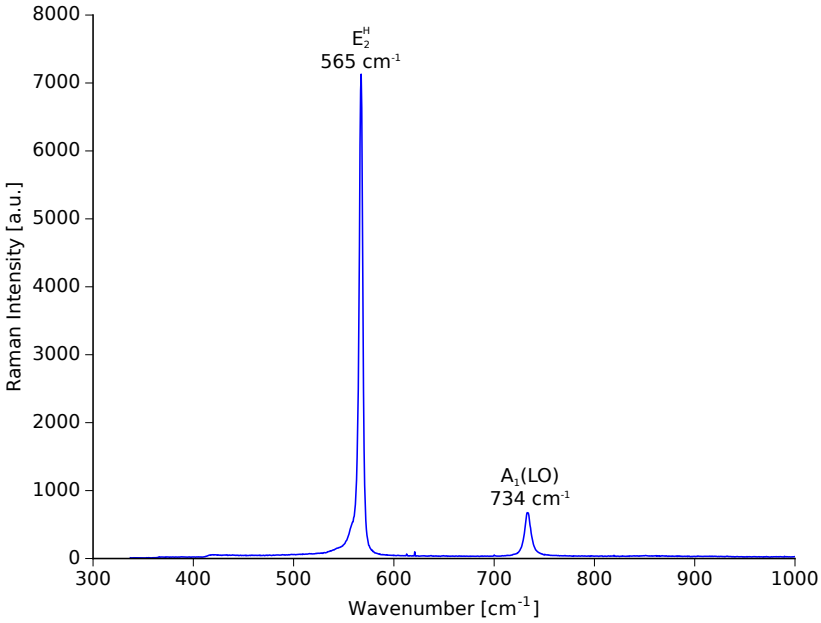

Figure 7.7: Raman modes found for the GaN single crystal sample.

Sample	Mode	Position (cm^{-1})	Peak width (cm^{-1})
GaN single crystal	$A_1(LO)$	733.494	6.771
	E_2^H	567.303	4.711
GaN on Si	$E_2^H(GaN)$	564.916	6.26
	$A_1(LO)(GaN)$	734.78	13.137
	$E_2^H(AlN)$	651.764	7.762
	$TO(Si)$	521.231	10.123
	$2TO(Si)$	965.998	49.224

Table 7.1: Raman modes encountered for both samples.

7.4 Second Harmonic Generation

For this experiment only the thickness of the GaN single crystal was estimated, since the thickness of the GaN on Si sample was too small for any Maker fringes to be visible, additionally since the OPO had a different intensity for each wavelength generated, a normalization sample was required. For this experiment the second order susceptibility was not estimated since in order to determine it the intensity of the fundamental frequency is required, and since the PMT had a different spectral response for two different frequencies, a calibration curve for the same PMT would had been required.

For normalizing the data a SHG measurement was made on a quartz crystal in reflection mode, for this sample the incident light was s polarized.

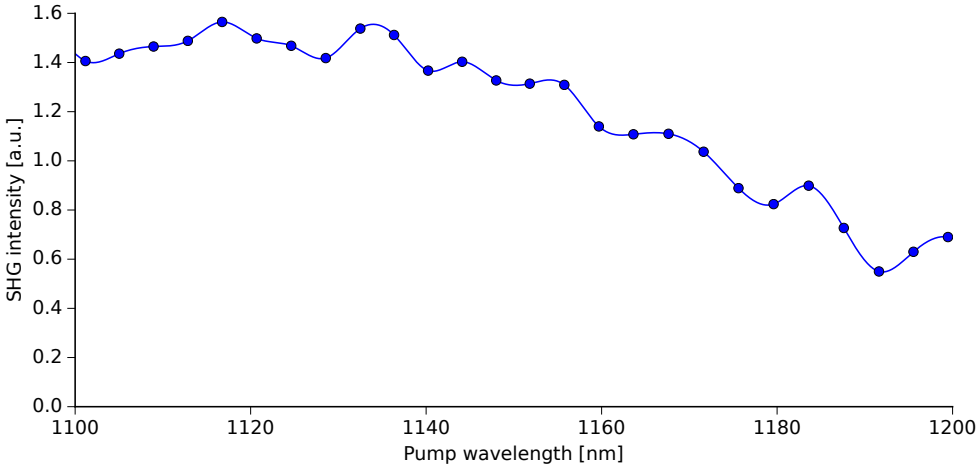

Figure 7.8: SHG signal for a quartz crystal in reflection mode.

By comparison, for the same quartz crystal (roughly 5.1 mm thick) measured in transmission mode with p polarized light it is clearly possible to observe Maker fringes, though the spectra needs to be normalized.

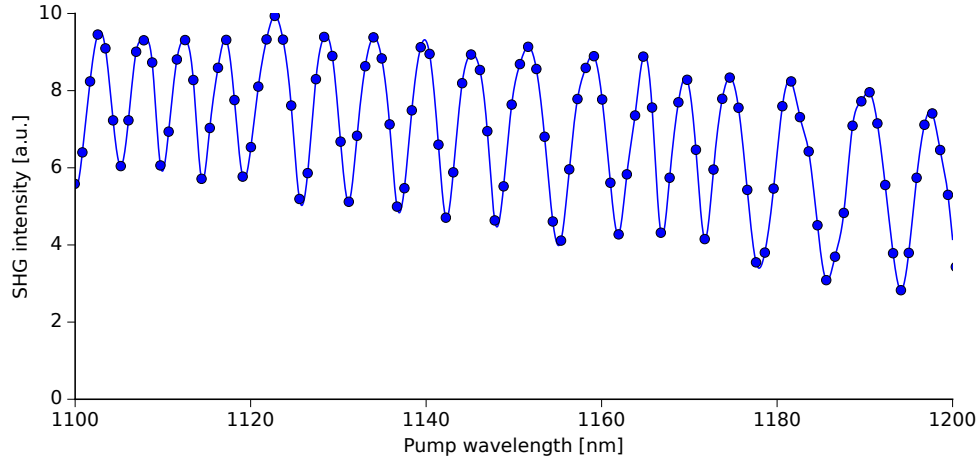

Figure 7.9: SHG signal for a quartz crystal in transmission mode.

For the GaN single crystal measurements, all spectra were normalized with the Quartz reference sample measured in reflection mode, and compared with the expected theoretical results from the Python script. In this script the ordinary and extraordinary refractive indices were obtained from a Sellmeier dispersion model [35]. The estimated thickness used for measurement was 0.3605 mm at 15° , 0.3285 mm at 30° and 0.364 mm at 45°.

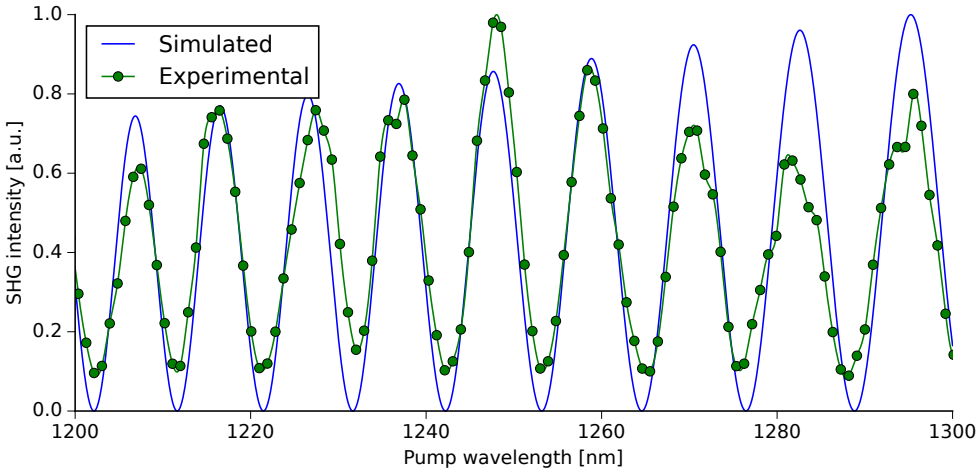

(a) 15° incidence

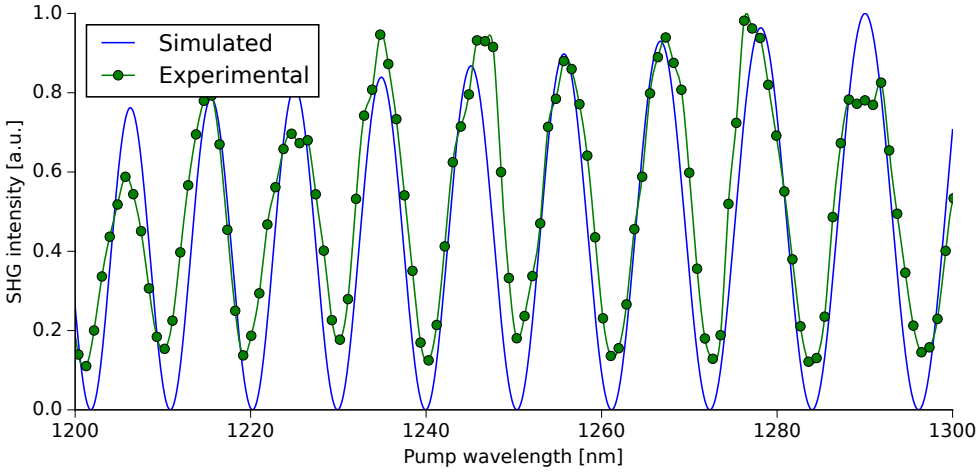

(b) 30° incidence

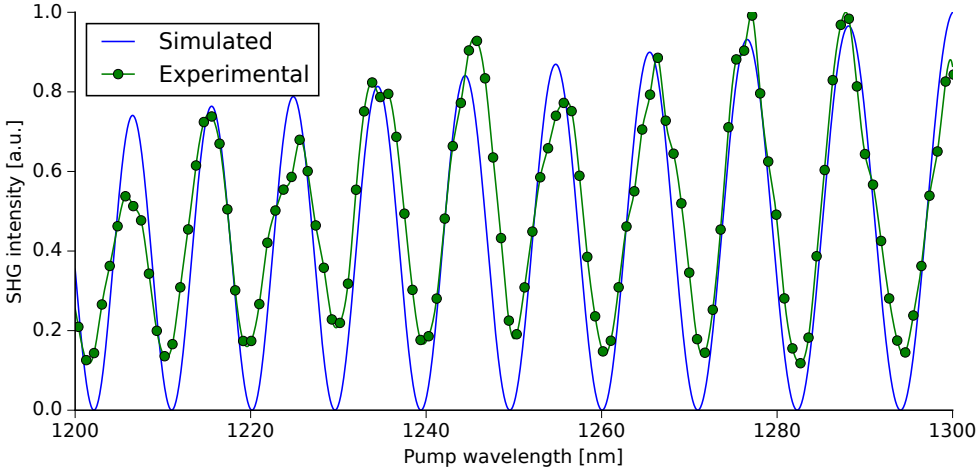

(c) 45° incidence

Figure 7.10: Normalized SHG spectra for the GaN single crystal, with p-polarized light.

Since the crystal was oriented on the (0001) plane, when s-polarized light was used, the electric field will oscillate perpendicularly to the crystal's optic axis, thus the refracted rays refract as ordinary rays, otherwise for p-polarized light the electric field would oscillate partially on the optic axis, thus a extraordinary ray. Since the thickness of the GaN on Si sample was very small, no Maker fringes could be observed, for the simulation a thickness of 590 nm was used from the previous ellipsometric results.

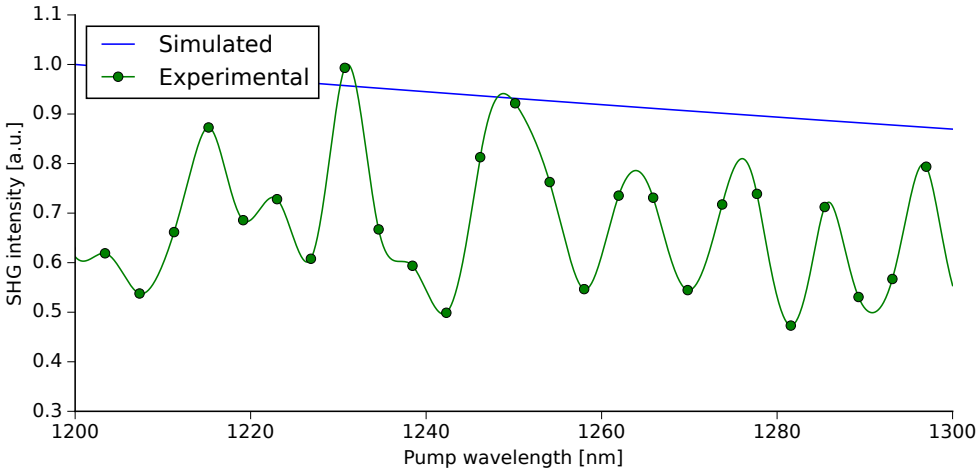

Figure 7.11: Normalized SHG spectra for the GaN on Si sample, with s-polarized light.

Given that the Sellmeier dispersion model used was fitted with wavelengths between 0.5μm and 5.2μm), to determine the SHG intensity for shorter pump wavelengths than 1000 nm would require to know the refractive index (both ordinary and extraordinary) at shorter wavelengths than 500 nm, thus only wavelengths above 1000 mn were compared.

Chapter 8

Conclusion

In this work spectra of photoluminescence, Raman, SHG and ellipsometry were obtained for two different GaN samples. While the first sample was a GaN sample deposited on a silicon substrate with an AlN buffer layer the second sample was a free standing GaN crystal. The chemical composition for each layer matched the chemical composition assumed for the SHG and ellipsometric simulated results, and the peaks encountered at both photoluminescence and Raman matched the peaks encountered in previous researches.

Both samples displayed a sharp bandgap emission at 3.4 eV, however different defects luminescence were observed for each sample. For the GaN single crystal a wide and very intense yellow luminescence band was observed, the origin of this band has been proposed to be related to the presence of carbon impurities [36], however for the GaN on Si sample a smaller red luminescence band was observed, however the origin of this band is not as clear as the yellow band, and multiple types of defects have been reported to contribute to the emission of this band [29]. While the geometry used for each sample was different, which might influence the intensity of the defects band, the thicker GaN single crystal displayed a higher density of defects (thus a higher defect luminescence band), however for a better understanding of these defects luminescence low temperature PL measurements would be required.

While ellipsometry allowed us to determine the thickness of each layer for the GaN on Si sample, for the GaN single crystal this could not be done, however the contrary happened with the obtained SHG spectra, where the thickness of the GaN on Si sample couldn't be determined due the absence of Maker fringes, thus SHG can be used to determine the thickness for thicker GaN samples, while ellipsometry for thin film samples.

Raman spectra for both sample also allowed to determine the composition of the samples, and the orientation of both samples. For both samples the only vibrational modes for GaN found were the $A_1(LO)$ and E_2^H, thus both samples were oriented on the

(0001) plane. The orientation of the GaN crystal could also be determined through the SHG spectra since for s-polarized light, the refracted rays were ordinary rays and not extraordinary, thus the crystal must be (0001) oriented.

In order to obtain a precise dispersion values for the second order susceptibility, from the SHG spectra, a calibration curve of the PMT would be required, however this dispersion formula would only be valid for a quartz reference sample, since there might also be some dispersion in the second order susceptibility of quartz. The values for the crystal thicknesses varied depending on the angle of incidence, this could be related to the shape of the crystal, for instance the crystal might be slightly wedge shaped. For the GaN single crystal measurements we can observe that the sampling rate was rather poor for such a thick sample, an apparent signal constant background (the oscillations do not seem to reach zero) suggest that a greater sampling frequency than 1 nm per point should be used for thick samples, otherwise SHG spectra for broader wavelength could be measured, thus allowing smaller sampling rates for a more accurate thickness determination, additionally given that the SHG is a very weak signal, a greater amount of samples per point would also be required to neglect any background noise.

Bibliography

[1] S. Pal and C. Jacob. "Silicon - A new substrate for GaN growth". In: *Bulletin of Materials Science* 27.6 (2004), pp. 501–504. ISSN: 02504707. DOI: 10.1007/BF02707276.

[2] M. Weyers and Î. U. Leds. *Substrates for GaN Technology Why GaN for optoelectronics? Applications in optoelectronics I*. URL: http://crysta.physik.hu-berlin.de/as2005/pdf/as2005_talk_08_Weyers.pdf (visited on 04/13/2016).

[3] U. Mishra. "Compound Semiconductors; GaN and SiC, Separating Fact from Fiction in both Research and Business". In: (2013), pp. 1–17. URL: http://www.transphormusa.com/sites/default/files/transphorm/news/Copy_of_Plenary%20presentation%20APEC%202013-HD-Final_14Mar2013.pdf (visited on 04/15/2016).

[4] A. Lidow and J. Strydom. "Gallium Nitride (GaN) Technology Overview". In: *White Paper WP001* (2012), pp. 1–6. URL: http://epc-co.com/epc/documents/papers/Gallium$\backslash$nNitride$\backslash$nGaN$\backslash$nTechnology$\backslash$nOverview.pdf (visited on 04/20/2016).

[5] A. Yariv and P. Yeh. *Optical Waves in Crystals: Propagation and Control of Laser Radiation*. Wiley Series in Pure and Applied Optics. Wiley, 2002. ISBN: 9780471430810.

[6] R. Ciechonski. *Growth and characterization of SiC and GaN*. 1151. 2007. ISBN: 9789185895267. DOI: ISBN:978-91-85895-26-7ISSN:0345-7524.

[7] B. Ridley. *Quantum Processes in Semiconductors*. Oxford science publications. OUP Oxford, 2013. ISBN: 9780199677214.

[8] M. Henini. *Handbook of Self Assembled Semiconductor Nanostructures for Novel Devices in Photonics and Electronics*. Elsevier Science, 2011. ISBN: 9780080560472.

[9] R. Willardson, E. Weber, T. Moustakas, and J. Pankove. *Gallium-Nitride (GaN) II*. Semiconductors and Semimetals. Elsevier Science, 1998. ISBN: 9780080864556.

[10] T. Fujita, T. Hasegawa, M. Haraguchi, T. Okamoto, M. Fukui, and S. Nakamura. "Determination of Second-Order Nonlinear Optical Susceptibility of GaN Films on Sapphire". In: *Japanese Journal of Applied Physics* 39.5R (2000), p. 2610.

[11] H. Morkoç. *Handbook of Nitride Semiconductors and Devices, Materials Properties, Physics and Growth*. Handbook of Nitride Semiconductors and Devices. Wiley, 2009. ISBN: 9783527628469.

[12] L. Liu and J. Edgar. "Substrates for gallium nitride epitaxy". In: *Materials Science and Engineering: R: Reports* 37 (2002), pp. 61–127. ISSN: 0927796X. DOI: 10.1016/S0927-796X(02)00008-6.

[13] J. S. Paek, K. K. Kim, J. M. Lee, D. J. Kim, M. S. Yi, D. Y. Noh, H. G. Kim, and S. J. Park. "Nitridation of sapphire substrate and its effect on the growth of GaN layer at low temperature". In: *Journal of Crystal Growth* 200.1-2 (1999), pp. 55–62. ISSN: 00220248. DOI: 10.1016/S0022-0248(98)01253-6.

[14] S. A. Kukushkin, A. V. Osipov, V. N. Bessolov, B. K. Medvedev, V. K. Nevolin, and K. A. Tcarik. "Substrates for epitaxy of gallium nitride: New materials and techniques". In: *Reviews on Advanced Materials Science* 17.1-2 (2008), pp. 1–32. ISSN: 16065131.

[15] Y. N. Ahn, S. H. Lee, S. K. Lim, K. J. Woo, and H. Kim. "The role of inversion domain boundaries in fabricating crack-free GaN films on sapphire substrates by hydride vapor phase epitaxy". In: *Materials Science and Engineering: B* 193 (2015), pp. 105–111. ISSN: 09215107. DOI: 10.1016/j.mseb.2014.11.012.

[16] R. Maria Kemper, T. Schupp, M. Häberlen, T. Niendorf, H. J. Maier, A. Dempewolf, F. Bertram, J. Christen, R. Kirste, A. Hoffmann, J. Lindner, and D. Josef As. "Anti-phase domains in cubic GaN". In: *Journal of Applied Physics* 110.12 (2011), pp. 5–10. ISSN: 00218979. DOI: 10.1063/1.3666050.

[17] S. Woo, M. Kim, B. So, G. Yoo, J. Jang, K. Lee, and O. Nam. "Defect reduction of SiNx embedded m-plane GaN grown by Hydride vapor phase epitaxy". In: *Journal of Crystal Growth* 407 (2014), pp. 6–10. ISSN: 00220248. DOI: 10.1016/j.jcrysgro.2014.08.014.

[18] C. D. Lee, A Sagar, R. M. Feenstra, W. L. Sarney, L Salamanca Riba, and J. W. P. Hsu. "Growth of GaN on Si(0001) by molecular beam epitaxy". In: *Physica Status Solidi a Applied Research* 188.2 (2001), pp. 595–599.

[19] J. R. Arthur. "Molecular Beam Epitaxy". In: *Surface Science* 500 (2002), pp. 189–217. ISSN: 0559-8516. DOI: 10.3131/jvsj.16.91.

[20] MBE Komponenten. *Knudsen Cell*. URL: http://www.mbe-komponenten.de/glossary/knudsen-cell{_}{_}48.php (visited on 05/17/2016).

[21] M. A. Materials. *Pyrolytic Boron Nitride (PBN)*. URL: http://www.morgantechnicalceramics.com/materials/pyrolytic-boron-nitride-pbn (visited on 05/17/2016).

[22] M Ohring. *The Materials Science of Thin Films*. Referex Engineering. Academic Press, 1992. ISBN: 9780125249904.

[23] K. Burak Üçer. *Vacuum Evaporation*. 2009. URL: users.wfu.edu/ucerkb/Nan242/L06-Vacuum{_}Evaporation.pdf (visited on 05/18/2016).

[24] Y Xu and X Yan. "Chapter 2 Physical Fundamentals of Chemical Vapour Deposition Gas Laws and Kinetic Theory". In: *Chemical Vapor Deposition: An integrated Engineering Design for Advanced materials* (2010), pp. 1–44.

[25] J. Coleman. "Metalorganic chemical vapor deposition for optoelectronic devices". In: *Proceedings of the IEEE* 85.11 (1997), pp. 1715–1729. ISSN: 0018-9219. DOI: 10.1109/5.649647.

[26] Y. Kokubun, J. Nishio, M. Abe, T. Ehara, and S. Nakagomi. "Properties of GaN epitaxial layers grown at high growth rates by metalorganic chemical vapor deposition". In: *Journal of Electronic Materials* 30.1 (2001), pp. 23–26. ISSN: 0361-5235. DOI: 10.1007/s11664-001-0210-0.

[27] P. R. Hageman, V. Kirilyuk, W. H. M. Corbeek, J. L. Weyher, B. Lucznik, M. Bockowski, S. Porowski, and S. Müller. "Thick GaN layers grown by hydride vapor-phase epitaxy: Hetero- versus homo-epitaxy". In: *Journal of Crystal Growth* 255.3-4 (2003), pp. 241–249. ISSN: 00220248. DOI: 10.1016/S0022-0248(03)01259-4.

[28] O. Kryliouk, M. Reed, T. Dann, T. Anderson, and B. Chai. "Growth of GaN single crystal substrates". In: *Materials Science and Engineering B: Solid-State Materials for Advanced Technology* 59.1-3 (1999), pp. 6–11. ISSN: 09215107. DOI: 10.1016/S0921-5107(98)00403-6.

[29] Y. Wei, Z. Xiao-Dong, Z. Li-Min, Y. Zhen, B. Hai, and L. Zheng-Min. "Yellow and red luminescence in Mg-implanted GaN epitaxial films". In: *Nuclear Instruments and Methods in Physics Research, Section B: Beam Interactions with Materials and Atoms* 264.1 (2007), pp. 41–46. ISSN: 0168583X. DOI: 10.1016/j.nimb.2007.07.023.

[30] W. Weber and R. Merlin. *Raman Scattering in Materials Science*. Springer Series in Materials Science. Springer Berlin Heidelberg, 2000. ISBN: 9783540672234.

[31] M. A. Reshchikov and H. Morko. "Luminescence properties of defects in GaN". In: *Journal of Applied Physics* 97.6 (2005). ISSN: 00218979. DOI: 10.1063/1.1868059.

[32] S. Chung, O. Cha, C.-H. Hong, E.-K. Suh, H. Lee, Y. Kim, and B. Kim. "Emission Mechanism of the Yellow Luminescence in Undoped GaN". In: *Journal of the Korean Physical Society* 37.6 (2000), p. 1003. ISSN: 0374-4884. DOI: 10.3938/jkps.37.1003.

[33] S. Adachi. *Optical Constants of Crystalline and Amorphous Semiconductors: Numerical Data and Graphical Information*. Springer US, 2013. ISBN: 9781461552475.

[34] M. A. Green and M. J. Keevers. "Optical properties of intrinsic silicon at 300 K". In: *Progress in Photovoltaics: Research and Applications* 3.3 (1995), pp. 189–192. ISSN: 1099-159X. DOI: 10.1002/pip.4670030303.

[35] S. R. Bowman, C. G. Brown, M. Brindza, G. Beadie, J. K. Hite, J. a. Freitas, C. R. Eddy, J. R. Meyer, and I. Vurgaftman. "Broadband measurements of the refractive indices of bulk Gallium Nitride". In: *Optical Materials Express* 4.7 (2014), p. 1287. ISSN: 2159-3930. DOI: 10.1364/OME.4.001287.

[36] D. O. Demchenko, I. C. Diallo, and M. A. Reshchikov. "Yellow luminescence of gallium nitride generated by carbon defect complexes". In: *Physical Review Letters* 110.8 (2013), pp. 1–5. ISSN: 00319007. DOI: 10.1103/PhysRevLett.110.087404.

APPENDIX A

ELLIPSOMETRY SIMULATION SCRIPT

```
1  import matplotlib.pyplot as plt
2  import numpy as np
3  import cmath as cmath
4  import scipy.interpolate as interpolate
5
6
7  def read_file(file_name):
8    # reads a file with file_name where the information for the refractive
9    # and extinction coefficient must be and returns a cubic interpolated
10   # function for the dispersion of both n and k
11
12   l = []
13   n = []
14
15   obj = open(file_name,"r").readlines()
16   for i in obj:
17     l.append(float(i.split()[0]))
18     n.append(float(i.split()[1]) + 1.0j * float(i.split()[2]))
19
20   fn = interpolate.interp1d(l,n,kind="linear")
21   return fn
22
23
24 #incidence angle
25 phi_1 = 65.0 * np.pi / 180.0
26 #GaN layer thickness
27 d2 = 585E-9
28 #AlN layer thickness
29 d3 = 85E-9
30
31 #complex refractive indices (layer one is assumed to always equal 1)
```

```
n2 = read_file("GaN.txt")
n3 = read_file("AlN.txt")
n4 = read_file("Si.txt")


def phi_2(wavelength) :
  # returns the phi_2 angle at the given wavelength in nm

  return cmath.asin(cmath.sin(phi_1)/n2(wavelength))


def phi_3(wavelength) :
  # returns the phi_2 angle at the given wavelength in nm

  return cmath.asin(cmath.sin(phi_1)/n3(wavelength))


def phi_4(wavelength) :
  # returns the phi_2 angle at the given wavelength in nm

  return cmath.asin(cmath.sin(phi_1)/n4(wavelength))


def beta_1(wavelength) :
  # returns the phase difference from layer 1 to layer 2 where wavelength
  # is given in nm

  ret = (cmath.sin(phi_1))**2.0
  ret = (n2(wavelength)**2.0) - ret
  ret = cmath.sqrt(ret)
  ret = 2*np.pi*(d2/wavelength)*ret*1.0E9

  return ret


def beta_2(wavelength) :
  # returns the phase difference from layer 2 to layer 3 where wavelength
  # is given in nm

  p_2 = phi_2(wavelength)
  p_3 = phi_3(wavelength)

  ret = n2(wavelength) * cmath.sin(p_3) * cmath.sin(p_2)
  ret = ret / cmath.cos(p_3)
  ret = n3(wavelength) / cmath.cos(p_3) - ret
  ret = 2.0*np.pi*d3*ret/wavelength
  ret = ret * 1E9

  return ret

```

```
82
83  def r_12_p(wavelength) :
84    # returns the complex reflection coefficient from layer 1 to 2 for
85    # p polarized light
86
87    num = n2(wavelength) * cmath.cos(phi_1) - cmath.cos(phi_2(wavelength))
88    den = n2(wavelength) * cmath.cos(phi_1) + cmath.cos(phi_2(wavelength))
89
90    return num / den
91
92
93  def r_12_s(wavelength) :
94    # returns the complex reflection coefficient from layer 1 to 2 for
95    # s polarized light
96
97    num = cmath.cos(phi_1) - n2(wavelength) * cmath.cos(phi_2(wavelength))
98    den = cmath.cos(phi_1) + n2(wavelength) * cmath.cos(phi_2(wavelength))
99
100   return num / den
101
102
103 def r_23_p(wavelength) :
104   # returns the complex reflection coefficient from layer 1 to 2 for
105   # p polarized light
106
107   num = n3(wavelength) * cmath.cos(phi_2(wavelength))
108   num = num - n2(wavelength) * cmath.cos(phi_3(wavelength))
109   den = n3(wavelength) * cmath.cos(phi_2(wavelength))
110   den = den + n2(wavelength) * cmath.cos(phi_3(wavelength))
111
112   return num / den
113
114
115 def r_23_s(wavelength) :
116   # returns the complex reflection coefficient from layer 1 to 2 for
117   # s polarized light
118
119   num = n2(wavelength) * cmath.cos(phi_2(wavelength))
120   num = num - n3(wavelength) * cmath.cos(phi_3(wavelength))
121   den = n2(wavelength) * cmath.cos(phi_2(wavelength))
122   den = den + n3(wavelength) * cmath.cos(phi_3(wavelength))
123
124   return num / den
125
126
127 def r_34_p(wavelength) :
128   # returns the complex reflection coefficient from layer 1 to 2 for
129   # p polarized light
130
131   num = n4(wavelength) * cmath.cos(phi_3(wavelength))
```

```
132   num = num - n3(wavelength) * cmath.cos(phi_4(wavelength))
133   den = n4(wavelength) * cmath.cos(phi_3(wavelength))
134   den = den + n3(wavelength) * cmath.cos(phi_4(wavelength))
135
136   return num / den
137
138
139 def r_34_s(wavelength) :
140   # returns the complex reflection coefficient from layer 1 to 2 for
141   # s polarized light
142
143   num = n3(wavelength) * cmath.cos(phi_3(wavelength))
144   num = num - n4(wavelength) * cmath.cos(phi_4(wavelength))
145   den = n3(wavelength) * cmath.cos(phi_3(wavelength))
146   den = den + n4(wavelength) * cmath.cos(phi_4(wavelength))
147
148   return num / den
149
150
151 def r_234_p(wavelength) :
152   # returns the complex reflection coefficient from layers 1, 2 and 3 for
153   # p polarized light
154
155   num = r_23_p(wavelength)
156   num = num + r_34_p(wavelength) * cmath.exp(2.0j * beta_2(wavelength))
157   den = r_23_p(wavelength) * r_34_p(wavelength)
158   den = den * cmath.exp(2.0j * beta_2(wavelength))
159   den = den + 1.0
160
161   return num / den
162
163
164 def r_234_s(wavelength) :
165   # returns the complex reflection coefficient from layers 1, 2 and 3 for
166   # p polarized light
167
168   num = r_23_s(wavelength)
169   num = num + r_34_s(wavelength) * cmath.exp(2.0j * beta_2(wavelength))
170   den = r_23_s(wavelength) * r_34_s(wavelength)
171   den = den * cmath.exp(2.0j * beta_2(wavelength))
172   den = den + 1.0
173
174   return num / den
175
176
177 def r_1234_p(wavelength) :
178   # returns the complex reflection coefficient from all layers for
179   # p polarized light
180
181   num = r_12_p(wavelength)
```

```
182   num = num + r_234_p(wavelength) * cmath.exp(2.0j * beta_1(wavelength))
183   den = r_12_p(wavelength) * r_234_p(wavelength)
184   den = den * cmath.exp(2.0j * beta_1(wavelength))
185   den = den + 1.0
186
187   return num / den
188
189
190 def r_1234_s(wavelength) :
191   # returns the complex reflection coefficient from all layers for
192   # s polarized light
193
194   num = r_12_s(wavelength)
195   num = num + r_234_s(wavelength) * cmath.exp(2.0j * beta_1(wavelength))
196   den = r_12_s(wavelength) * r_234_s(wavelength)
197   den = den * cmath.exp(2.0j * beta_1(wavelength))
198   den = den + 1.0
199
200   return num / den
201
202
203 def get_s1(wavelength) :
204   # returns the absolute value of rho as a function of wavelength, where
205   # wavelength is a vector
206
207   ret = []
208   for i in wavelength:
209     aux = r_1234_p(i) / r_1234_s(i)
210
211     psi = cmath.atan(abs(aux))
212
213     ret.append(-cmath.cos(2.0*psi))
214   return ret
215
216
217 def get_s2(wavelength) :
218   # returns the real part of rho as a function of wavelength, where
219   # wavelength is a vector
220
221   ret = []
222   for i in wavelength:
223     aux = r_1234_p(i) / r_1234_s(i)
224
225     psi = cmath.atan(abs(aux))
226     cos_delta = aux.real/cmath.tan(psi)
227
228     ret.append(cmath.sin(2.0*psi)*cos_delta)
229
230   return ret
231
```

```
232
233 l = np.linspace(340.0,820.0,200,endpoint=True)
234 #s1 = get_s1(l)
235 s2 = get_s2(l)
236
237
238 def read_file2(file_name) :
239   # reads the experimental data
240   l = []
241   tan_psi = []
242   tan_psi_cos_delta = []
243
244   obj = open(file_name,'r').readlines()
245   for i in obj :
246     l.append(float(i.split()[0]))
247     tan_psi.append(float(i.split()[1]))
248     tan_psi_cos_delta.append(float(i.split()[2]))
249
250
251   return l, tan_psi, tan_psi_cos_delta
252
253
254 l_exp, s1_exp, s2_exp = read_file2("data_ellip.dat")
255
256 plt.figure(figsize=(10,4.5))
257 plt.plot(l,s2)
258 plt.plot(l_exp,s2_exp)
259
260 plt.legend(["Simulated","Experimental"],loc=1)
261 plt.xlabel("Wavelength [nm]")
262 plt.ylabel("$\mathregular{sin(2\Psi)cos(\Delta)}$")
263
264 plt.gca().spines['top'].set_visible(False)
265 plt.gca().spines['right'].set_visible(False)
266 plt.tick_params(top='off', right='off', bottom='on', left='on',
267     direction='out', length=5)
268
269 plt.show()
```

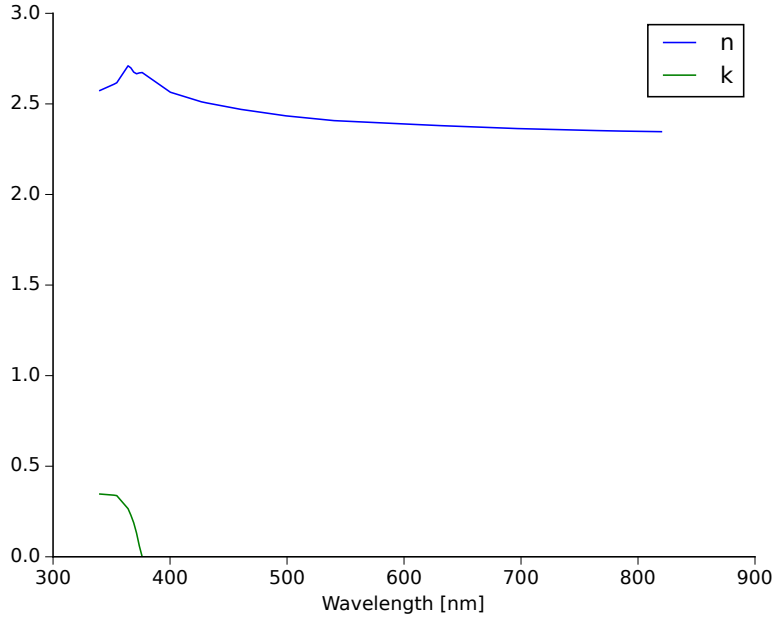

Figure A.1: Refractive index and extinction coefficients used for GaN [33].

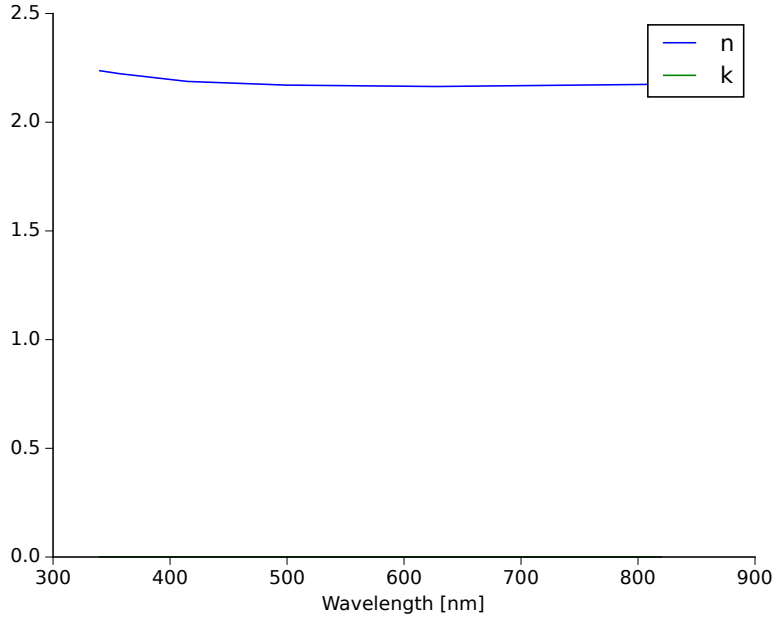

Figure A.2: Refractive index and extinction coefficients used for AlN [33].

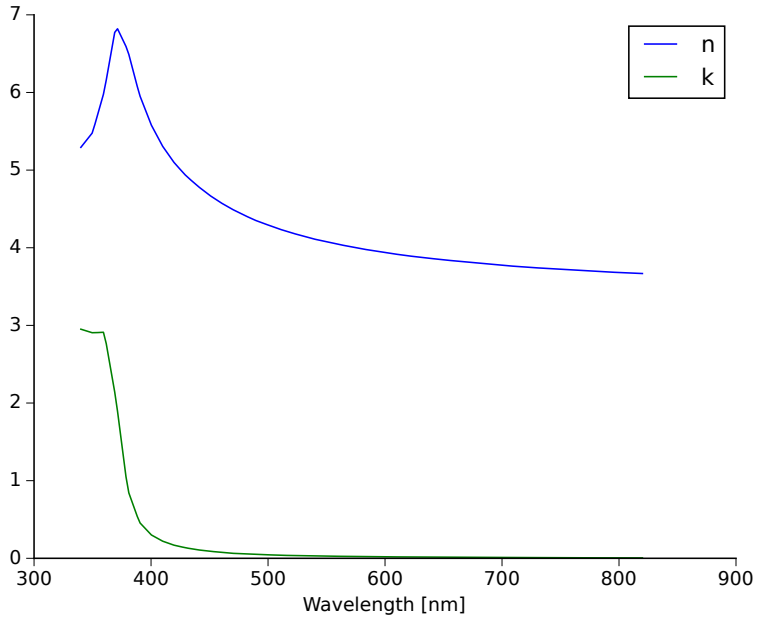

Figure A.3: Refractive index and extinction coefficients used for Si [34].

APPENDIX B

SHG SIMULATION SCRIPT

```
1  import matplotlib.pyplot as plt
2  import numpy as np
3  import scipy.interpolate as interpolate
4  import cmath as cmath
5
6
7  def read_file(file_name):
8    # reads the experimental data
9
10   X = []
11   Y = []
12   obj = open(file_name,'r').readlines()
13   for i in obj:
14     X.append(float(i.split()[0]))
15     Y.append(float(i.split()[1]))
16
17   f = interpolate.interp1d(X,Y,kind="cubic")
18
19   return f
20
21 #f_GaN = read_file("Quartz1(30deg)(p-pol).dat")
22
23 #f_GaN = read_file("GaNonSi(0deg)(s-pol).dat")
24 #f_GaN = read_file("GaNcrystal(15deg)(p-pol).dat")
25 #f_GaN = read_file("GaNcrystal(30deg)(p-pol).dat")
26 f_GaN = read_file("GaNcrystal(45deg)(p-pol).dat")
27
28 # Experimental normalization values, these values where measured in
29 # reflectance mode, thus no Maker fringes patterns should be visible,
30 # so that the PMT, optical filters and OPO spectrals responses get
31 # canceled out
```

```
32 f_Qrt = read_file("Quartz-1000-1400.dat")
33
34
35 def GaN_no(wavelength) :
36   # returns the ordinady refractive index for GaN at the
37   # given wavelength in nm
38
39   wavelength = wavelength * 1E-3
40
41   r1 = 1
42
43   r2 = 4.199 * (wavelength**2.0)
44   r2 = r2 / (wavelength**2.0 - 0.1753**2.0)
45
46   r3 = 3.625 * (wavelength**2.0)
47   r3 = r3 / (wavelength**2.0 - 17.05**2.0)
48
49   ret = r1 + r2 + r3
50   ret = cmath.sqrt(ret)
51
52   return ret
53
54
55 def GaN_ne(wavelength) :
56   # returns the ordinady refractive index for GaN at the
57   # given wavelength in nm
58
59   wavelength = wavelength * 1E-3
60
61   r1 = 1
62
63   r2 = 4.347 * (wavelength**2.0)
64   r2 = r2 / (wavelength**2.0 - 0.1781**2.0)
65
66   r3 = 2.964 * (wavelength**2.0)
67   r3 = r3 / (wavelength**2.0 - 15.23**2.0)
68
69   ret = r1 + r2 + r3
70   ret = cmath.sqrt(ret)
71
72   return ret
73
74
75 def Quartz_no(wavelength) :
76   # returns the ordinady refractive index for Quartz at the
77   # given wavelength in nm
78
79   wavelength = wavelength * 1E-3
80
81   r1 = 1.28604141
```

```
82
83    r2 = 1.07044083 * (wavelength**2.0)
84    r2 = r2 / (wavelength**2.0 - 1.00585997E-2)
85
86    r3 = 1.10202242 * (wavelength**2.0)
87    r3 = r3 / (wavelength**2.0 - 100.0)
88
89    ret = r1 + r2 + r3
90    ret = cmath.sqrt(ret)
91
92    return ret
93
94
95  def Quartz_ne(wavelength) :
96    # returns the extraordinady refractive index for Quartz at the
97    # given wavelength in nm
98
99    wavelength = wavelength * 1E-3
100
101   r1 = 1.28851804
102
103   r2 = 1.09509924 * (wavelength**2.0)
104   r2 = r2 / (wavelength**2.0 - 1.02101864E-2)
105
106   r3 = 1.15662475 * (wavelength**2.0)
107   r3 = r3 / (wavelength**2.0 - 100.0)
108
109   ret = r1 + r2 + r3
110   ret = cmath.sqrt(ret)
111
112   return ret
113
114
115 def theta_1_o(theta_0,no,wavelength):
116   # returns the theta_1 angle for a ordinary ray for a given
117   # wavelength in nm
118
119   return cmath.asin(cmath.sin(theta_0)/no(wavelength))
120
121
122 def theta_2_o(theta_0,no,wavelength):
123   # returns the theta_1 angle for a ordinary ray for a given
124   # wavelength in nm
125
126   return cmath.asin(cmath.sin(theta_0)/(no(wavelength/2.0)))
127
128
129 def psi_o(theta_0,no,wavelength,L):
130   # returns the psi SHG interference parameter for a given
131   # wavelength in nm, and a given length n m for a ordinary ray
```

```
132
133   r1 = no(wavelength)
134   r1 = r1*cmath.cos(theta_1_o(theta_0,no,wavelength))
135   r2 = no(wavelength/2.0)
136   r2 = r2*cmath.cos(theta_2_o(theta_0,no,wavelength))
137
138   ret = (r2 - r1) * L * 2.0*np.pi / wavelength
139   ret = ret * 1E9
140
141   return ret
142
143
144 def n_eq(theta_0,no,ne,wavelength):
145   # returns the effective refractive index for a extraordinary ray for
146   # a uniaxial crystal
147
148   n1 = (cmath.cos(theta_0)**2.0) / (no(wavelength)**2.0)
149   n2 = (cmath.sin(theta_0)**2.0) / (ne(wavelength)**2.0)
150   n_eq = 1.0 / cmath.sqrt(n1 + n2)
151
152   return n_eq
153
154
155 def theta_1_e(theta_0,no,ne,wavelength):
156   # returns the theta_1 angle for a extraordinary ray for a given
157   # wavelength in nm
158
159   ret = cmath.asin(cmath.sin(theta_0))
160   ret = ret / n_eq(theta_0,no,ne,wavelength)
161
162   return ret
163
164
165 def theta_2_e(theta_0,no,ne,wavelength):
166   # returns the theta_2 angle for a extraordinary ray for a given
167   # wavelength in nm
168
169   ret = cmath.asin(cmath.sin(theta_0))
170   ret = ret / n_eq(theta_0,no,ne,wavelength/2.0)
171
172   return ret
173
174
175 def psi_e(theta_0,no,ne,wavelength,L):
176   # returns the psi SHG interference parameter for a given
177   # wavelength in nm, and a given length n m for a extraordinary ray
178
179   r1 = n_eq(theta_0,no,ne,wavelength)
180   #r1 = ne(wavelength)
181   r1 = r1*cmath.cos(theta_1_e(theta_0,no,ne,wavelength))
```

```
182     r2 = n_eq(theta_0,no,ne,wavelength/2.0)
183     #r2 = ne(wavelength/2.0)
184     r2 = r2*cmath.cos(theta_2_e(theta_0,no,ne,wavelength))
185 
186     ret = (r2 - r1) * L * 2.0*np.pi / wavelength
187     ret = ret * 1E9
188 
189     return ret
190 
191 
192 def t_o_1(theta_0,no,wavelength):
193     # transmission coefficient for fundamental frequency
194     # for a ordinary ray
195 
196     r1 = 2*cmath.cos(theta_0)
197     r2 = no(wavelength)*cmath.cos(theta_1_o(theta_0,no,wavelength))
198     r2 = r2 + cmath.cos(theta_0)
199 
200     return r1/r2
201 
202 
203 def t_o_2(theta_0,no,wavelength):
204     # transmission coefficient for the two photon frequency
205     # for a ordinary ray
206 
207     r1 = 2.0*no(wavelength/2.0)*cmath.cos(theta_2_o(theta_0,no,wavelength))
208 
209     r2 = cmath.cos(theta_0)
210     r2 = r2 + no(wavelength)*cmath.cos(theta_1_o(theta_0,no,wavelength))
211 
212     r31 = no(wavelength)*cmath.cos(theta_1_o(theta_0,no,wavelength))
213     r32 = no(wavelength/2.0)*cmath.cos(theta_2_o(theta_0,no,wavelength))
214     r3 = r31 + r32
215 
216     r4 = no(wavelength/2.0)*cmath.cos(theta_2_o(theta_0,no,wavelength))
217     r4 = r4 + cmath.cos(theta_0)
218     r4 = r4**3.0
219 
220     ret = (r1*r2*r3) / r4
221 
222     return ret
223 
224 
225 def t_e_1(theta_0,no,ne,wavelength):
226     # transmission coefficient for fundamental frequency
227     # for a extraordinary ray
228 
229     r1 = 2*cmath.cos(theta_0)
230 
231     r21 = n_eq(theta_0,no,ne,wavelength)
```

```
232   r21 = r21 * cmath.cos(theta_1_e(theta_0,no,ne,wavelength))
233   r22 = cmath.cos(theta_0)
234   r2 = r21 + r22
235
236   return r1/r2
237
238
239 def t_e_2(theta_0,no,ne,wavelength):
240   # transmission coefficient for the two photon frequency
241   # for a extraordinary ray
242
243   r1 = 2.0*n_eq(theta_0,no,ne,wavelength)
244   r1 = r1*cmath.cos(theta_2_e(theta_0,no,ne,wavelength))
245
246   r21 = cmath.cos(theta_1_e(theta_0,no,ne,wavelength))
247   r22 = n_eq(theta_0,no,ne,wavelength)*cmath.cos(theta_0)
248   r2 = r21 + r22
249
250   r31 = n_eq(theta_0,no,ne,wavelength)
251   r31 = r31 * cmath.cos(theta_2_e(theta_0,no,ne,wavelength))
252   r32 = n_eq(theta_0,no,ne,wavelength/2.0)
253   r32 = r32 * cmath.cos(theta_1_e(theta_0,no,ne,wavelength))
254   r3 = r31 + r32
255
256   r41 = n_eq(theta_0,no,ne,wavelength/2.0)
257   r41 = r41 * cmath.cos(theta_0)
258   r42 = cmath.cos(theta_2_e(theta_0,no,ne,wavelength))
259   r4 = r41 + r42
260
261   ret = (r1*r2*r3) / r4
262
263   return ret
264
265
266 def shg_power(theta_0,no,ne,wavelength,L,kind="p") :
267   # returns the power for the SHG for a ordinary ray all multiplying
268   # constants are omitted since the spectra is normalized with the
269   # maxvalue, also the second order dielectric tensor values are
270   # considered as constants, thus also omitted
271
272   ret = []
273   for i in wavelength:
274     if (kind == "s"):
275       aux = cmath.sin(psi_o(theta_0,no,i,L))
276       aux = aux / psi_o(theta_0,no,i,L)
277
278       aux = (aux ** 2.0)
279
280       aux = aux  / (i*no(i/2.0))
281       aux = aux * 1E9
```

```
282       aux = aux / (no(i)**2.0)
283
284       aux = aux * t_o_2(theta_0,no,i)
285       aux = aux * (t_o_1(theta_0,no,i)**4.0)
286
287     elif (kind == "p") :
288       aux = cmath.sin(psi_e(theta_0,no,ne,i,L))
289       aux = aux / psi_e(theta_0,no,ne,i,L)
290
291       aux = (aux ** 2.0)
292
293       aux = aux  / (i*n_eq(theta_0,no,ne,i/2.0))
294       aux = aux * 1E9
295       aux = aux / (n_eq(theta_0,no,ne,i)**2.0)
296
297       aux = aux * t_e_2(theta_0,no,ne,i)
298       aux = aux * (t_e_1(theta_0,no,ne,i)**4.0)
299
300     ret.append(aux.real)
301
302   ret = ret / max(ret)
303
304   return ret
305
306
307 # incidence angle
308 theta_0 = 45.0 * np.pi / 180.0
309
310 # GaN crystal thickness
311 L = 0.381E-3
312 #L = 0.3875E-3
313 #L = 585E-9
314
315 l = np.linspace(1200.0,1300,3E2,endpoint=True)
316 shg1 = shg_power(theta_0,GaN_no,GaN_ne,l,L,"p")
317
318 shg_exp = []
319 for i in l:
320   shg_exp.append(f_GaN(i)/f_Qrt(i))
321
322 shg_exp = shg_exp / max(shg_exp)
323
324 plt.figure(figsize=(10,4.5))
325 plt.plot(l,shg1)
326 plt.plot(l,shg_exp)
327
328 plt.gca().spines['top'].set_visible(False)
329 plt.gca().spines['right'].set_visible(False)
330 plt.tick_params(top='off', right='off', bottom='on', left='on',
331     direction='out', length=5)
```

```
332
333 plt.legend(["Simulated","Experimental"],loc=2)
334 plt.xlabel("Fundamental wavelength [nm]")
335 plt.ylabel("SHG intensity [a.u.]")
336
337 plt.show()
```

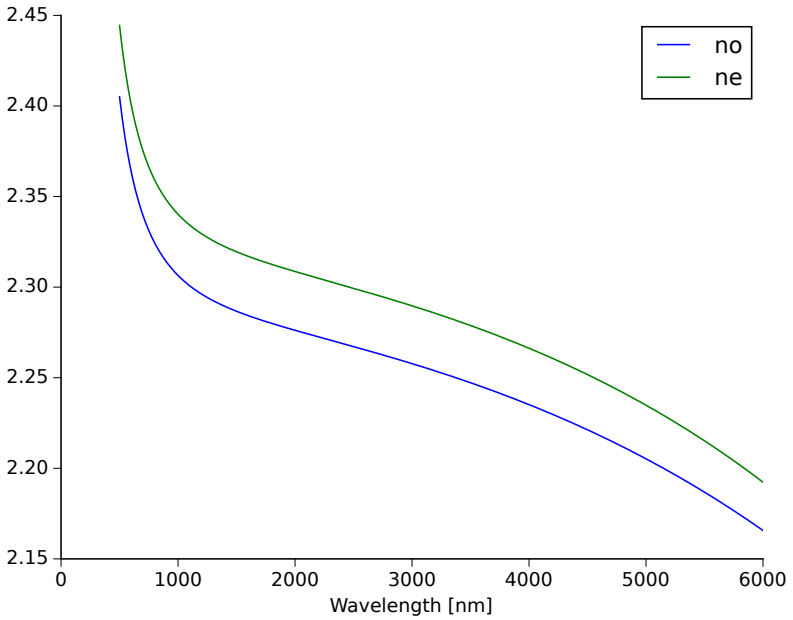

Figure B.1: Ordinary and extraordinary refractive indices used for GaN [35].